Solitons, spatiotemporal chaos and synchronization in arrays of damped driven nonlinear oscillators

William Michael Lewin Robinson

Thesis presented for the degree of

Master of Science

Department of Mathematics and Applied Mathematics

University of Cape Town

May 2008

Abstract

We explore periodic and chaotic motion in a soliton-bearing chain of nonlinear oscillators and study the effect of disorder on the spatiotemporal chaos. The chain we consider consists of torsionally coupled, damped, parametrically driven pendulums. We show that the amplitudes of the pendulums satisfy a system of equations in slow time, the "nonlinear Schrödinger (NLS) oscillators". The evolution of the chain of NLS oscillators is simulated numerically.

Simulating the homogeneous chain, we demonstrate the existence of periodically oscillating solitons, the period-doubling sequence of transitions to temporal chaos and the degeneration into spatiotemporal chaos for larger driving strengths. Next, we explore the effect of introducing weak disorder in the simplest form, a single impurity, into the chain. We describe how a long impurity can induce a pinned soliton to form and prevent spatiotemporal chaos, synchronizing the oscillators in the chain. Lastly, we study chains with several impurities in various configurations. Cases considered include chains with multiple impurities of different strengths, equal equidistant impurities (both long and short), and equal impurities which are positioned randomly along the chain.

We show that all the previously reported features of the continuous NLS equation are reproduced in the dynamics of the discrete chain. Our results indicate that the dominant structures of the spatiotemporal chaos are unstable solitons. We show how spatiotemporally chaotic motion can be suppressed by disordering the chain through the inclusion of one or more impurities, synchronizing the oscillators.

A comprehensive analysis of chains with identical equidistant long impu-

rities reveals an unexpectedly complex relationship between the number and strength of impurities and the dynamics observed. As a result of disordering the positions of impurities, we find that oscillating solitons form between impurities when the gaps are large enough. The oscillations may be periodic or chaotic. Equidistant short impurities may also stabilize the chain.

We conclude that for a set of impurities to prevent spatiotemporal chaos from emerging in the array, the intervals between the impurities should be sufficiently small, and the strength of the impurities should be sufficiently large. The required number and strength of impurities depends on the oscillator parameters and the initial condition of the chain.

Acknowledgements

Many thanks go to my supervisors, Igor Barashenkov and Nora Alexeeva, for their patience and guidance throughout this project. It has been a privilege to work on projects with Igor over the last six years. Nora's assistance with computing aspects in particular has been invaluable.

Thank you to my office mates Oliver Oxtoby and Teresa Lu for all the help, support and continuous entertainment.

To all my friends at the UCT Athletics and Cycling clubs, thank you for all the good times. And thank you for pretending to show an interest in nonlinear dynamical systems. My apologies if my explanations were perhaps not always satisfactory; hopefully, if nothing else, you will appreciate my equations and graphs herein from an aesthetic perspective.

To my family, thank you for your quiet encouragement and interest in my work. Having parents who are experts in comma placement has certainly proven to be useful. My sister Philippa is a constant inspiration.

I was unfortunate to suffer some serious personal setbacks during the course of this project, but happily there have been many highlights over the years as well. In all circumstances, the sympathies and congratulations of all my friends and colleagues have been overwhelming.

I must thank Professor Reinhard Richter and the staff of Experimentalphysik V at Universität Bayreuth, Germany, for their hospitality during my visit in 2005. It was a privilege to see some of the magnetic fluid experiments, especially the appearance of stable two-dimensional solitons [34].

I acknowledge the financial support of the National Research Foundation.

I had two lines open on this page, and right at the end, Debbie, you have filled them. There is just enough space for me to simply say... "Thank you."

Table of Contents

Chapter 1

Introduction

"Synchronization" is described as "an adjustment of rhythm of oscillating objects due to their weak interaction" by Pikovsky, Rosenblum and Kurths [31]. This phenomenon is observed across the full spectrum of scientific fields including physics, chemistry, engineering, biology and even social science.

The synchronization phenomenon has been a topic of great interest in the field of nonlinear dynamics in recent years. Of particular interest is the result that synchronization is sometimes less likely to occur in an array of identical coupled oscillators than in a disordered array which includes variations in the parameters of the oscillators.

In this work, we study an array of nonlinear Schrödinger oscillators which is reduced from a chain of coupled pendulums. The discrete damped driven NLS equations describing these oscillators form a soliton-bearing system. The array becomes prone to spatiotemporal chaos for a range of parameters. Suppression of this chaos amounts to the synchronization of the oscillators in the chain.

Under certain conditions, introducing disorder can synchronize our NLS chain and suppress spatiotemporal chaos. We employ pendulums which are longer or shorter than the others in the chain as a form of weak disorder. We study how varying the number, strength and position of such impurities can promote synchronization.

1.1 First observation of synchronization

The earliest recorded scientific description relating to synchronization dates back to the 17th century [31]. Dutch mathematician Christiaan Huygens had a strong interest in pendulum clocks. According to his accounts, during a voyage in 1665, he became ill. He had set up two clocks suspended from a single wooden beam which he could observe from his bed for a few days, in order to track their accuracy relative to each other.

Unexpectedly, he noticed that the pendulums of the two clocks swung with exactly the same rhythm, but in opposite directions. The ticks from the two clocks always sounded at the same instant. Furthermore, if one pendulum was slightly disturbed, the synchronous rhythm was soon reestablished.

This type of system, where the two oscillators always reach their maximum amplitude at the same instant but move in opposite directions, is said to be in a state of anti-phase synchronization. The motions of the two oscillators are identical, but they have a phase difference of 180 degrees.

The phenomenon observed was the mutual synchronization of the clocks as a result of their coupling through the beam. The motion of the beam was barely perceptible, but it was sufficient to entrain the oscillations of the pendulums in anti-phase. In-phase synchronization is also possible; that happens when the oscillators have zero phase difference. In general, the synchronization of two oscillators is more likely to occur when the difference between their natural frequencies (called frequency detuning) is small. Stronger coupling tends to make synchronization possible for a wider range of detunings.

In this study, we simulate the evolution of a coupled array of self-sustained nonlinear oscillators over a period of time. A self-sustained oscillator is driven by some force, meaning that if it were to be isolated from the rest of the system, it would continue oscillating under the action of the force. Also, the oscillations are stable under small perturbations: the oscillator quickly returns to the original rhythm after being disturbed if the perturbation is not too large. Such an oscillator can be described mathematically without explicit time dependence — it is autonomous.

1.2 Types of synchronization

Different types of synchronization occur in different configurations of oscillators. For example, studies have been performed on the synchronization of pairs of chaotic lasers [36], phase synchronization of an electrochemical oscillator through forcing [21], synchronization of chaotic oscillations in an electric circuit [39], phase synchronization of chaos in a plasma discharge tube [43], phase locking of relativistic magnetrons [9], synchronous flashing of large populations of fireflies [14], acoustic synchrony of the chirping of snowy tree crickets [44], the synchrony of menstrual cycles of women living together in a college dormitory [24] and the synchronization of circadian rhythms through exposure to bright light [4].

In this section, we describe synchronization characteristics in three types of systems: systems containing two oscillators, systems containing N oscillators, and oscillatory media. We also introduce the ideas of phase synchronization and complete synchronization of chaotic signals.

1.2.1 Two oscillators

The pair of pendulum clocks in the previous section is an example of a system which exhibits the mutual synchronization of two interacting oscillators. Following the exposition of Pikovsky *et al.* [31], suppose the natural frequencies of two oscillators are different, say ω_1 and ω_2. If the oscillators are coupled in some way, then the rhythms of both oscillators may be adjusted to some common frequency ω^*, different from both ω_1 and ω_2. If the coupling is dependent on the phases of the two oscillators, then the phases can be described by the equations

$$\frac{d\phi_1}{dt} = \omega_1 + kQ_1(\phi_1, \phi_2),$$
$$\frac{d\phi_2}{dt} = \omega_2 + kQ_2(\phi_2, \phi_1).$$

Here k is the coupling constant and $Q_{1,2}$ are some coupling functions.

Another form of synchronization involving two oscillators occurs when

the adjustment of frequency is unidirectional. In this case, one oscillator has a set rhythm which cannot be influenced by the other. The first oscillator acts as an external periodic force. If the detuning (frequency mismatch) $\Delta\omega = \omega_1 - \omega_2$ is not too large, the second oscillator can be entrained by the first. It will then also oscillate with frequency ω_1. This is known as synchronization by an external force.

Two examples in nature are the entrainment of daily rhythms of living organisms by the revolution of the Earth and the regulation of seasonal rhythms by the motion of the Earth around the sun. In both these cases, the coupling action is clearly unidirectional. Note that while the period of each individual's internal clock will normally be exactly locked to the length of a day (24 hours), the phase shift may differ. This is evident from the fact that some people are more active early in the morning, while others prefer to work till late at night.

1.2.2 Arrays of oscillators

Often a system consists of many oscillators. The ensemble could be arranged in a chain or lattice, where the position of each oscillator in the structure is fixed and the oscillators are evenly spaced. Alternatively, the spatial distribution of the ensemble could be without a fixed or regular structure.

Local coupling

In a chain or lattice, it is common to assume that only adjacent oscillators interact. In such cases, one models the interactions with nearest-neighbour coupling. Often the same coupling function q is used for all interactions. The function q can depend, for example, on the phase difference of the oscillators or on their spatial separation. According to Pikovsky *et al.*, in a chain with typical diffusive coupling, the phase of the n-th oscillator (which we say has natural frequency ω_n) can be described with the equation

$$\frac{d\phi_n}{dt} = \omega_n + \epsilon q(\phi_{n-1} - \phi_n) + \epsilon q(\phi_{n+1} - \phi_n). \tag{1.1}$$

A simple attractive coupling function which is commonly used has the coupling proportional to the sine of the phase differences:

$$q(\phi_j - \phi_n) = \sin(\phi_j - \phi_n).$$

The coupling effect is thus greatest between oscillators which are 90 degrees out of phase.

The oscillators may be numbered from 1 to N, regularly spaced and placed symmetrically about the origin on some domain of length L. The distance between adjacent oscillators is $\Delta x = L/N$. Different boundary conditions are possible. For a chain with free ends, one would use the boundary conditions

$$\phi_0 = \phi_1, \qquad \phi_{N+1} = \phi_N.$$

The phases ϕ_0 and ϕ_{N+1} are not real quantities but must be specified in order to use equation (1.1) to calculate the phase derivatives at the boundaries, which in this case are simply equal to the natural frequency ω_n. If the chain forms a ring, the equations of motion for ϕ_1 and ϕ_N are

$$\frac{d\phi_1}{dt} = \omega_1 + \epsilon q(\phi_N - \phi_1) + \epsilon q(\phi_2 - \phi_1),$$
$$\frac{d\phi_N}{dt} = \omega_N + \epsilon q(\phi_{N-1} - \phi_N) + \epsilon q(\phi_1 - \phi_N).$$

Note that if there is no coupling ($\epsilon = 0$), then each oscillator simply rotates with its own natural frequency. The system thus evolves in a quasi-periodic manner with N different frequencies. On the other hand, for very strong coupling, the differences between the natural frequencies ω_n become negligible, and all oscillators synchronize eventually. For intermediate coupling values, clusters of synchronized oscillators tend to form. The transition between states with different clusters depends on the distribution of the frequencies ω_n.

Consider the transition from the state of complete synchronization to the state containing two clusters. We follow the pioneering work [31]. The phase difference between adjacent oscillators can be written as $\psi_n = \phi_{n+1} - \phi_n$.

Using this in equation (1.1) gives a set of $N-1$ equations,

$$\frac{d\psi_n}{dt} = \Delta_n + \epsilon\left[q(\psi_{n-1}) - 2q(\psi_n) + q(\psi_{n+1})\right], \qquad n = 1, \ldots, N-1.$$

Here the frequency differences between adjacent oscillators are denoted by $\Delta_n = \omega_{n+1} - \omega_n$.

When all oscillators become synchronized, $\dot{\psi}_n = 0$. This leads to a tridiagonal algebraic system with a unique solution for $u_n = q(\psi_n)$. Inverting this relation gives an expression for the phase differences, $\psi_n = q^{-1}(u_n)$, but because $q(\psi)$ is periodic, many inverse solutions exist. Ermentrout and Kopell [16] showed that if q has one minimum and one maximum per period, only one root is stable. All other fixed points are saddles or unstable nodes. For the inverse solution to exist, all components u_k must lie in the interval $(q_{\min}, q_{\max})$. At some critical coupling value, where $u_c = q_{\min}$ or $u_c = q_{\max}$, a saddle-node bifurcation occurs, the stable fixed point disappears and a periodic orbit emerges. The result is that oscillators $n = 1, \ldots, c$ have frequency Ω_1 while oscillators $n = c+1, \ldots, N$ have a different frequency Ω_2. Subsequent bifurcations could split the clusters into smaller groups.

Global coupling

An alternative to nearest-neighbour coupling is global coupling [35], where each oscillator influences every other oscillator in the system. For a system of N oscillators where the coupling is dependent on all the phase differences in the system, the equations for the phases are

$$\frac{d\phi_n}{dt} = \omega_n + \frac{k}{N}\sum_{j=1}^{N} q(\phi_j - \phi_n),$$

where q is a general coupling function [31].

Systems of globally coupled oscillators are not considered in this work.

1.2.3 Oscillatory media

In situations when we cannot identify distinct oscillators, we can speak of a continuous oscillatory medium. A well-known example in chemistry is the Belousov-Zhabotinsky reaction. This reaction between liquids takes place in a container, with oscillations at different sites exhibiting different phases and frequencies. For a light-sensitive version of the reaction, it has been shown that frequency locking can be induced by a periodic optical forcing [30]. A result was the observation of resonant pattern formation.

Pikovsky *et al.* describe the complex amplitude of weakly nonlinear oscillations in a uniform one-dimensional lattice with the equation

$$\frac{dA_k}{dt} = \mu A_k + (\beta + i\delta)(A_{k+1} - 2A_k + A_{k-1}) - (\gamma + i\alpha)|A_k|^2 A_k.$$

By scaling the coupling constants β and δ, and by normalizing time and the amplitude to eliminate μ and γ, the Ginzburg-Landau equation

$$\frac{\partial a(x,t)}{\partial t} = a + (1 + ic_1)\nabla^2 a - (1 + ic_2)|a|^2 a \tag{1.2}$$

may be obtained. The first term describes the linear growth of oscillations. The second term describes the spatial interaction, and the third term describes the nonlinear effect.

If the medium is driven by an external periodic forcing, an additional term accounting for the amplitude of the forcing e and the frequency mismatch ν is added to equation (1.2), giving

$$\frac{\partial a(x,t)}{\partial t} = (1 - i\nu)a + (1 + ic_1)\nabla^2 a - (1 + ic_2)|a|^2 a - ie$$

for the weakly nonlinear one-dimensional case. The driving frequency should be close to the natural frequency of the medium. An important observation is that if the system is not in a spatially homogeneous state (with the phase at each point in the medium being equal), the synchronized solution $a =$ constant can lose its stability as a result of the growth of any spatially inhomogeneous perturbations.

1.2.4 Chaotic oscillators

In many systems, self-sustained oscillators generate a signal which is chaotic. The amplitude of such oscillations may vary, and the time differences between successive maxima may not be equal. Nevertheless, chaotic oscillators may also undergo synchronization through coupling. We must, however, specify what we mean by synchronization in this context.

Often it is helpful to define the average frequency of an oscillator. Following the recipe of Osipov and Sushchik [28], we do this by counting the number of times n_j that a signal $\phi_j(t)$ reaches a maximum over a long time period τ. The average frequency of oscillator j is then calculated as

$$\Omega_j = \frac{2\pi n_j}{\tau}. \tag{1.3}$$

When chaotic oscillators interact, two forms of synchronization may be observed for different coupling strengths. If the coupling is weak, it does not affect the amplitudes of the oscillators which may remain irregular and uncorrelated. However, the frequencies may be adjusted so that the average frequencies become equal and the phase shift between the signals may become constant. This is known as phase synchronization. For stronger coupling, complete synchronization is possible. In this case, the amplitudes as well as the frequencies in the system coincide.

1.3 Taming chaos with disorder

1.3.1 The phenomenon

Intuitively, one might expect synchronization of an array of nonlinear oscillators to be more easily achieved if all oscillators are identical. In technological applications, frequency locking of such arrays is often highly desirable but difficult to achieve in practice.

A key example in electronics involves an array of Josephson junctions. The aim is to produce high power, high frequency voltage oscillations from a direct current. A single Josephson junction can produce extremely fast

oscillations, but with a very low power output. A goal is to use an array or lattice of junctions to increase the power output to levels useful for practical applications, but obtaining synchronized oscillations in such an array is difficult in practice. A potential problem is that the in-phase state may be dynamically unstable, causing the system to evolve to some other asynchronous state [18]. The failure to obtain a system of synchronized junctions was often thought to be because of the small variations between oscillator parameters which are inevitable in any real system. However, in contrast to this conclusion, researchers have demonstrated in recent years that in many cases, synchronization can in fact be induced by *increasing* the disorder in a system [2, 37, 41, 42].

Braiman, Ditto, Wiesenfeld and Spano studied an array of current-biased Josephson junctions connected in parallel [11]. The phase difference across the j-th junction, ϕ_j, is governed by the dynamical equations

$$\ddot{\phi}_j + \gamma\dot{\phi}_j + I_j \sin\phi_j = I + \kappa(\phi_{j+1} - 2\phi_j + \phi_{j-1}),$$

numbered $j = 1, 2, \ldots, N$. Free-end boundary conditions, $\phi_0 = \phi_1$ and $\phi_{N+1} = \phi_N$, are used. An array of $N = 21$ junctions was simulated. The disorder in the system was introduced as a spread in critical currents

$$I_j = 1 + \epsilon\xi_j,$$

with each ξ_j being a random number uniformly distributed between -0.5 and 0.5, modified by the disorder parameter ϵ. It was shown that for a wide range of parameter values, an increase in ϵ would often enhance the synchronization of the array. On the other hand, the opposite, more expected behaviour was also observed for different critical currents.

In another study, a series array of nonidentical Josephson junctions subject to a load was analysed by Wiesenfeld, Colet and Strogatz [45]. The N governing equations for the wave-function phase difference across the j-th

junction, ϕ_j, were given as

$$\frac{\hbar}{2er_j}\dot{\phi}_j + I_j \sin\phi_j + \dot{Q} = I_B,$$

$$L\ddot{Q} + R\dot{Q} + \frac{1}{C}Q = \frac{\hbar}{2e}\sum_{k=1}^{N}\dot{\phi}_k.$$

In this case, the circuit analysis gave rise to a globally coupled system. The authors found two transitions in the dynamics as the spread in the critical currents of the junctions was varied. As the level of disorder was reduced, frequency locking appeared in the dynamics at the first transition. At the second transition, complete synchronization was observed.

1.3.2 Synchronization and chaos in pendulum arrays

Let us consider a single periodically driven damped pendulum

$$m\ell^2\ddot{\theta} + \gamma\dot{\theta} = -mg\ell\sin\theta + \tau' + \tau\sin\omega t.$$

Depending on the parameters chosen (pendulum mass and length, driving strength and frequency), three qualitatively different motions are possible: libration, whirling or chaos. Whirling occurs when the length of the pendulum is short. It completes a full rotation for each period of the driving force. Longer pendulums librate backwards and forwards, while for intermediate lengths, the pendulum alternates between the two motions in a chaotic fashion.

Braiman, Lindner and Ditto [12] simulated a chain of $N = 128$ forced, damped, coupled pendulums governed by the equation

$$m\ell_n^2\ddot{\theta}_n + \gamma\dot{\theta}_n = -mg\ell_n\sin\theta_n + \tau' + \tau\sin\omega t + \kappa(\theta_{n+1} - 2\theta_n + \theta_{n-1}). \quad (1.4)$$

Free-end boundary conditions were assumed:

$$\theta_0 = \theta_1 \qquad \text{and} \qquad \theta_{N+1} = \theta_N. \quad (1.5)$$

The model parameters were chosen such that each pendulum would exhibit a chaotic motion if isolated from the chain. The authors showed that when the chain was homogeneous (all lengths equal), the spatiotemporal evolution was chaotic. However, when some disorder was introduced into the system, a periodic pattern emerged. The disorder chosen was a uniformly distributed variation in the lengths of the pendulums, with the distribution of the variations symmetric about zero.

The researchers suggested that the stabilization of the chaotic array was a result of the removal of certain pendulums from their chaotic band. Clusters of periodic oscillators formed, and they induced the remaining chaotic clusters to lock on to a common frequency, creating periodic solutions to the equations of motion.

Similar results were obtained in a practical experiment with an array of ten real pendulums [41]. The pendulums were driven, damped and coupled torsionally with springs. The centre of mass of each pendulum was adjustable, effectively allowing the length of each pendulum to be set independently as required. Digitized videotape was used to record the motion. When all pendulums were set equally (i.e. the chain was homogeneous), the spatiotemporal evolution was chaotic. After disordering the chain, however, periodic patterns emerged. Under such configurations, all pendulums oscillated with the same frequency — the driving frequency — but with different amplitudes.

Lindner, Prusha and Clay simulated a similar array of 32 pendulums [22]. They chose parameter values such that the evolution of the homogeneous chain would be chaotic if the pendulum lengths were set to $\ell_n = 1$ for all n. They varied the amount by which the pendulum lengths were disordered using three different methods to disorder the array. For the first method, alternate pendulums were given different lengths so that $\ell_n = 1 - \delta$ for odd n and $\ell_n = 1 + \delta$ for even n. For the second method, the pendulum lengths increased linearly from $\ell_1 = 1 - \delta$ to $\ell_{32} = 1 + \delta$. In the final method, the lengths were randomly selected from a uniform distribution $[1 - \delta, 1 + \delta]$. In each case, they calculated the largest Lyapunov exponent which they used as a measure for the degree of chaos in the system. When

the Lyapunov exponent was larger, the evolution was more chaotic, while the smallest observed Lyapunov exponent was found when the system was most regular. The authors concluded that there was an optimal level of disorder for taming chaos and that this level depended on the type of disorder introduced.

The model (1.4)–(1.5) with $N = 128$ was also studied by Gravielides, Kottos, Kovanis and Tsironis [17]. They showed that often a single impurity placed appropriately was sufficient to tame chaos. For larger coupling constants, self-organization of the array was observed for a wider domain of impurity pendulum lengths. The authors noted that for longer chains, synchronization could still be achieved by placing more than one impurity of appropriate strength at selected sites.

A different strategy for taming chaos was studied by Qi, Hou and Xin [33]. They modified the model (1.4) by allowing a small number of random shortcuts, i.e. additional coupling between pairs of non-adjacent oscillators. They found that there was an optimum number of shortcuts, expressed as a fraction of total possible connections, which resulted in the highest degree of synchronized periodic spatiotemporal motion in the system. The explanation given was that a few shortcuts would create local structures. These could have an effective average pendulum length different from unity, bringing them out of the chaotic regime. They could then entrain the rest of the array in periodic motion.

1.3.3 Various examples

Synchronization phenomena and the effect of disorder have been observed in a wide variety of nonlinear systems. Some examples are listed in this section.

For a chain of N diffusively coupled Rössler oscillators, numbered $j = 1, 2, \ldots, N$, with (nonidentical) natural frequencies ω_j,

$$\begin{aligned} \dot{x}_j &= -\omega_j y_j - z_j, \\ \dot{y}_j &= \omega_j x_j + a y_j + \epsilon(y_{j+1} - 2y_j + y_{j-1}), \\ \dot{z}_j &= 0.4 + (x_j - 8.5) z_j, \end{aligned}$$

phase synchronization effects were studied [27]. Two types of synchronization were observed for sufficiently strong coupling, namely, the formation of clusters of synchronized oscillators as well as global synchronization of all oscillators. For small coupling strengths, the transition to global synchronization was via a gradual adjustment of frequencies, while for large couplings a jump in the frequencies was observed.

Several of the effects observed in the lattice of coupled Rössler oscillators were also found to be evident in a system of diffusively coupled periodic Van der Pol oscillators [29]. Both global and cluster synchronization was shown to be possible. As a result of multistability, different types of transitions were found between states containing a different number of clusters

Spatial disorder in a regular monotonic trend of natural frequencies was found to increase oscillation intensity in an array of diffusively coupled limit-cycle oscillators [38]. The result was to eliminate oscillator death, even in the presence of strong dissipative coupling.

Phase synchronization has been studied in systems of coupled circle maps [25], limit cycle oscillators [23], chaotic rotators [26], chaotic oscillators which exhibit intermittency behaviour [20] and ensembles of bursting oscillators [19].

1.4 Objectives of this thesis

In our work, we study a soliton-bearing chain of oscillators which we simulate numerically. For some parameters, the homogeneous chain exhibits spatiotemporally chaotic behaviour. Spatiotemporal chaos can be suppressed in favour of periodic motion or a stationary state if the oscillators can be synchronized. We explore how introducing disorder can synchronize some or all of the oscillators in the chain.

We disorder the chain by adding impurities, that is by altering the lengths of one or more of the oscillators. We vary the number, strength and position of the impurities. Since we only change the lengths of a few of the oscillators (the lengths of most oscillators remain identical), we describe our chain as being *weakly* disordered.

One of our tasks is to analyse the spatiotemporally chaotic motion. We wish to determine what structures, if any, this motion consists of. Understanding this may help us to determine how and why chaos is suppressed after the introduction of impurities.

The outline of the thesis is as follows.

In Chapter 2, we reduce a chain of damped driven pendulums to the chain of nonlinear Schrödinger oscillators which we simulate. We show that the chain of NLS oscillators has the NLS equation as its continuum limit.

In Chapter 3, we consider a homogeneous chain. We discuss the stability of solitons and the attractors which occur for different damping and driving strengths. We analyse the spatiotemporal chaos which arises.

In Chapter 4, we demonstrate how a single impurity in the chain can cause a soliton to form and tame spatiotemporal chaos. We produce examples highlighting the properties of both short and long impurities.

In Chapter 5, we study chains with several impurities. Cases we consider include sets of impurities of equal strength placed equidistantly along the chain, as well as equal impurities which have been positioned which some randomness.

The results are summarized and conclusions are given in Chapter 6.

Chapter 2

Model

In this project, we perform simulations of the evolution of a nonhomogeneous chain of nonlinear Schrödinger oscillators. In this chapter, we show in Section 2.1 that the equations for our NLS chain can be derived from those for a chain of pendulums with an impurity. In Section 2.2, we show that when the distance between oscillators $\Delta x \to 0$, the chain of Schrödinger oscillators may be reduced to the continuous nonlinear Schrödinger equation. We conclude this chapter with some notes on our numerical model and simulations in Section 2.3.

We consider a driven Frenkel-Kontorova chain of N pendulums, meaning that each pendulum is driven by a periodic force and each pendulum in the chain interacts only with the two nearest neighbours through harmonic diffusive coupling [13]. Under this model, with the addition of damping due to friction, the interaction of the pendulums is described by the differential equations of motion

$$m\ell_n^2\ddot{\theta}_n + \alpha\ell_n\dot{\theta}_n - k\left(\theta_{n+1} - 2\theta_n + \theta_{n-1}\right) = -m\ell_n\left(g + 4\omega^2\rho\cos 2\omega t\right)\sin\theta_n, \tag{2.1}$$

where θ_n is the angle of the n-th pendulum. Each pendulum has mass m, and we choose to set this and the gravitational constant g equal to 1. The damping constant is α, the coupling strength is k and the driving amplitude is $4\omega^2\rho$, each of which we assume to be small. The length of each pendulum is $\ell_n = 1$ for all $n \neq 0$, while we allow the central pendulum to differ by a

small amount. The natural frequency of each pendulum (except the central pendulum) is $\sqrt{g/\ell_n} = 1$. We assume that the driving frequency 2ω is slightly less than double the natural frequency, and so $\omega \lesssim 1$.

2.1 Amplitude equations for coupled pendulums

We wish to derive amplitude equations for the chain of pendulums (2.1). Employing a similar multiple-scaling technique to that used by Alexeeva *et al.* [2, 3] and Chen *et al.* [15], we make the following assumptions, where ε is a small parameter:

$$\begin{aligned} &\omega = 1 - \frac{\varepsilon^2}{2}, \qquad && \omega^2 \approx 1 - \varepsilon^2, \qquad && 4\omega^2\rho = 2h\varepsilon^2, \\ &\alpha = \gamma\varepsilon^2, && k = \varepsilon^2\kappa^2, && \ell_n = 1 + 2Q\varepsilon^2\delta_{n,0}. \end{aligned} \tag{2.2}$$

We look for solutions θ_n, $n = 0, \pm 1, \ldots$, for small amplitude waves of the form

$$\theta_n = 2\varepsilon\left[\psi_n(T)e^{-i\omega t} + \overline{\psi}_n(T)e^{i\omega t}\right], \qquad T = \frac{\varepsilon^2}{2}t. \tag{2.3}$$

Differentiating, we get

$$\dot{\theta}_n = \varepsilon^3\frac{d\psi_n}{dT}e^{-i\omega t} - 2i\omega\varepsilon\psi_n e^{-i\omega t} + \text{c.c.}, \tag{2.4}$$

$$\ddot{\theta}_n = -2i\omega\varepsilon^3\frac{d\psi_n}{dT}e^{-i\omega t} - 2\omega^2\varepsilon\psi_n e^{-i\omega t} + \text{c.c.} \tag{2.5}$$

Also, we use the approximation $\sin\theta_n \approx \theta_n - \theta_n^3/6$, where

$$\theta_n^3 = 8\varepsilon^3\left(3\psi_n^2\overline{\psi}_n e^{-i\omega t} + 3\psi_n\overline{\psi}_n^2 e^{i\omega t} + \cdots\right) \tag{2.6}$$

and the identity

$$\cos 2\omega t = \frac{e^{2i\omega t} + e^{-2i\omega t}}{2}. \tag{2.7}$$

Substituting (2.2)–(2.7) into (2.1) and keeping terms up to those proportional to ε^3 and $e^{-i\omega t}$ gives, for $n \neq 0$,

$$-2i\varepsilon^3\frac{d\psi_n}{dT} - 2\varepsilon\left(1-\varepsilon^2\right)\psi_n + \gamma\varepsilon^2\left(-2i\varepsilon\psi_n\right) - 2\varepsilon^3\kappa^2\left(\psi_{n+1} - 2\psi_n + \psi_{n-1}\right) \\ = -2\varepsilon\psi_n + 4\varepsilon^3\left|\psi_n\right|^2\psi_n - 2h\varepsilon^3\overline{\psi}_n.$$

We compare like powers of ε. We note that terms of order ε cancel. For terms of order ε^3,

$$i\frac{d\psi_n}{dT} + \kappa^2\left(\psi_{n+1} - 2\psi_n + \psi_{n-1}\right) - \psi_n + 2\left|\psi_n\right|^2\psi_n = h\overline{\psi}_n - i\gamma\psi_n. \tag{2.8}$$

For $n = 0$ we get

$$\left(1+2Q\varepsilon^2\right)^2\left[-2i\varepsilon^3\frac{d\psi_0}{dT} - 2(1-\varepsilon^2)\varepsilon\psi_0\right] \\ + \gamma\varepsilon^2\left(-2i\varepsilon\psi_0\right) - 2\varepsilon^3\kappa^2\left(\psi_1 - 2\psi_0 + \psi_{-1}\right) \\ = -\left(1+2Q\varepsilon^2\right)\left(2\varepsilon\psi_0 - 4\varepsilon^3\left|\psi_0\right|^2\psi_0 + 2h\varepsilon^3\overline{\psi}_0\right).$$

Again terms proportional to ε cancel, and we need to equate terms proportional to ε^3:

$$i\frac{d\psi_0}{dT} + \kappa^2\left(\psi_1 - 2\psi_0 + \psi_{-1}\right) - \psi_0 + 2Q\psi_0 + 2\left|\psi_0\right|^2\psi_0 = h\overline{\psi}_0 - i\gamma\psi_0. \tag{2.9}$$

Equations (2.8) and (2.9) can be combined into the following equation, valid for all n [5]:

$$i\frac{d\psi_n}{dT} + \kappa^2\left(\psi_{n+1} - 2\psi_n + \psi_{n-1}\right) - \psi_n + 2Q\delta_{n,0}\psi_n + 2\left|\psi_n\right|^2\psi_n = h\overline{\psi}_n - i\gamma\psi_n. \tag{2.10}$$

The advantage that equation (2.10) has over the original chain of pendulums (2.1) is that the NLS oscillators evolve on a much faster time scale. (Recall that $T = \varepsilon^2 t/2$ and that ε is a small parameter.) This is preferable for computational reasons.

2.2 Continuum limit: the nonlinear Schrödinger equation

We will now show that the chain of Schrödinger oscillators can be reduced to the nonlinear Schrödinger equation. The motivation for this is that the parametrically driven NLS equation has a variety of stationary and periodic solutions with well-understood stability properties. The availability of these solutions is useful as they can serve as benchmarks in the analysis of the discrete system (2.10) in the large-coupling limit.

We introduce the spatial variable x so that $\psi_n = \psi(x_n)$. Then $x_{n+1} = x_n + \Delta x$ where $\Delta x \to 0$, and we set $(\Delta x)^2 = 1/\kappa^2$.

For $n \neq 0$, the Taylor expansion of $\psi(x_n)$ gives

$$\psi_{n\pm1} = \psi_n \pm \psi'(\Delta x) + \frac{1}{2!}\psi_n''(\Delta x)^2 \pm \frac{1}{3!}\psi_n'''(\Delta x)^3 + \cdots,$$

and so

$$\psi_{n+1} + \psi_{n-1} = 2\psi_n + \psi_n''(\Delta x)^2 + \cdots.$$

Neglecting $(\Delta x)^3$ and higher terms, we rearrange to get

$$\begin{aligned}\psi_n'' &\approx \left(\psi_{n+1} - 2\psi_n + \psi_{n-1}\right)/(\Delta x)^2 \\ &= \kappa^2\left(\psi_{n+1} - 2\psi_n + \psi_{n-1}\right).\end{aligned}$$

We can now rewrite equation (2.8) as

$$i\psi_t + \psi_{xx} - \psi + 2\left|\psi\right|^2\psi = h\overline{\psi} - i\gamma\psi. \tag{2.11}$$

For $n = 0$ the Taylor expansions for $\psi_{\pm1}$ around ψ_0 are

$$\psi_1 = \psi_0 + \Delta x\psi'\Big|_{x\to+0} + \frac{(\Delta x)^2}{2!}\psi_0'' + \cdots \tag{2.12}$$

and

$$\psi_{-1} = \psi_0 - \Delta x\psi'\Big|_{x\to-0} + \frac{(\Delta x)^2}{2!}\psi_0'' + \cdots. \tag{2.13}$$

Here, we are assuming that the second derivative is continuous while the first derivative is not necessarily so. This will be justified by the following results. Adding equations (2.12) and (2.13) gives

$$\psi_1 - 2\psi_0 + \psi_{-1} = \Delta x \left(\psi' \Big|_{x \to +0} - \psi' \Big|_{x \to -0} \right) + (\Delta x)^2 \psi_0'' + \cdots . \tag{2.14}$$

We choose to use the scaling $Q = \kappa q$, remembering that $\kappa = 1/\Delta x$ is a large parameter. When we use this and equation (2.14) in equation (2.9), equating terms proportional to κ^1 gives us the boundary condition

$$\psi' \Big|_{x \to +0} - \psi' \Big|_{x \to -0} + 2q\psi_0 = 0. \tag{2.15}$$

Terms of order κ^0 give us the equation

$$i\frac{d\psi_0}{dT} + \psi_0'' - \psi_0 + 2|\psi_0|^2\psi_0 = h\overline{\psi}_0 - i\gamma\psi_0.$$

Combining the boundary condition (2.15) with equation (2.11) gives the continuous NLS equation

$$i\psi_t + \psi_{xx} - \psi + 2q\delta(x)\psi + 2|\psi|^2\psi = h\overline{\psi} - i\gamma\psi. \tag{2.16}$$

We will be interested in continuous solutions to this equation. Such solutions obviously have a continuous second derivative, justifying our assumption above.

We can verify that equation (2.16) is indeed the continuous analogue of equation (2.10) by integrating equation (2.16) in the neighbourhood of $x = 0$, that is from $-\mu$ to μ where $\mu \to +0$. The integral of each term vanishes as the interval becomes infinitely small, with the exception of the terms ψ_{xx} and $2q\delta(x)\psi$. Calculating the integrals of these terms gives

$$\int_{-\mu}^{+\mu} \psi_{xx} dx + 2q \int_{-\mu}^{+\mu} \delta(x)\psi dx = \psi_x \Big|_{-\mu}^{+\mu} + 2q\psi(0).$$

The integrals above must sum to zero for consistency, and equation (2.15)

shows that this is indeed the case.

2.3 Numerical simulations

Having shown that the chain of pendulums can be reduced to the nonlinear Schrödinger chain (2.10), we simulate this chain on a ring from $-L/2$ to $L/2$ on the x domain. In all simulations, the length of our array is $L = 150$, with the origin ($x = 0$) at the centre of the chain. In most cases, a chain consisting of 500 oscillators is used, except in a few examples where we prefer the higher resolution provided by 1000 oscillators.

The results of simulations on the ring should be a close approximation to results for an array with free-end boundary conditions. This is because the length of the chain is much larger than the spacing between the oscillators ($\Delta x = 0.3$ for $N = 500$) and the damping constants used in our simulations are not very close to zero.

The system is solved numerically using the fifth-order Cash-Karp Runge-Kutta method with adaptive step-size control [32].

In the next chapter, we illustrate the dynamical behaviour which occurs in a homogeneous chain of NLS oscillators.

Chapter 3

Homogeneous chain

The first objective of our work is to review some features of a homogeneous chain of NLS oscillators,

$$i\frac{d\psi_n}{dT} + \kappa^2\left(\psi_{n+1} - 2\psi_n + \psi_{n-1}\right) - \psi_n + 2\left|\psi_n\right|^2\psi_n = h\overline{\psi}_n - i\gamma\psi_n, \qquad (3.1)$$

which is equation (2.10) with $Q = 0$. (We remind that $\kappa = 1/\Delta x$.) This chain is a discretization of the parametrically driven, damped NLS equation,

$$i\psi_t + \psi_{xx} - \psi + 2|\psi|^2\psi = h\overline{\psi} - i\gamma\psi, \qquad (3.2)$$

which is equation (2.16) with $q = 0$. This equation describes the dynamics of a variety of physical and biological systems (see [1, 7, 8, 40]). In particular, the equation was derived by Barashenkov *et al.* to describe small-amplitude breathers in the easy-plane ferromagnet [6].

We review the stability of soliton solutions of equation (3.2) in Section 3.1 and the types of attractors which arise in Section 3.2. We demonstrate and describe the period-doubling transition to chaos in Section 3.3. Aspects of spatiotemporally chaotic evolution are described in Section 3.4. We summarize our results from Chapter 3 and give conclusions in Section 3.5.

3.1 Stability of solitons

Equation (3.2) has two soliton solutions, even when the damping is nonzero, expressed explicitly as

$$\psi_{\pm}(x,t) = A_{\pm} e^{-i\theta_{\pm}} \operatorname{sech} A_{\pm} x \tag{3.3}$$

with

$$A_{\pm} = \sqrt{1 + h\cos 2\theta_{\pm}}, \qquad \theta_{+} = \frac{1}{2}\arcsin\frac{\gamma}{h}, \qquad \theta_{-} = \frac{\pi}{2} - \frac{1}{2}\arcsin\frac{\gamma}{h}.$$

Barashenkov *et al.* [6] show that the ψ_{-} soliton is always unstable for all values of the driving amplitude h and the damping constant γ. Thus it is disregarded in what follows, and henceforth the term "soliton" will always refer to ψ_{+}. The stability domain of the soliton ψ_{+} was analysed; the results of that analysis are summarized in Fig. 3.1. The chart consists of four regions in which qualitatively different stability behaviour is found, and two of these regions overlap.

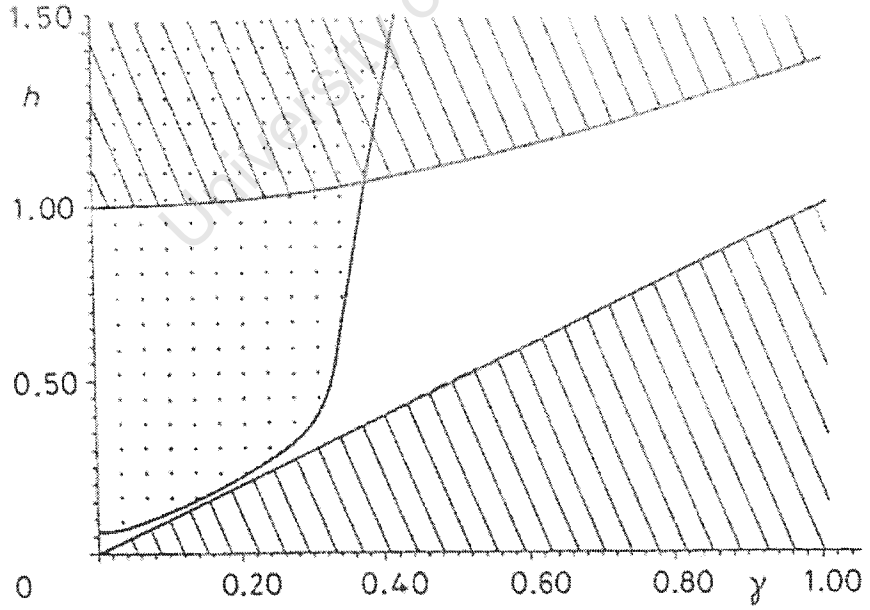

Figure 3.1: Stability diagram for the ψ_{+} soliton on the (γ, h)-plane. (Reproduced from [6].)

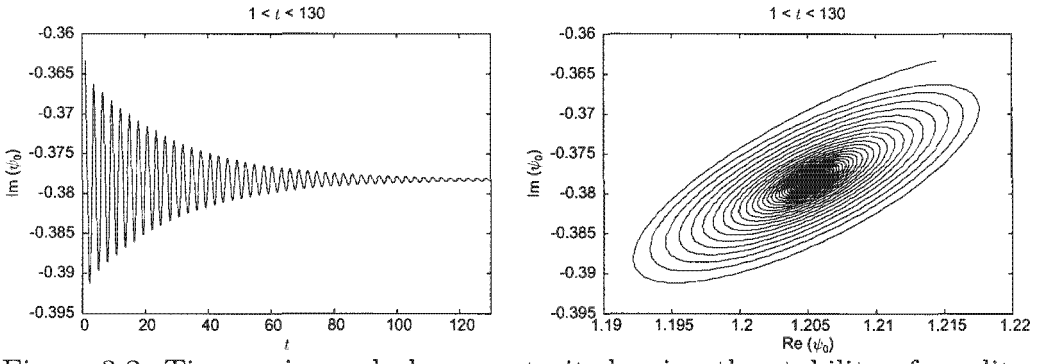

Figure 3.2: Time series and phase portrait showing the stability of a soliton in the empty region of (Fig. 3.1). Here $\gamma = 0.4$, $h = 0.7$ and $\Delta x = 0.3$.

1. Below the straight line $h = \gamma$, no solitons exist. The only attractor in this region is the trivial one, $\psi \equiv 0$.

2. Above the curve $h = \sqrt{1+\gamma^2}$, the soliton exists, but it is unstable with respect to extended modes (radiation).

3. In the dotted region, the ψ_+ soliton is unstable with respect to a local mode.

4. The soliton is stable in the empty region.

We illustrate case 4 in Fig. 3.2 with a result from our own simulations. [Note that we are simulating not the continuous NLS equation, but a discrete chain of oscillators (3.1).] We show the time series and phase portrait for the central oscillator ψ_0. It is clearly seen that oscillations cease as the real and imaginary parts of ψ_0 converge to a fixed point. This result for the discrete system is in agreement with the stability diagram for the continuous NLS equation, at least for our choice of discreteness parameter ($\Delta x = 0.3$).

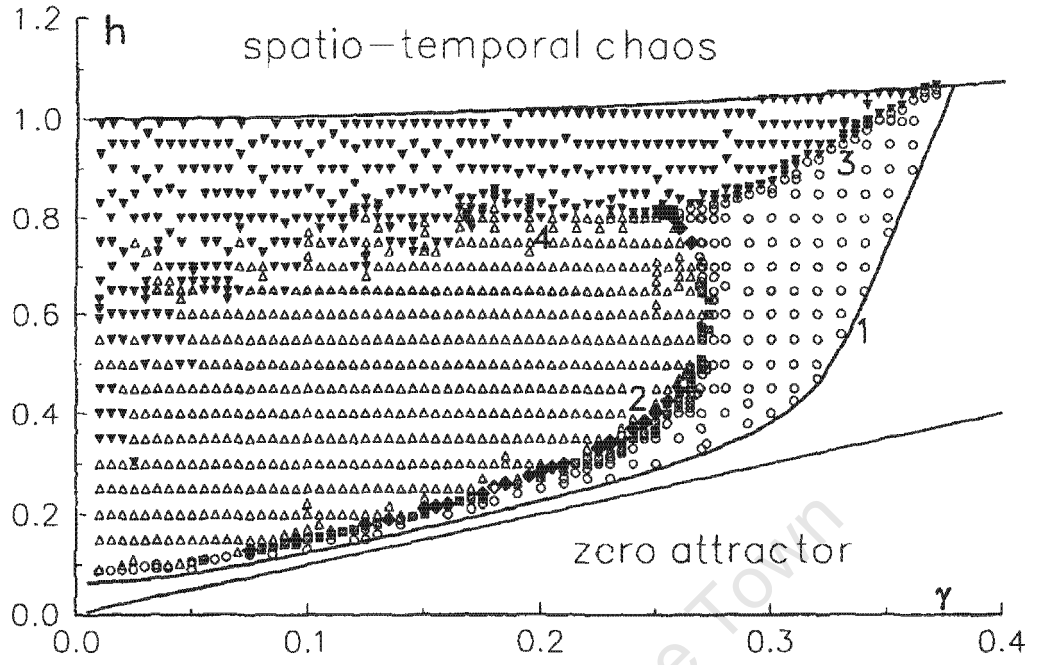

Figure 3.3: Attractor chart of the continuous NLS equation (3.2) on the (γ, h)-plane. (Reproduced from [10].)

3.2 Topography of attractors

Equation (3.2) was analysed numerically [10] with the ψ_+ soliton (3.3) being used as the initial condition for the simulations. The authors of [10] systematically determined which types of attractors arise from this initial condition for the range of the parameters h and γ spanning the dotted region of Fig. 3.1 below the curve $h = \sqrt{1+\gamma^2}$. The chart of Ref. [10] is reproduced in Fig. 3.3.

Within the parameter space which was explored, four distinct classes of attractor were identified. We illustrate each of these in Fig. 3.4–Fig. 3.7 with results from our own simulations of the chain of oscillators (3.1).

1. Open circles and shadowed boxes denote periodic solitons; that is, the solitons are not stationary as in the empty region to the right of the curve, but their amplitudes and phases oscillate periodically. Open circles denote period-1 solitons, examples of which are shown in Fig.

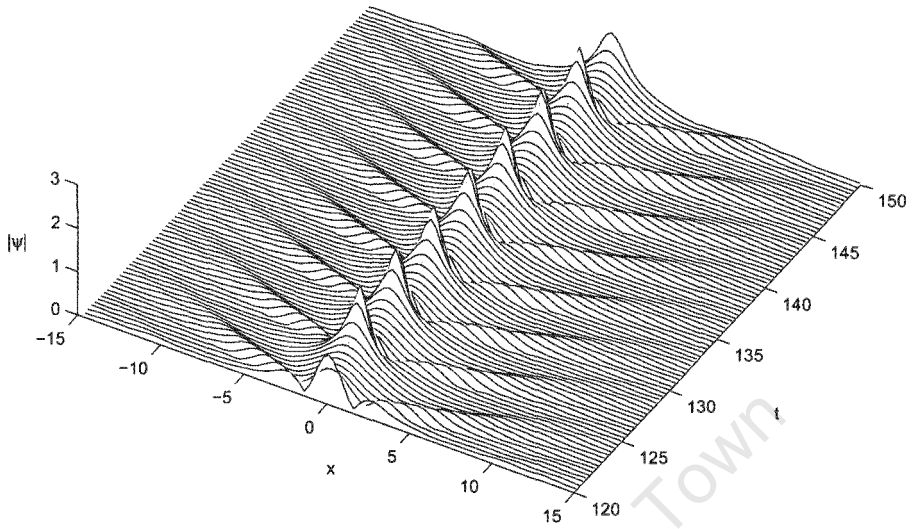

Figure 3.4: Evolution of a period-1 soliton. Here $\gamma = 0.315$, $h = 0.8$ and $\Delta x = 0.3$.

3.4, Fig. 3.5 and Fig. 3.6a. Shadowed boxes denote period-2, period-4, and period-8 solitons, such as those illustrated in Fig. 3.6b–d.

2. Along the narrow band marked 2 between the regions of periodic solitons and the trivial attractors, shadowed diamonds are used to denote strange attractors. These solutions are spatially localized but temporally chaotic, as illustrated in Fig. 3.6f.

3. The trivial solution $\psi \equiv 0$ is the only attractor found in the area marked with open triangles (Fig. 3.7).

4. At the points covered by black triangles, the evolution from the soliton initial condition degenerates into spatiotemporal chaos (Fig. 3.8). By spatiotemporal chaos, we mean that no periodic patten for ψ is observed in either space or time. The evolution is unpredictable and irregular, over the whole x-axis.

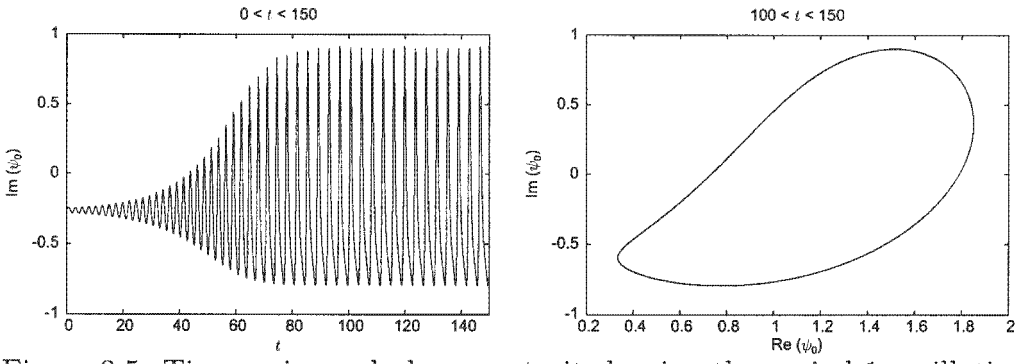

Figure 3.5: Time series and phase portrait showing the period-1 oscillations of the soliton in Fig. 3.4. Here $\gamma = 0.315$, $h = 0.8$ and $\Delta x = 0.3$.

3.3 Period-doubling transition to chaos

A phenomenon which is interesting to demonstrate is the period-doubling transition to chaos. For fixed damping γ, the period of the soliton doubles and redoubles as the driving strength h is increased. A strange attractor then emerges briefly before disappearing in favour of the zero attractor as h is increased further. We were able to reproduce this effect with our simulations of a discrete chain as shown in Fig. 3.6. With the interval $\Delta x = 0.3$, we used the damping value $\gamma = 0.265$ with the driving strength increasing from $h = 0.38$ (period-1) to $h = 0.42$ (strange attractor). For much stronger driving strengths (for example $h = 0.9$), evolution becomes spatiotemporally chaotic.

It is interesting to measure the average frequency Ω_j of each oscillator in the array for the different types of evolution described above using equation (1.3). Here we use the signal $\phi_j = \text{Re}\,\psi_j$, the real part of each oscillator. We simply count the maxima of $\text{Re}\,\psi_j$ in a chosen time period, and there could be more than one maximum per phase cycle. Some results are shown in Fig. 3.9 to Fig. 3.21. In each case, we denote the frequency of the central oscillator as $\Omega_{N/2} = \omega$, so that we can measure other frequencies in terms of ω.

Our average frequency measurements of the whole array of oscillators are particularly useful because they allow us to study the radiation component of

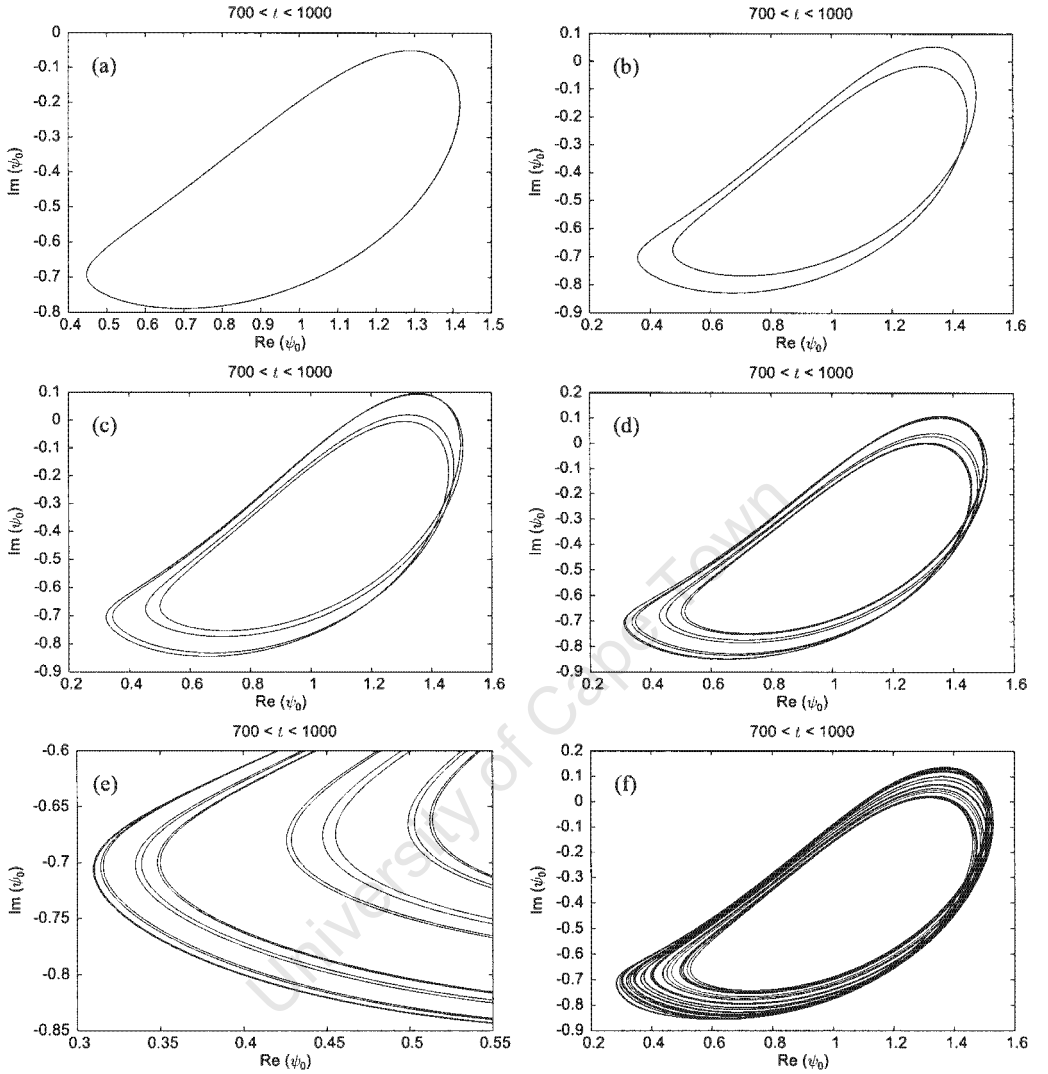

Figure 3.6: Our simulations of the discrete system (3.1) demonstrate the period-doubling transition to chaos which was previously observed for the continuous NLS equation. Using $\Delta x = 0.3$, we fix $\gamma = 0.265$. We increase h as follows: (a) $h = 0.38$ for the period-1 solution, (b) $h = 0.4$ for the period-2 solution, (c) $h = 0.41$ for the period-4 solution, (d) $h = 0.4132$ for the period-8 solution, (e) $h = 0.4134$ for the period-16 solution, (f) $h = 0.42$ for the strange attractor. Note that only a portion of the phase diagram for the period-16 solution is displayed. This is necessary in order for the trajectories to be distinguishable.

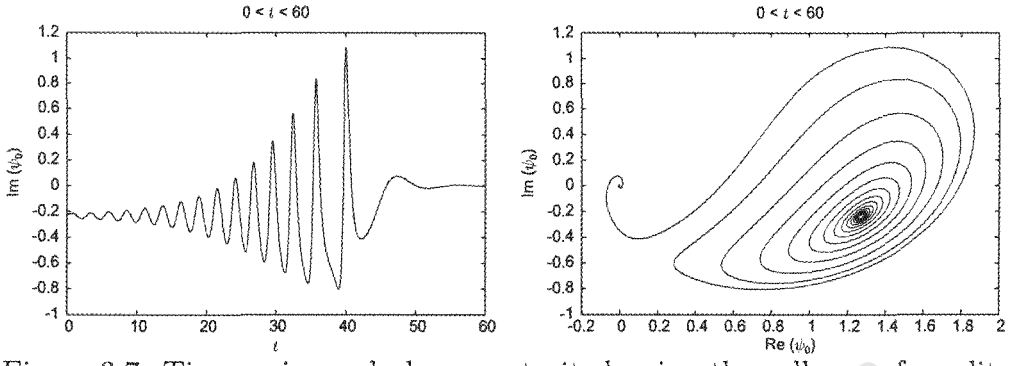

Figure 3.7: Time series and phase portrait showing the collapse of a soliton to the zero attractor. Here $\gamma = 0.25$, $h = 0.7$ and $\Delta x = 0.3$.

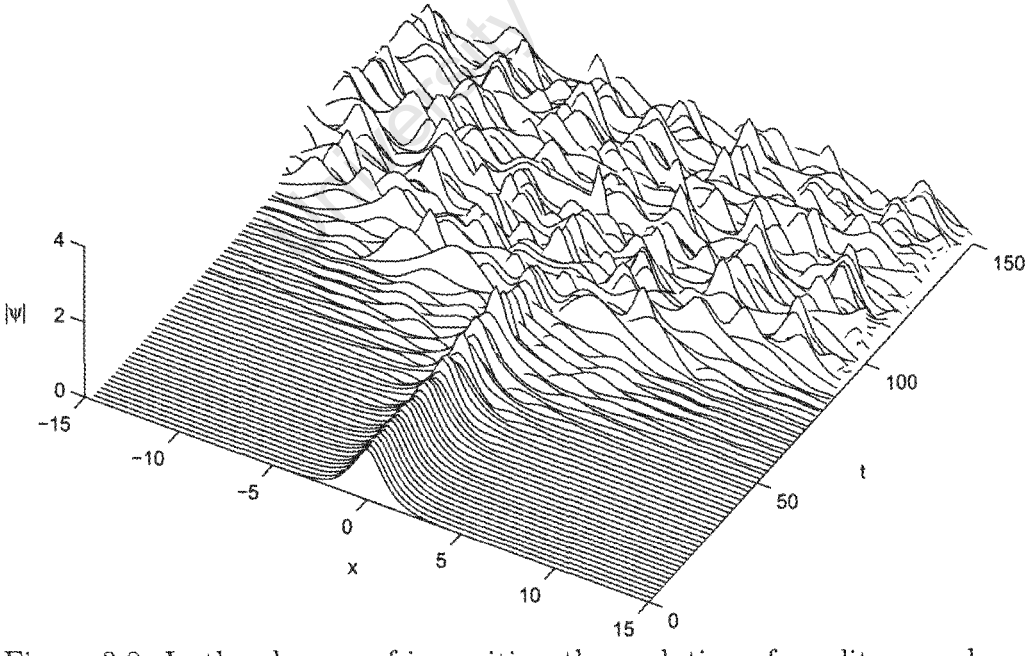

Figure 3.8: In the absence of impurities, the evolution of a soliton produces spatiotemporal chaos. Here $\gamma = 0.315$, $h = 0.9$ and $\Delta x = 0.3$.

the system. The radiation waves are emitted by the oscillating soliton. (The radiation is generally difficult to study because the radiation waves typically have a very small amplitude, but our method overcomes these problems.)

Recall that the oscillating soliton observed for these parameters typically lies in the region $-5 < x < 5$. We have included the soliton in Fig. 3.10, Fig. 3.13, Fig. 3.16 and Fig. 3.19 so that its position and width can be directly compared with the pattern of the average frequency data in each case. The long tails of the soliton also oscillate, but with very small amplitudes (typically of order 10^{-3} to 10^{-5}, decreasing as $|x|$ increases). We observe that higher harmonics are present in the tails.

We plot phase portraits for selected oscillators in the array for $h = 0.38$ (period-1), $h = 0.40$ (period-2), $h = 0.41$ (period-4) and $h = 0.42$ (strange attractor) in Fig. 3.11, Fig. 3.14, Fig. 3.17 and Fig. 3.20 respectively. The phase portraits for the central oscillator ($x = 0$) clearly show the doubling of the period as the number of loops increases. From the phase portraits of the side oscillators, we can better understand the results of the frequency measurements, as we illustrate the formation of new loops in the phase portrait as x increases.

Let us explain the progression of the average frequency plots with the aid of the associated phase portraits. In Fig. 3.10 (the period-1 regime), we see that the soliton oscillates with an average frequency of $\Omega = \omega \approx 1$. We denote the period of these oscillations as T. Fig. 3.11 confirms that the phase portraits of oscillators with $\Omega \approx 1$ are single loops where $\mathrm{Re}\,\psi$ has only one maximum. We see that there are also oscillations of frequency $\Omega = 2\omega \approx 2$. This value of Ω occurs in two cases: either the phase portrait consists of a single loop with two maxima, or it consists of a double loop where each loop has only one maximum. This double frequency arises because second harmonic radiation waves are superimposed over the oscillations of the soliton.

Next, compare the frequency measurements in the period-1 and period-2 regimes. In the period-2 regime (Fig. 3.13), we see that the average frequency of the central oscillator is $\Omega = \omega \approx 1$, which is the same as the value observed in the case of the period-1 regime. Since the period-2 soliton has a

period of $2T$, the frequency corresponding to this period is $\omega/2$. There is no contradiction, however, because each period in the phase portrait consists of two loops, and hence contains two maxima, so that we measure $\Omega = \omega$.

The frequencies of some oscillators have the additional values of $\Omega \approx \frac{3}{2}$ and $\Omega \approx \frac{5}{2}$. The frequency $\Omega \approx \frac{3}{2}$ appears when the phase portrait consists of a double loop, and $\mathrm{Re}\,\psi$ has two maxima in one of the loops. We see this in Fig. 3.14 in graphs (c) and (e). Thus, we have identified radiation with the frequency $\frac{3}{2}\omega$ in the period-2 regime, which was unexpected.

When the period doubles again (becoming period-4), and the phase portrait for ψ_0 consists of four loops, average frequency measurements of $\Omega \approx \frac{5}{4}$ and $\Omega \approx \frac{7}{4}$ are also observed (Fig. 3.16). These frequencies occur when one out of four loops in the phase portrait has two maxima (Fig. 3.17c) or three out of four (Fig. 3.17e). These average frequencies are caused by radiation with a mixture of the frequencies 2ω, $\frac{3}{2}\omega$ and $\frac{5}{4}\omega$. The higher the periodicity, the more different possibilities there are for values of Ω. The limit of the period-doubling process is seen in the case of the strange attractor (Fig. 3.18), where the range of possible values of Ω is effectively continuous. This is a result of the soliton emitting a practically continuous band of radiation frequencies.

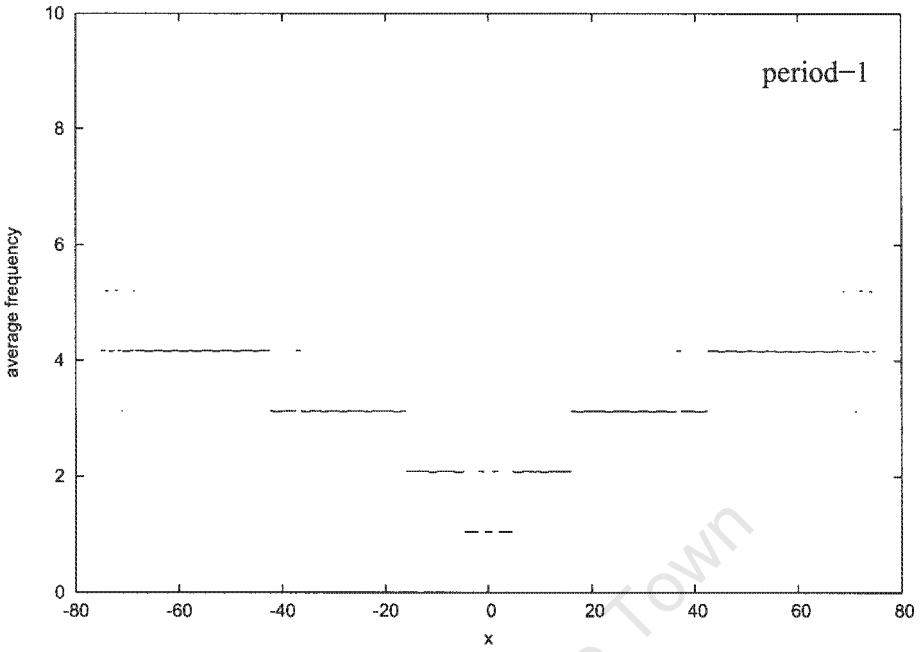

Figure 3.9: Average frequency of each oscillator, for the case of the period-1 soliton (Fig. 3.6a). Here $\gamma = 0.265$, $h = 0.38$ and $\Delta x = 0.3$.

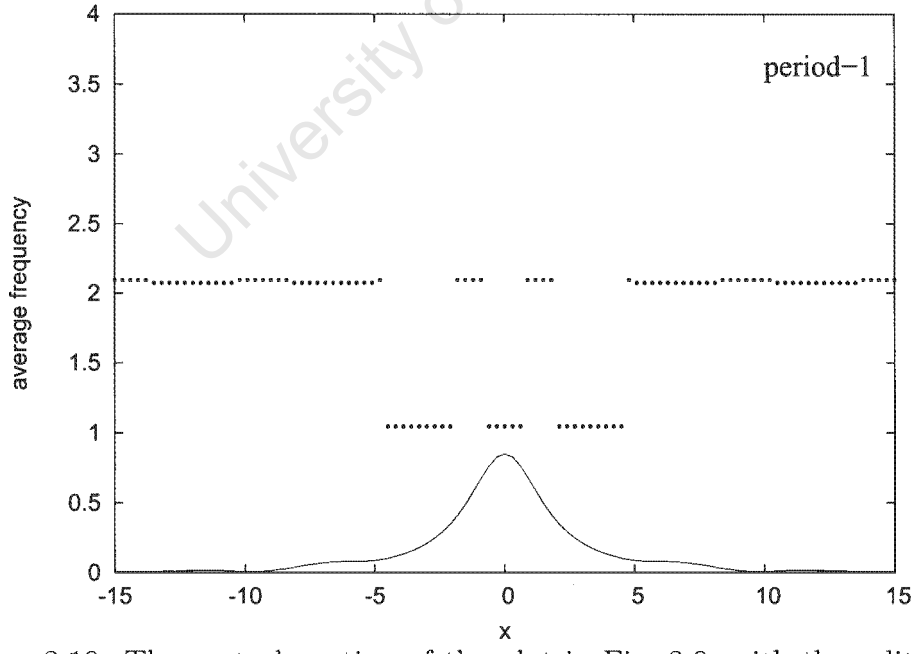

Figure 3.10: The central portion of the plot in Fig. 3.9, with the soliton at $t = 1000$ superimposed. Here $\gamma = 0.265$, $h = 0.38$ and $\Delta x = 0.3$.

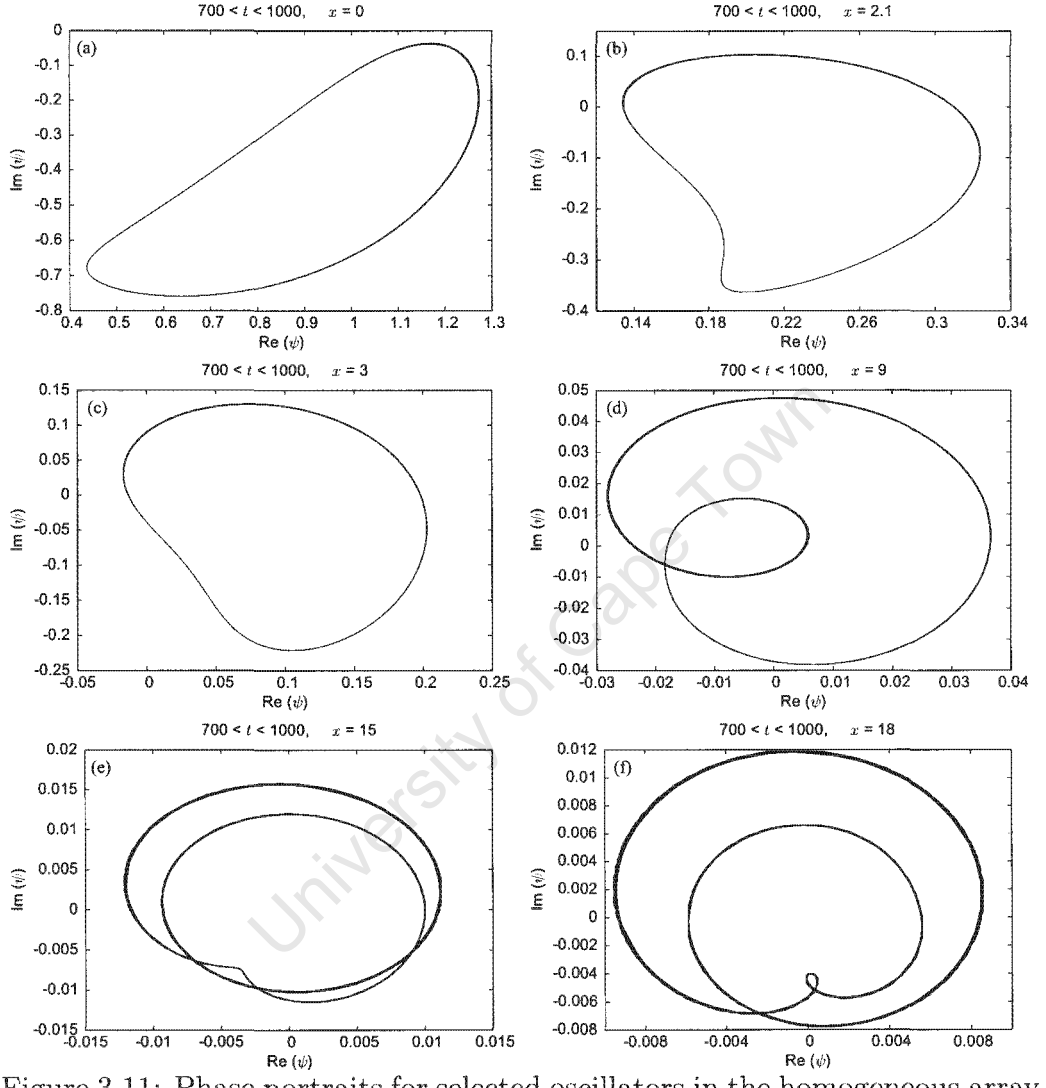

Figure 3.11: Phase portraits for selected oscillators in the homogeneous array for $\gamma = 0.265$, $h = 0.38$ and $\Delta x = 0.3$. The central oscillator, shown in graph (a), is period-1. In graphs (a) and (c), $\mathrm{Re}\,\psi$ has only one maximum ($\Omega = \omega$), while a second maximum appears in graph (b) ($\Omega = 2\omega$). We observe a double loop in graphs (d) and (e) ($\Omega = 2\omega$), and a triple loop in graph (f) ($\Omega = 3\omega$).

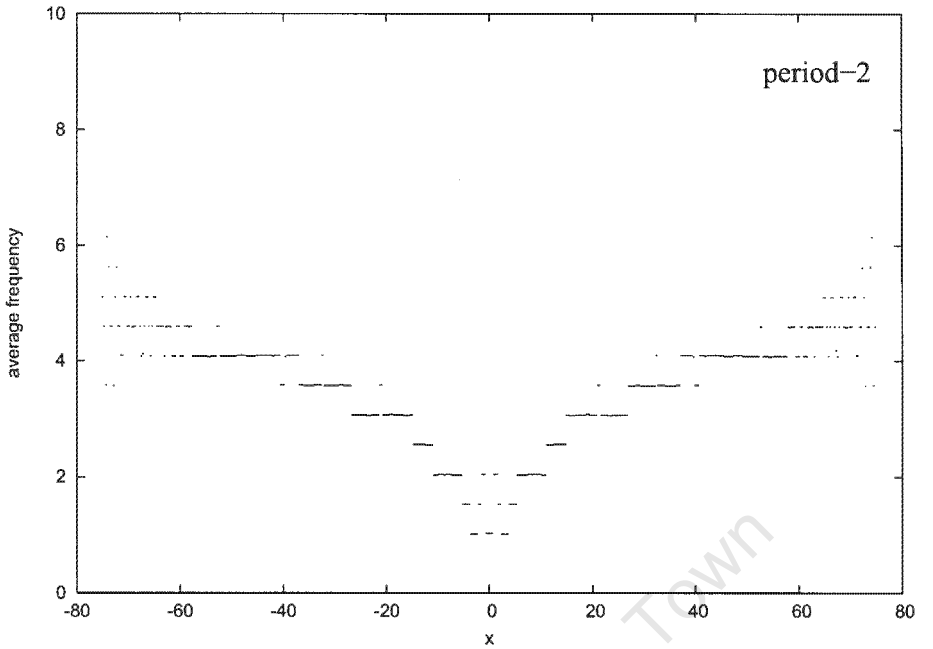

Figure 3.12: Average frequency of each oscillator, for the case of the period-2 soliton (Fig. 3.6b). Here $\gamma = 0.265$, $h = 0.4$ and $\Delta x = 0.3$.

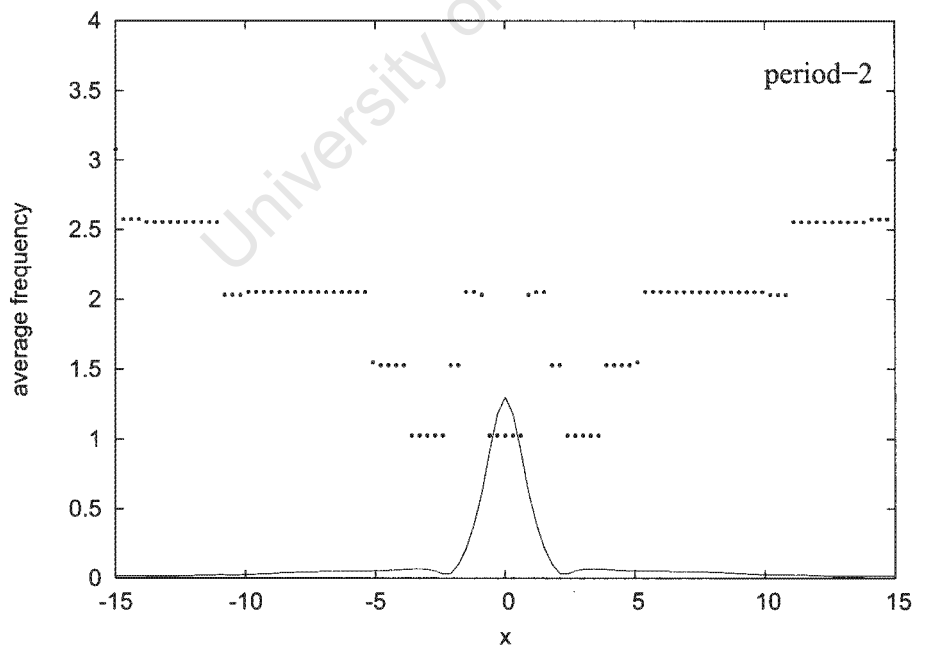

Figure 3.13: The central portion of the plot in Fig. 3.12, with the soliton at $t = 1000$ superimposed. Here $\gamma = 0.265$, $h = 0.4$ and $\Delta x = 0.3$.

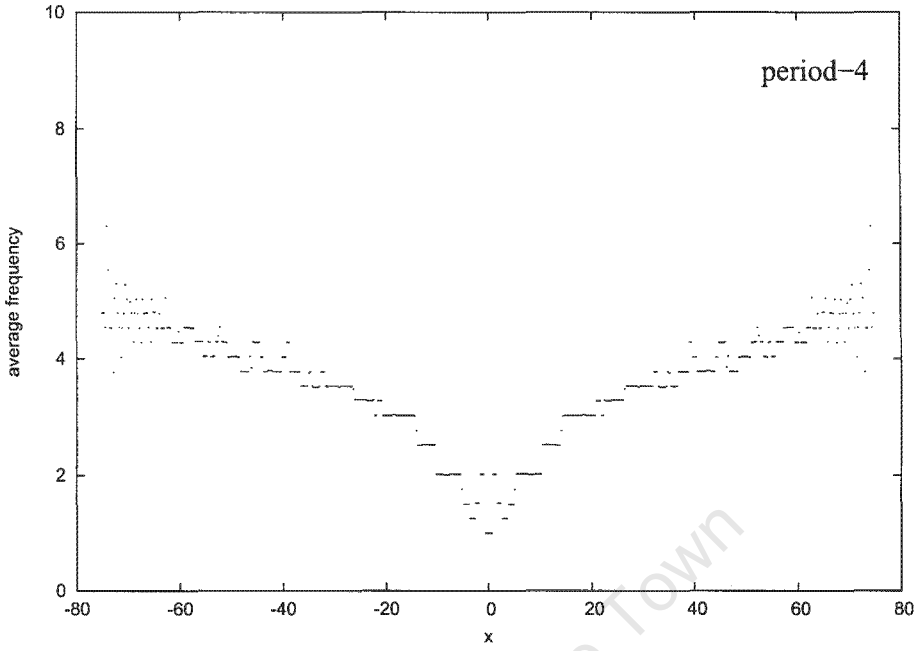

Figure 3.15: Average frequency of each oscillator, for the case of the period-4 soliton (Fig. 3.6c). Here $\gamma = 0.265$, $h = 0.41$ and $\Delta x = 0.3$.

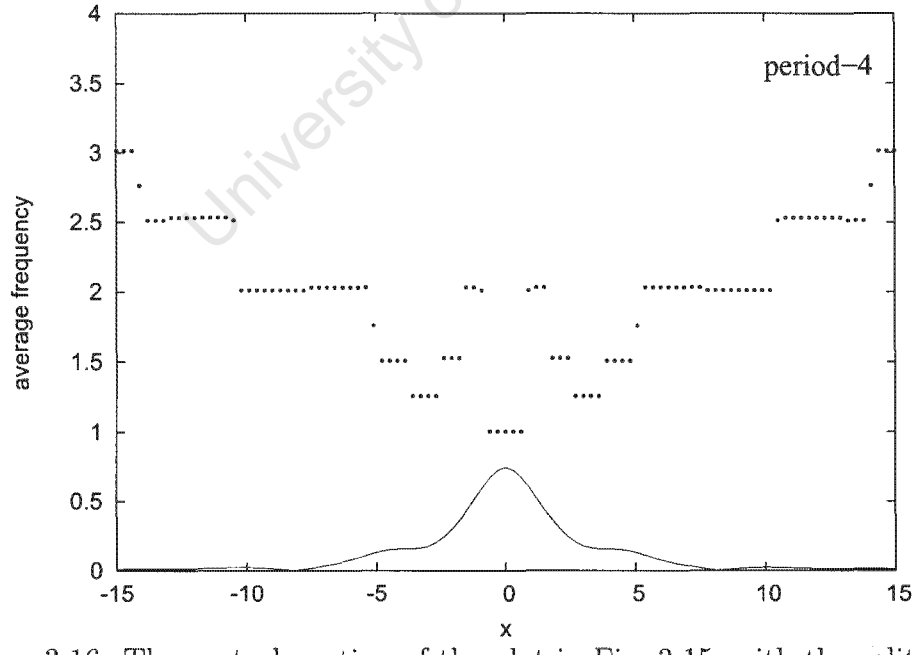

Figure 3.16: The central portion of the plot in Fig. 3.15, with the soliton at $t = 1000$ superimposed. Here $\gamma = 0.265$, $h = 0.41$ and $\Delta x = 0.3$.

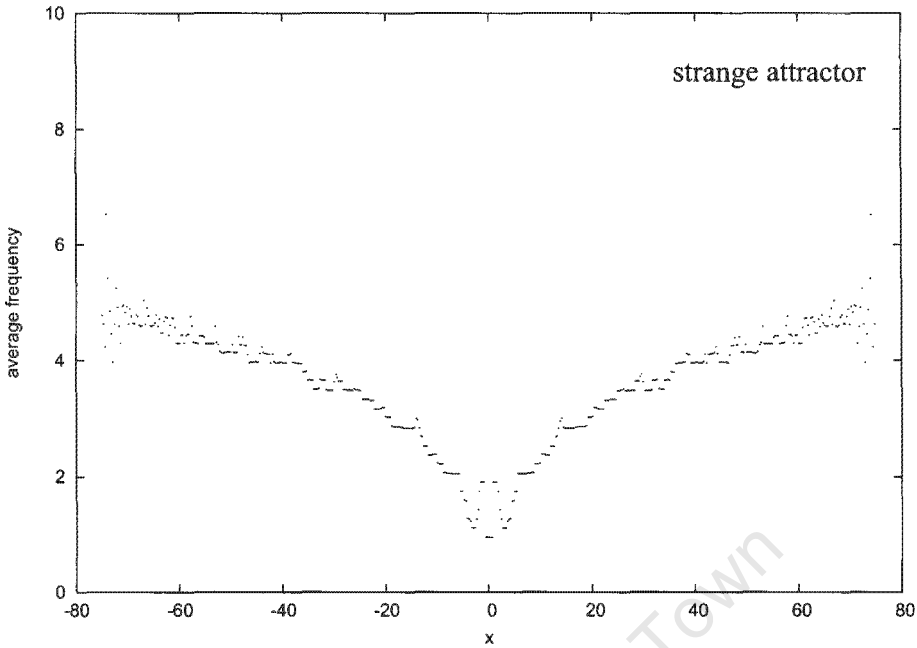

Figure 3.18: Average frequency of each oscillator, for the case of the strange attractor (Fig. 3.6f). Here $\gamma = 0.265$, $h = 0.42$ and $\Delta x = 0.3$.

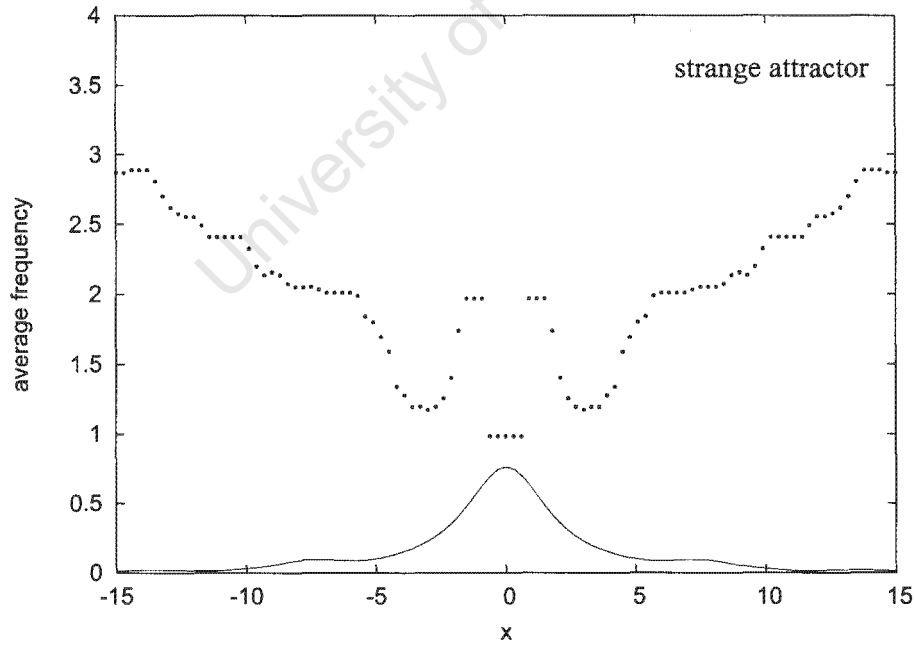

Figure 3.19: The central portion of the plot in Fig. 3.18, with the soliton at $t = 1000$ superimposed. Here $\gamma = 0.265$, $h = 0.42$ and $\Delta x = 0.3$.

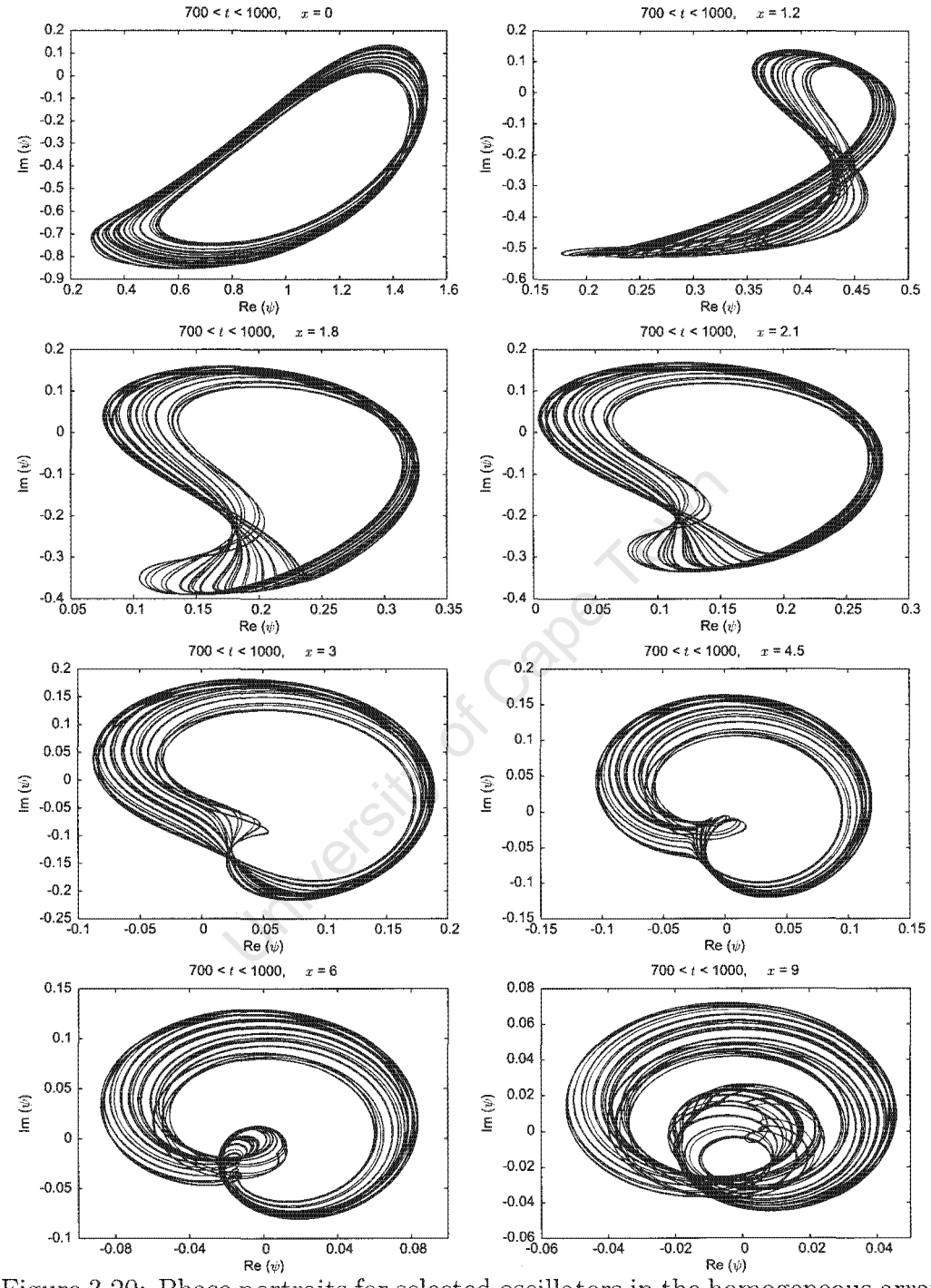

Figure 3.20: Phase portraits for selected oscillators in the homogeneous array for $\gamma = 0.265$, $h = 0.42$ and $\Delta x = 0.3$, where we see the appearance of the strange attractor.

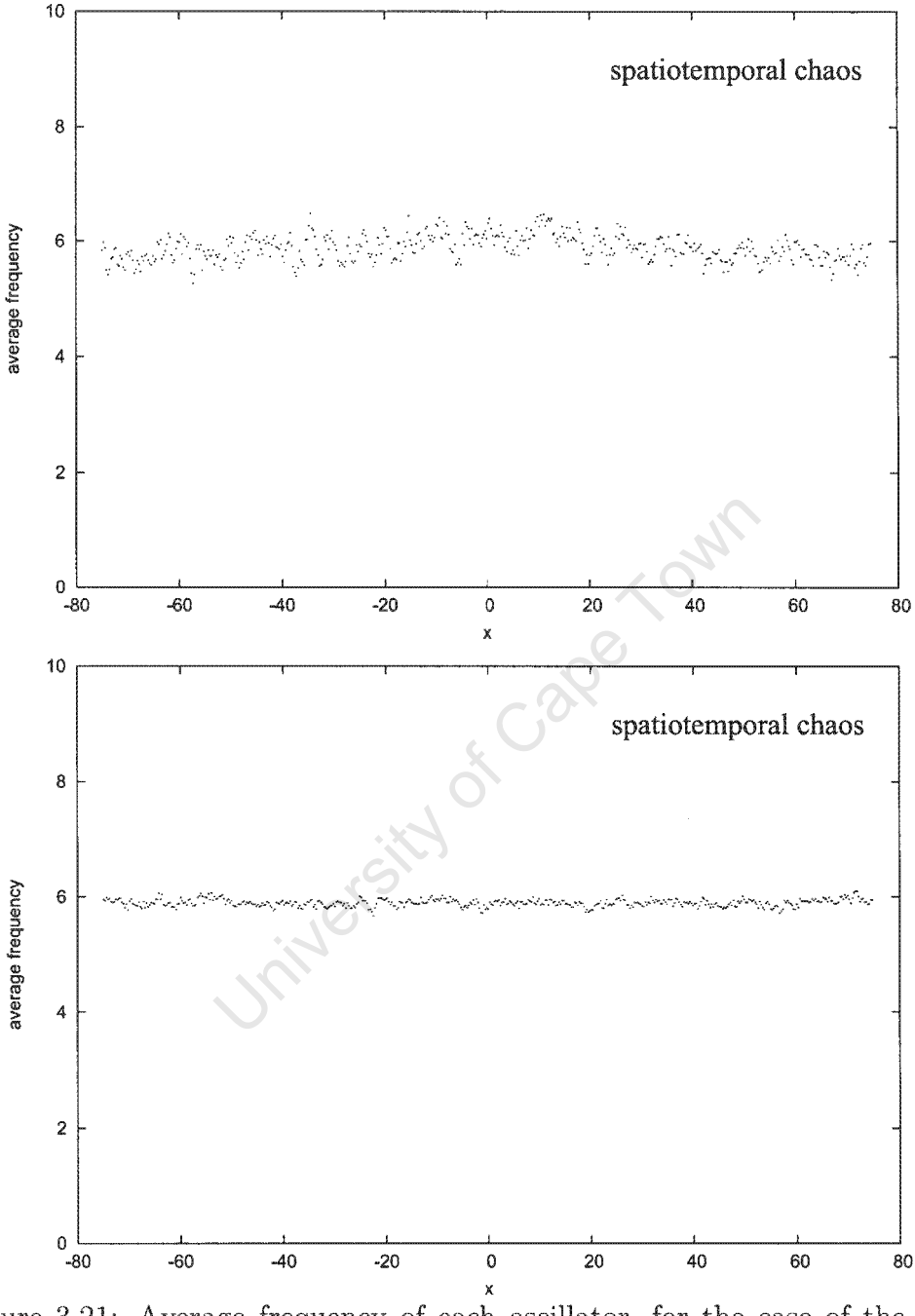

Figure 3.21: Average frequency of each oscillator, for the case of the spatiotemporally chaotic evolution. Here $\gamma = 0.265$, $h = 0.9$ and $\Delta x = 0.3$. In the top picture, the average is taken over a total period of $\tau = 500$, while in the bottom picture $\tau = 5000$. Note that the frequency measurements for all oscillators in the array are converging to a common value, $\Omega \approx 5.9$.

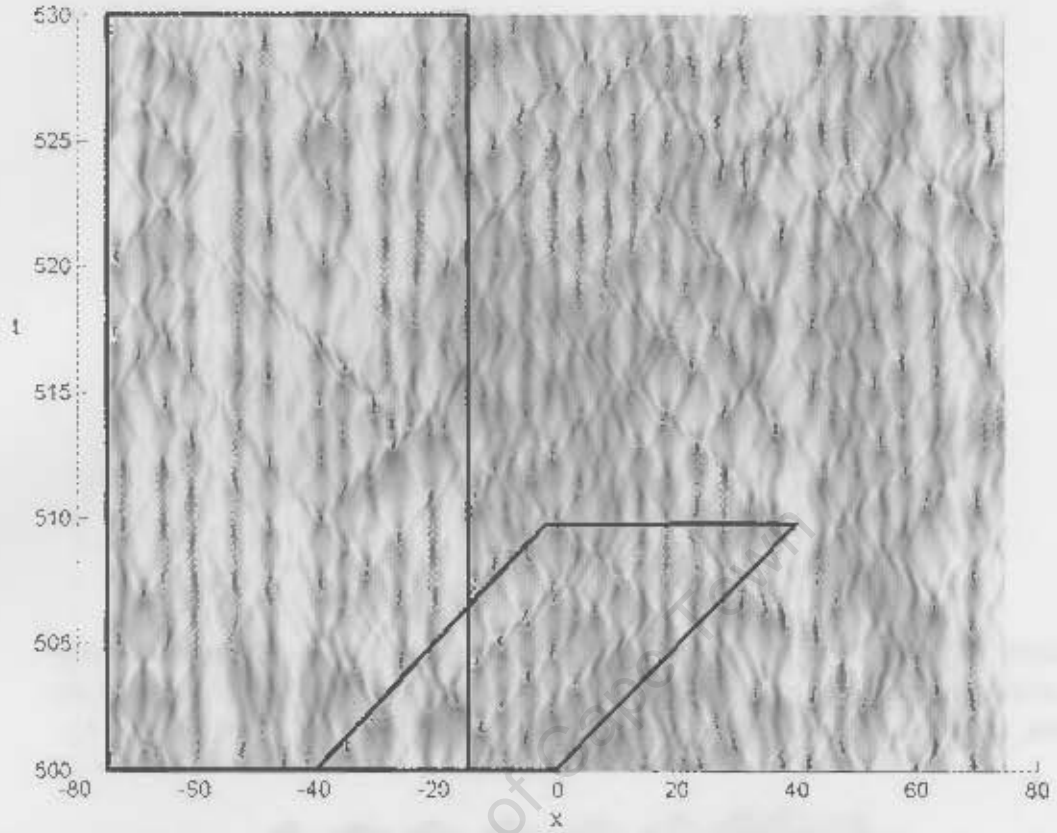

Figure 3.22: Evolution of the spatiotemporal chaos where $\gamma = 0.265$, $h = 0.9$ and $\Delta x = 0.3$. The shading is proportional to $|\psi|$, with $|\psi| = 0$ shown as white. The portion in the large rectangle is displayed in Fig. 3.23, and the portion in the small parallelogram is displayed in Fig. 3.24.

The corresponding group velocity is

$$v_{\rm gr} = \frac{d\omega}{dk} = \frac{2k(k^2+1)}{\omega}.$$

If we assume that the measured average frequency $\omega = 5.9$ is due to linear radiations of the wave number k, then, for $h = 0.9$,

$$k = \sqrt{\sqrt{\omega^2 + h^2} - 1} = 2.23$$

and

$$v_{\rm gr} = \frac{2k(k^2+1)}{\omega} = 4.51.$$

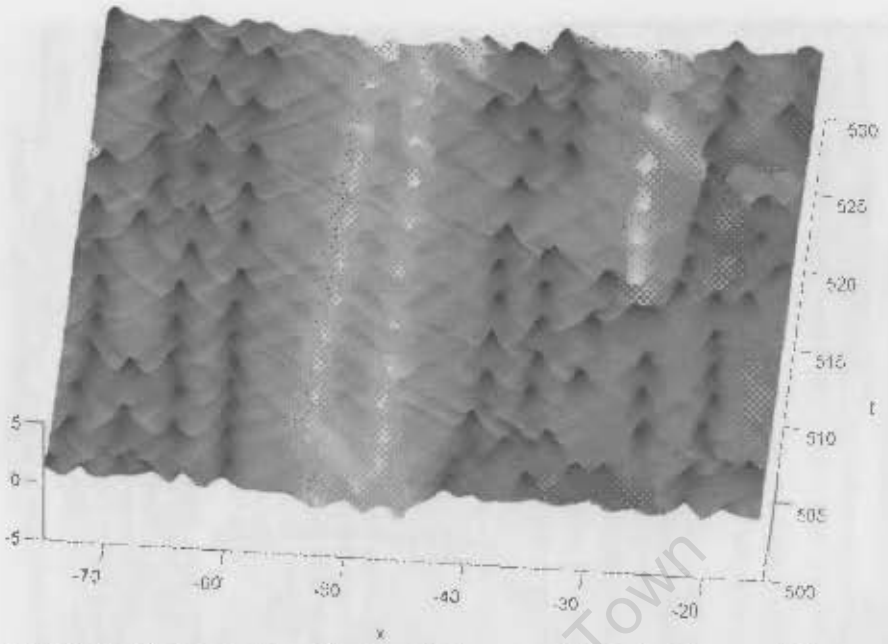

Figure 3.23: Solitons with a finite lifetime oscillate in the spatiotemporally chaotic regime. (Here $\gamma = 0.265$, $h = 0.9$ and $\Delta x = 0.3$.) Such solitons are seen, for example, near $x = -60$ and $x = -47.7$. Here, we show $\mathrm{Re}\,\psi(x, t)$.

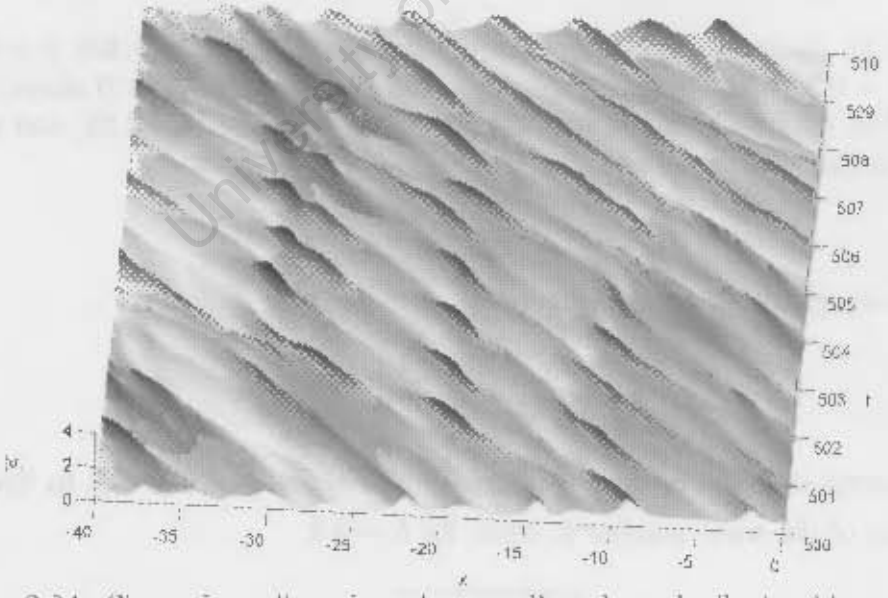

Figure 3.24: Since the solitons' peaks are aligned vertically in this moving reference frame, the oscillations of adjacent solitons are synchronized with a constant phase shift. Here, we show $\mathrm{Re}\,\psi(x + vt, t)$ with $\gamma = 0.265$, $h = 0.9$, $\Delta x = 0.3$ and $v = 4.6$.

This figure is in very close agreement with our estimate for the velocity of the ripples ($v = 4.6$). This strongly suggests that the measured frequency $\Omega \approx 5.9$ is indeed a result of the radiation waves.

3.5 Summary and conclusions

The continuous NLS equation (3.2) has two soliton solutions (3.3), one of which is always unstable (ψ_-). The stability of the other solution (ψ_+), which depends on the parameters h and γ, was described in detail. The types of attractors found in the system are stationary solitons, periodic solitons, chaotic solitons (strange attractors) and the trivial solution $\psi \equiv 0$. For some parameter values, an initial condition in the form of a soliton degenerates into spatiotemporal chaos. Each distinct type of solution was illustrated with a simulation of the discrete system (3.1). We consistently found agreement between the dynamics produced by the continuous and discrete system with $\Delta x = 0.3$.

We have demonstrated that the period-doubling transition to chaos, previously observed in the continuous NLS equation, also occurs in the discrete system. An analysis was made of the frequency of maxima of Re ψ of each oscillator in the chain for systems with increasing periodicity. The average frequency plots Fig. 3.9, Fig. 3.12, Fig. 3.15 and Fig. 3.18 were interpreted with the aid of phase portraits for selected oscillators in each system. We conclude from our phase portraits and average frequency measurements for the oscillator at $x = 0$ that the strange attractor is the limit of the period-doubling process.

The difference between the average frequency plot for the strange attractor (Fig. 3.18), where oscillations are spatially localized, and those for the spatiotemporally chaotic regime (Fig. 3.21) is interesting. The measured frequencies of all the oscillators in the spatiotemporally chaotic regime converge over a long time period τ to the same value (here $\Omega \approx 5.9$). In contrast, the range of possible values of Ω is practically continuous in the case of the strange attractor. Although oscillations are temporally chaotic here, the plot of measured frequencies is remarkably similar to the case of the period-4

regime.

We used Fig. 3.22 to estimate the frequency of two solitons in the spatiotemporally chaotic regime, obtaining values for ω of 2.51 and 2.74. We noticed that these values were close to half of the observed value of $\Omega \approx 5.9$.

The linear wave frequency equation (3.4) enables us to calculate the wave number ($k = 2.23$) and hence the group velocity ($v_{\mathrm{gr}} = 4.51$). This value is remarkably close to our measurements for the velocity of the diagonal ripples in Fig. 3.22 ($v = 4.6$).

The vertical stripes and diagonal ripples observed in the spatiotemporally chaotic regime are both interesting and surprising. In particular, we discovered that adjacent solitons typically oscillate with a constant phase shift, which persists for the duration of the lifetime of the solitons. This means that frequency locking is evident in the chaotic system. We presume that this form of synchronization is a result of radiation-coupling. The frequency locking is possible because the natural frequencies of the solitons are closely matched in the homogeneous system.

In the next chapter, we introduce an impurity into the chain which we simulate. We examine how varying the strength of the impurity influences the evolution of the chain.

Chapter 4

Single impurity

As described in Section 1.3.2, impurities can sometimes synchronize a chain of oscillators, thus eliminating spatiotemporal chaos [17]. Our goal is to identify and study the effect of such disorder on our discrete NLS equations.

In this chapter, we describe the evolution of the chain of oscillators (2.10) containing a single impurity — a slow-time oscillator corresponding to a pendulum with a different length to all the others in the chain. The anomalous oscillator is always placed at the centre of the chain (at position $x = 0$). We consider both "long" impurities ($q > 0$) and "short" impurities ($q < 0$). Altering the length of the pendulum changes the natural frequency of the corresponding slow-time oscillator.

The discrete chain reduces to the continuous equation (2.16) in the limit $\kappa \to \infty$ (see Section 2.2). This continuous equation (which includes a δ-function impurity) was studied by Alexeeva *et al.* [2] using the pseudospectral method. We expect that, for sufficiently small Δx, simulations of the discrete NLS chain will reproduce the behaviour of the continuous equation. Our aim is to demonstrate the proximity of the discrete NLS to its continuum limit.

The main results of the analysis in Ref. [2] are summarized in Section 4.1. We then produce results from our own simulations in order to show that all the phenomena are reproducible using the discrete NLS chain. In Section 4.2 we describe the effects of a long impurity, and in Section 4.3 we describe the effects of a short impurity. We give our conclusions in Section 4.4.

4.1 Analysis

The continuous NLS equation containing a δ-function impurity (2.16),

$$i\psi_t + \psi_{xx} - \psi + 2q\delta(x)\psi + 2|\psi|^2\psi = h\overline{\psi} - i\gamma\psi,$$

has two stationary soliton solutions,

$$\psi_\pm(x) = A_\pm \operatorname{sech}(A_\pm|x| + \tilde{x})\, e^{-i\theta_\pm}, \tag{4.1}$$

where

$$\cos 2\theta_\pm = \pm\sqrt{1-\gamma^2/h^2}, \qquad A_\pm^2 = 1 \pm \sqrt{h^2-\gamma^2}, \qquad \tilde{x} = \operatorname{arctanh}(q/A_\pm).$$

It was demonstrated [2] that the solution ψ_- is always unstable. While it may be interesting to explore what comes from this instability, that is beyond the scope of this work. Thus, as in the previous chapter, we consider only the ψ_+ soliton in our investigations.

The stability atlas for the ψ_+ soliton [2] is reproduced in Fig. 4.1 for easy reference. We summarize the main results here. If the impurity is weak ($|q| < 1$), the ψ_+ soliton exists for any h and γ such that $h > \gamma$. For strong impurities ($|q| > 1$), the ψ_+ soliton exists only if $h > \mathfrak{h}_{q,\gamma}$, where $\mathfrak{h}_{q,\gamma}^2 = (1-q^2)^2 + \gamma^2$. The family of curves $h = \mathfrak{h}_{q,\gamma}$ is the set of nearly horizontal curves in the middle of the diagram. Solitons are formed spontaneously by a long impurity ($q > 0$) between the dashed line $h = \sqrt{1+\gamma^2}$ and the relevant $\mathfrak{h}_{q,\gamma}$ curve. Pinned solitons are stable to the right of the parabola-shaped curves. Note that the stability domain increases in area as q is increased. Short impurities ($q < 0$) repel solitons below the corresponding $\mathfrak{h}_{q,\gamma}$ curves.

We now illustrate these properties in the following two sections.

4.2 Long impurity effects

In this section, we simulate a chain of NLS oscillators (2.10) with a single long impurity at $x = 0$. The length of the interval occupied by oscillators

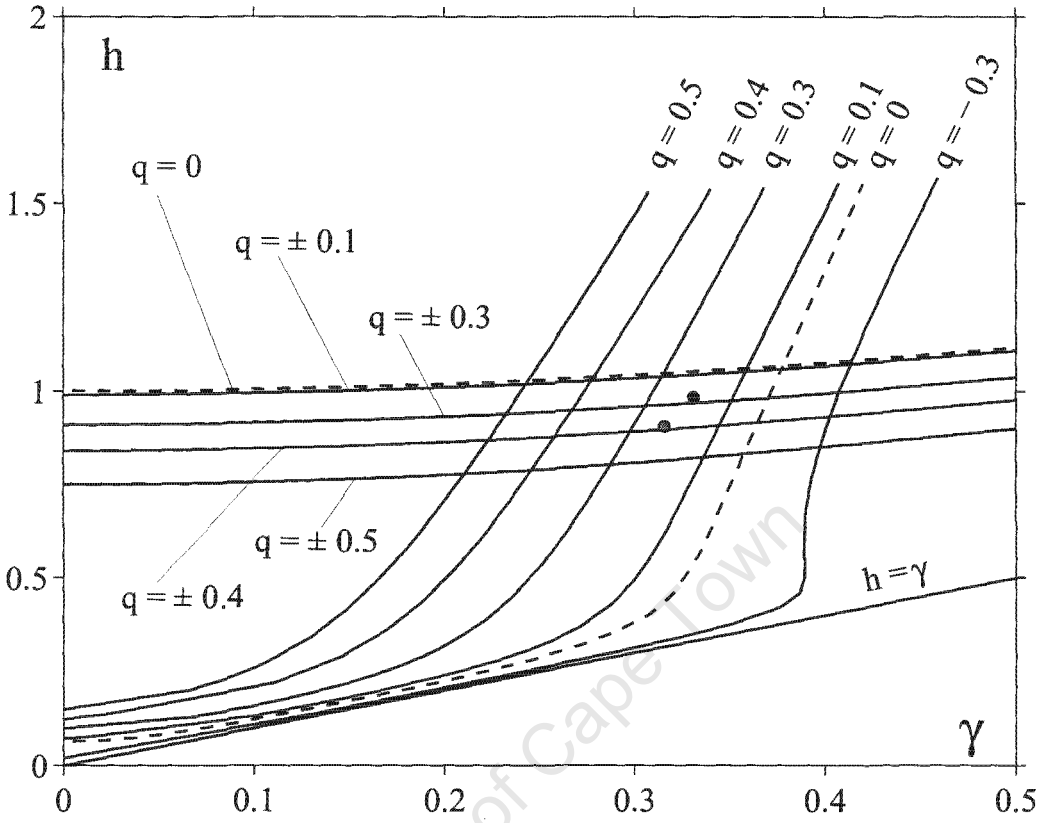

Figure 4.1: Stability charts on the (γ, h)-plane for various values of the impurity q, reproduced from [2]. The point $(\gamma = 0.315, h = 0.9)$ is marked with a grey blob. The point $(\gamma = 0.33, h = 0.99)$ is marked with a black blob. We use parameter values corresponding to these points in our simulations in Chapter 4 and Chapter 5 respectively.

is $L = 150$, from $x = -75$ to $x = 75$. (Generally, we only show part of this range in our diagrams.) We show results of simulations with both $N = 500$ and $N = 1000$ oscillators, which have a spacing of $\Delta x = 0.3$ and $\Delta x = 0.15$ respectively. The other parameters are $\gamma = 0.315$ and $h = 0.9$. The corresponding point is marked with a grey blob on the (γ, h)-plane in Fig. 4.1. For increasing values of q, we demonstrate how the impurity can prevent spatiotemporal chaos, nucleate a stable soliton and suppress a soliton. Lastly, for a different set of parameters $(\gamma = 0.35, h = 0.6)$, we show how a long impurity can attract a soliton.

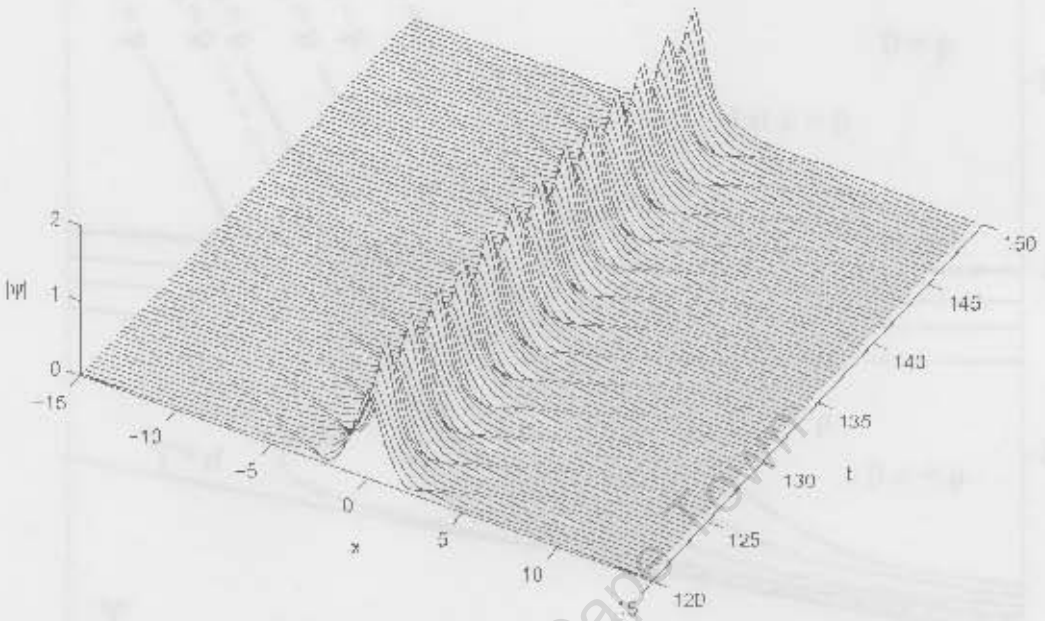

Figure 4.2: A long impurity at $x = 0$ prevents an oscillating soliton centred at the origin from degenerating into spatiotemporal chaos. Here $\gamma = 0.315$, $h = 0.9$ and $q = 0.3$. The oscillations persist for all time when $\Delta x = 0.3$ (shown here), while the soliton becomes stationary when $\Delta x = 0.15$.

4.2.1 Prevention of chaos

In Chapter 3, we showed that when the chain is homogeneous an initial condition in the form of a free-standing soliton

$$\psi_n = A_+ \operatorname{sech}(A_+ x_n) e^{-i\theta_+} \tag{4.2}$$

is unstable for our choice of parameter values ($\gamma = 0.315, h = 0.9$). Consistent with the attractor chart (Fig. 3.3), spatiotemporal chaos sets in if there is no impurity [10] (see Fig. 3.8 on page 28).

If we introduce an impurity which is strong enough, it is able to stabilize the soliton (Fig. 4.2), preventing the system from degenerating into spatiotemporal chaos. Here, the strength of our impurity is $q = 0.3$.

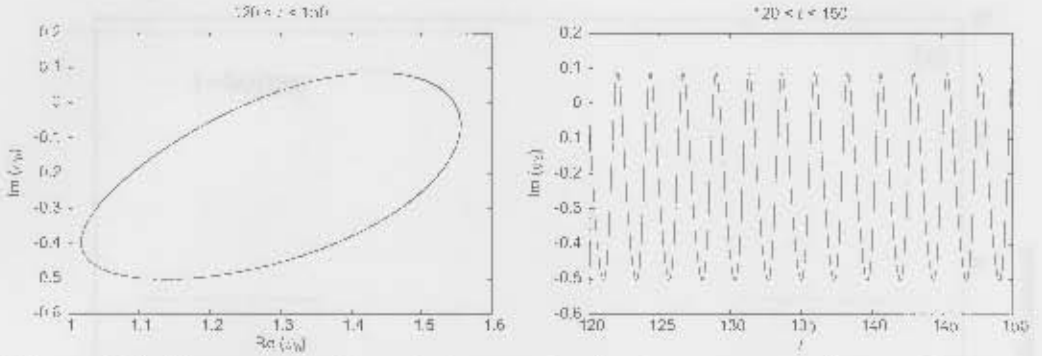

Figure 4.3: Phase portrait and time series for ψ_0 corresponding to Fig. 4.2.

As the phase portrait for the central oscillator ψ_0 shows, the oscillations of the amplitude are regular, and we observe a period-1 limit cycle when $\Delta x = 0.3$ (Fig. 4.3).

Note that, according to the stability chart (Fig. 4.1), the soliton should be stationary in the continuous equation for the parameter values used to generate the results shown in Fig. 4.2. When simulating the corresponding discrete equations, we have noticed that the soliton indeed becomes stationary by $t = 400$ for $\Delta x \quad 0.15$. However, when we use $\Delta x = 0.3$, the periodic oscillations persist for all time.

We measured the average frequency Ω of each oscillator in the array using equation (1.3). The results are displayed in Fig. 4.4. In contrast to the case of the homogeneous array (where we found phase portraits with double loops even very close to the soliton), we observe that when an impurity is present, *all* the oscillators close to the impurity exhibit a period-1 limit cycle (Fig. 4.3 and Fig. 4.5). This indicates that the impurity reduces higher-harmonic radiation. There is, however, some evidence of second-harmonic radiation in Fig. 4.5f and Fig. 4.5h.

4.2.2 Nucleation of a soliton

For the next demonstration, we use the initial condition

$$\mathrm{Re}\,\psi_n = \mathrm{Im}\,\psi_n = \xi_n,$$

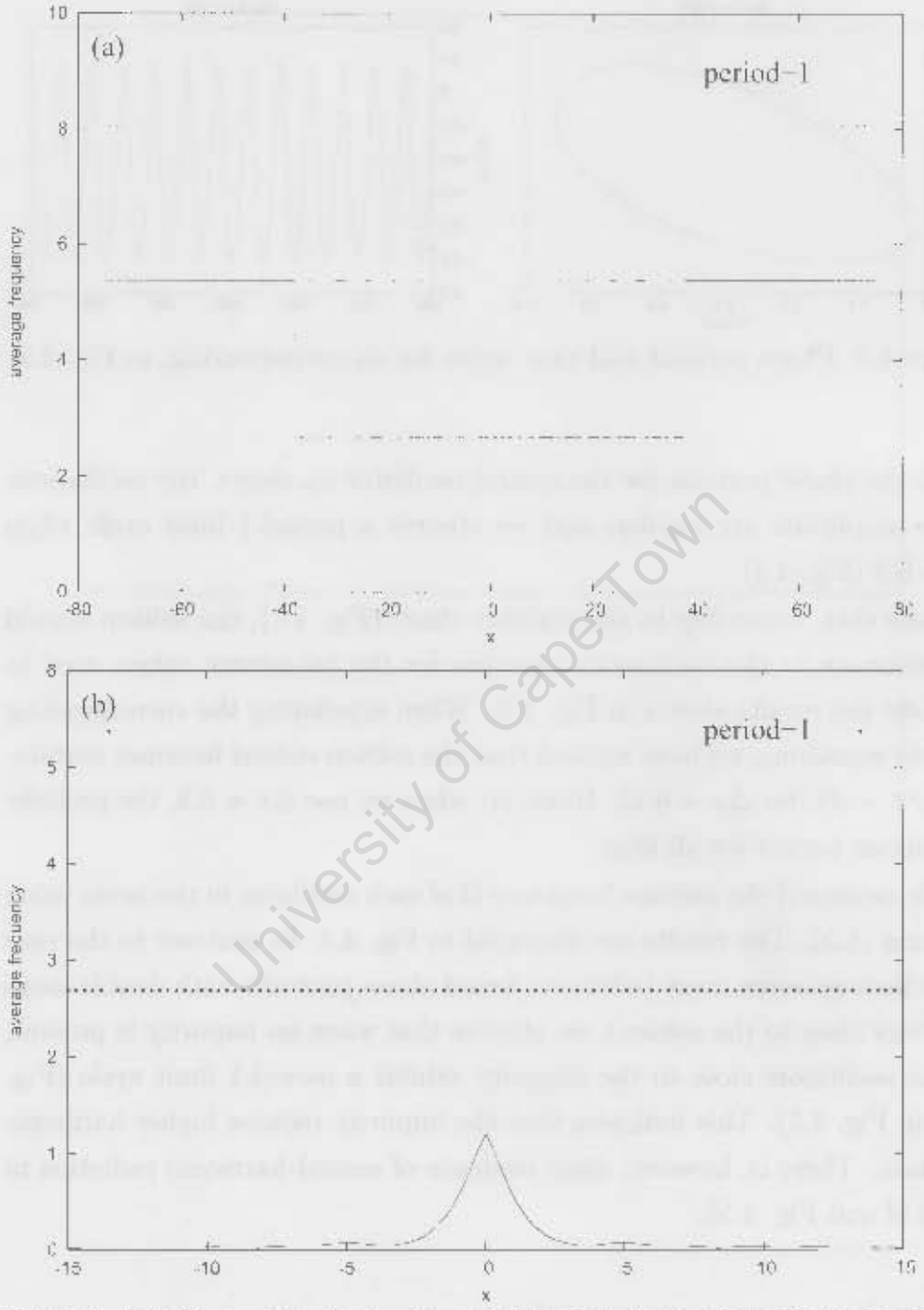

Figure 4.4: (a) The average frequency of oscillators in an array which exhibits a period-1 soliton pinned on a long impurity. Here $\gamma = 0.315$, $h = 0.9$, $q = 0.3$ and $\Delta x = 0.3$. (b) The central portion of the chain is redisplayed, with the soliton at $t = 600$ superimposed.

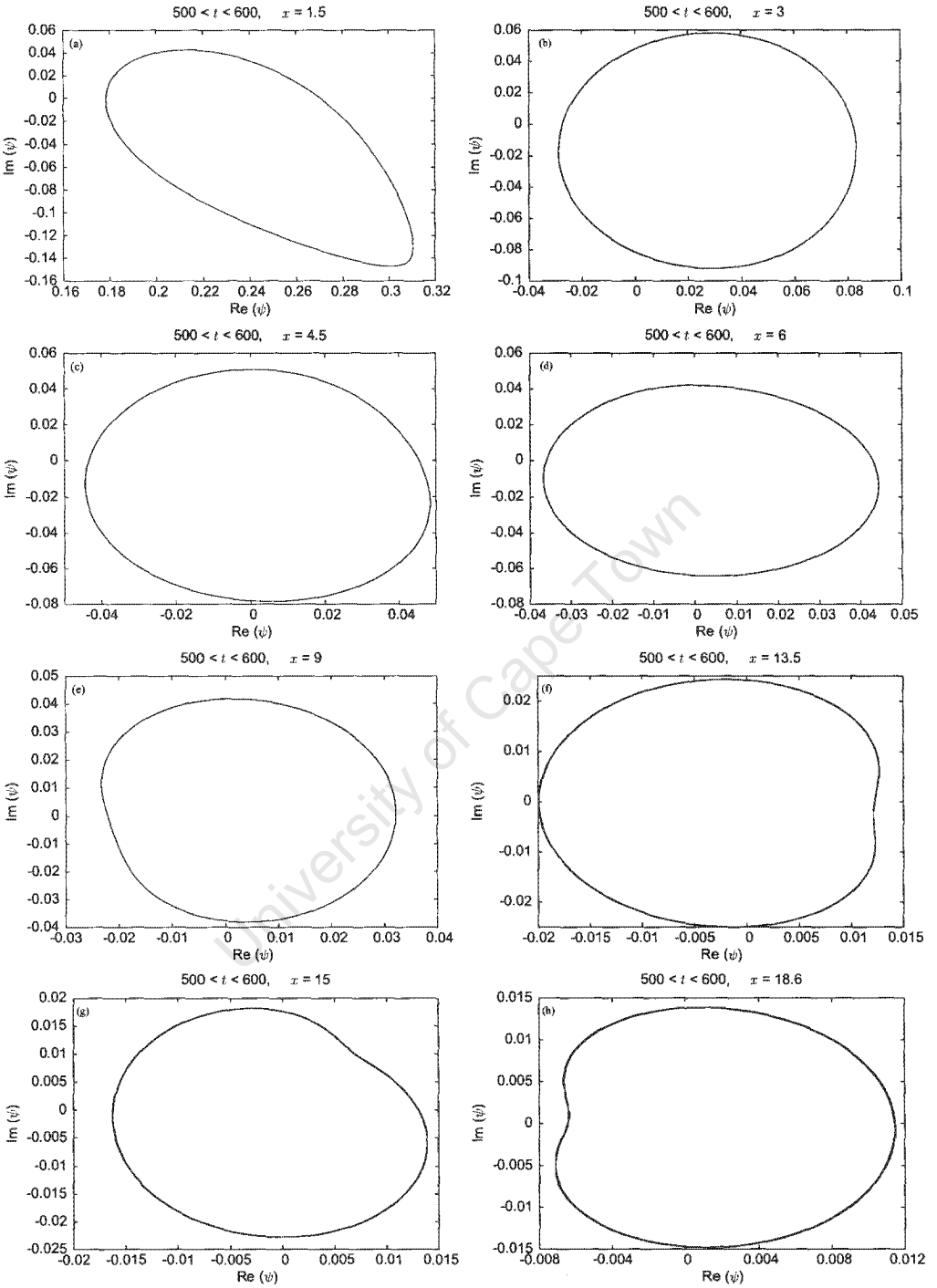

Figure 4.5: Phase portraits of selected oscillators in the array with a single long impurity at $x = 0$ for $\gamma = 0.315$, $h = 0.9$, $q = 0.3$ and $\Delta x = 0.3$. Note the slight deformities in graphs (f) and (h) resulting in $\Omega = 2\omega$ in Fig. 4.4.

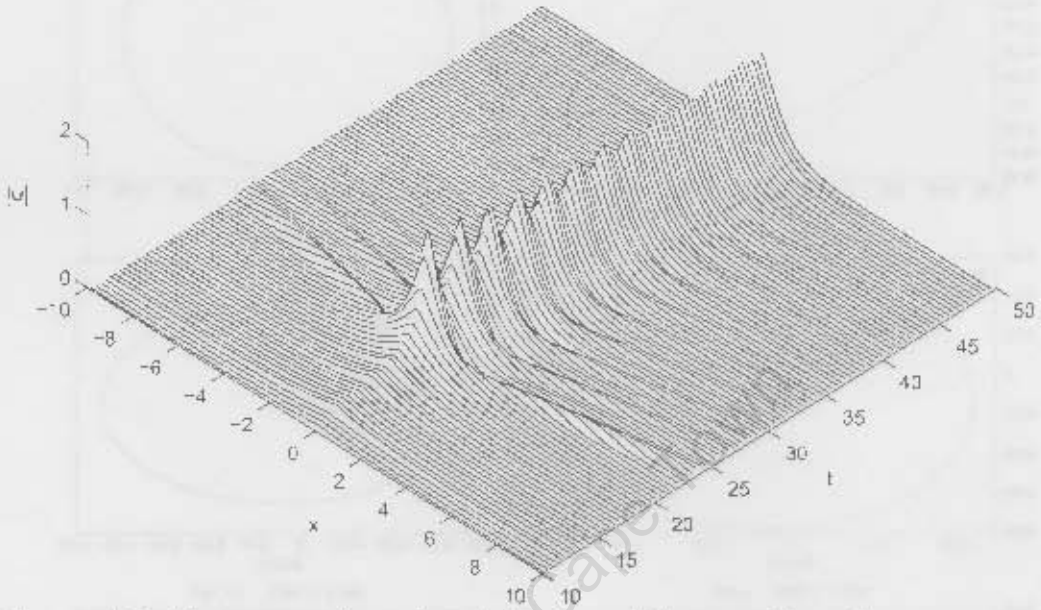

Figure 4.6: From a small random initial condition, a soliton forms spontaneously, pinned on a single impurity at $x = 0$. Here $\gamma = 0.315$, $h = 0.9$, $q = 0.5$ and $\Delta x = 0.15$. The oscillations gradually settle and the soliton becomes stationary.

where each ξ_n is a uniformly distributed random number between 0 and 0.01. For the parameters ($\gamma = 0.315, h = 0.9$), this initial condition would evolve to $\psi = 0$ in the absence of an impurity.

When an impurity of strength $q = 0.5$ is added to the chain at $x = 0$, a soliton spontaneously forms (Fig. 4.6), centred at the site of the impurity. The soliton is stable: the oscillations gradually decrease until the soliton is stationary. This is consistent with the stability chart (Fig. 4.1) since $h > h_{q,\gamma}$ and the parameters fall into the stability domain. The result is in agreement with that of a similar simulation of the continuous equation (2.16) in [2].

(We have checked that a spacing of $\Delta x = 0.3$ gives qualitatively similar results here, but we prefer to show the smoother picture which the smaller spacing produces.)

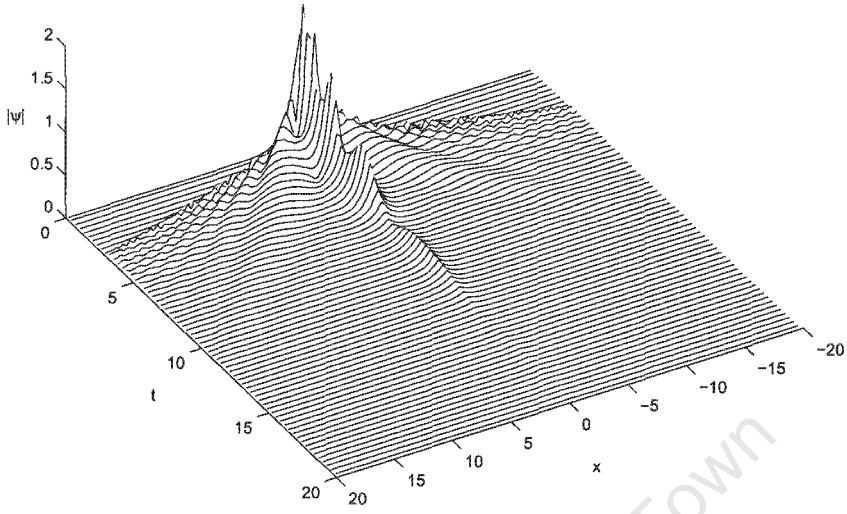

Figure 4.7: A soliton initially centred at $x = 0$ decays to $\psi \equiv 0$ under the influence of a very strong impurity, $q = 1.4$. Here $\gamma = 0.315$, $h = 0.9$ and $\Delta x = 0.15$.

4.2.3 Suppression of a soliton

If the impurity is too strong, the soliton will be suppressed (Fig. 4.7). Here, we have used the initial condition in the form of the free-standing soliton (4.2) and the impurity strength $q = 1.4$. When $h < \mathfrak{h}_{q,\gamma}$ there can be no soliton pinned on the impurity, as is the case here. [The initial radiation which is evident in the diagram is produced while the soliton is adjusting to the pinned form (4.1).]

4.2.4 Attraction of a soliton

Long impurities are attractive. If the soliton is not initially centred at the site of the long impurity (which in this case is at the origin), it can be attracted by the impurity, if it is close enough (Fig. 4.8). Here, the initial condition is in the form of a free-standing soliton centred at $x = -3$,

$$\psi_n = A_+ \operatorname{sech}[A_+(x_n + 3)]e^{-i\theta_+}.$$

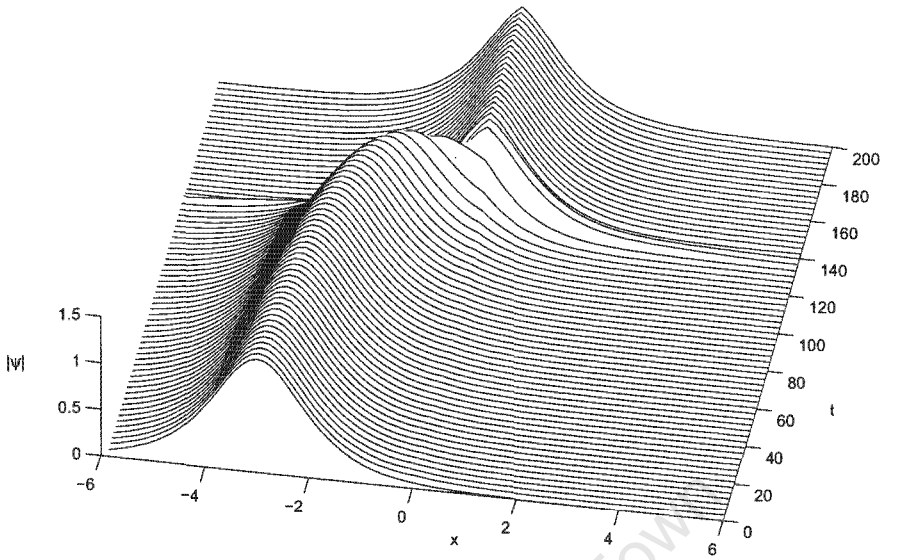

Figure 4.8: A soliton initially centred at $x = -3$ is attracted by an impurity at the origin. Here $\gamma = 0.35$, $h = 0.6$, $q = 0.3$ and $\Delta x = 0.15$.

4.3 Short impurity effects

We show two examples of the effect of a short impurity on the evolution of the chain of NLS oscillators. In both examples, we use the pinned ψ_+ soliton (4.1) as the initial condition.

In the first case ($h < \mathfrak{h}_{q,\gamma}$) the soliton is unpinned and repelled from the impurity (Fig. 4.9).

In the second case, $h > \mathfrak{h}_{q,\gamma}$. The impurity is not repulsive here, and we see a double-humped soliton evolving with the two humps oscillating alternately (Fig. 4.10).

For the second case, we have done the frequency analysis using equation (1.3) on the long-term oscillatory motion of the double-humped soliton. The results are displayed in Fig. 4.11. The results are similar to the case of the period-1 soliton in the homogeneous system (Fig. 3.9), apart from at the origin where we see oscillations at double the frequency of oscillations at other points in the array. This is clearly shown in the time series plots in Fig. 4.12. This is perhaps because ψ_0 lies at the cusp between the two humps

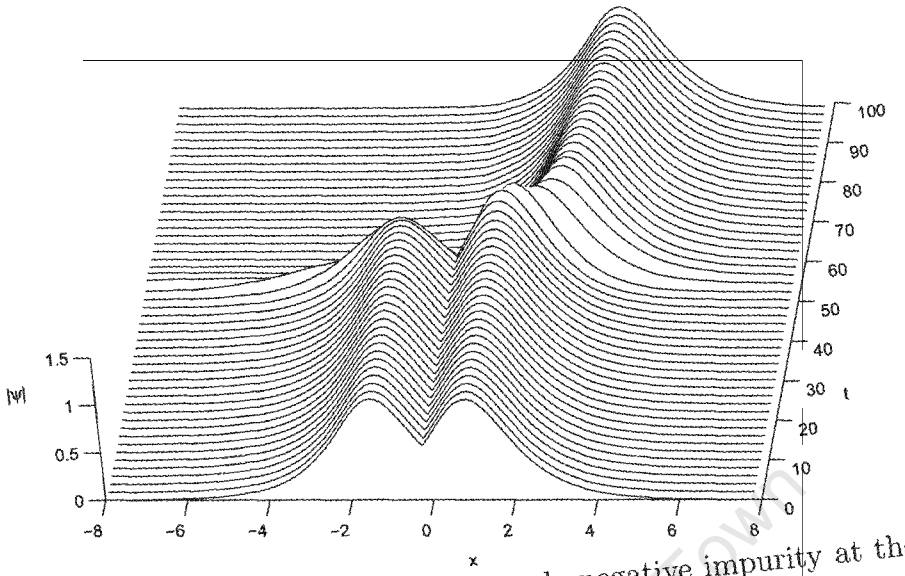

Figure 4.9: A soliton is repelled by a single negative impurity at the origin when $h < \mathfrak{h}_{q,\gamma}$. Here $q = -0.9$, $\gamma = 0.45$, $h = 0.47$ and $\Delta x = 0.15$.

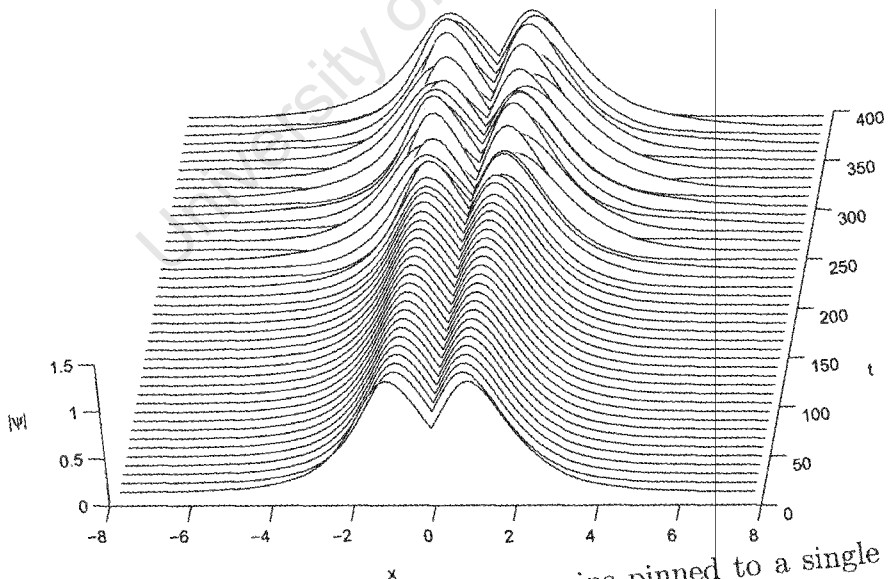

Figure 4.10: A double-humped soliton remains pinned to a single negative impurity at the origin when $h > \mathfrak{h}_{q,\gamma}$. Here $q = -0.9$, $\gamma = 0.45$, $h = 0.6$ and $\Delta x = 0.15$.

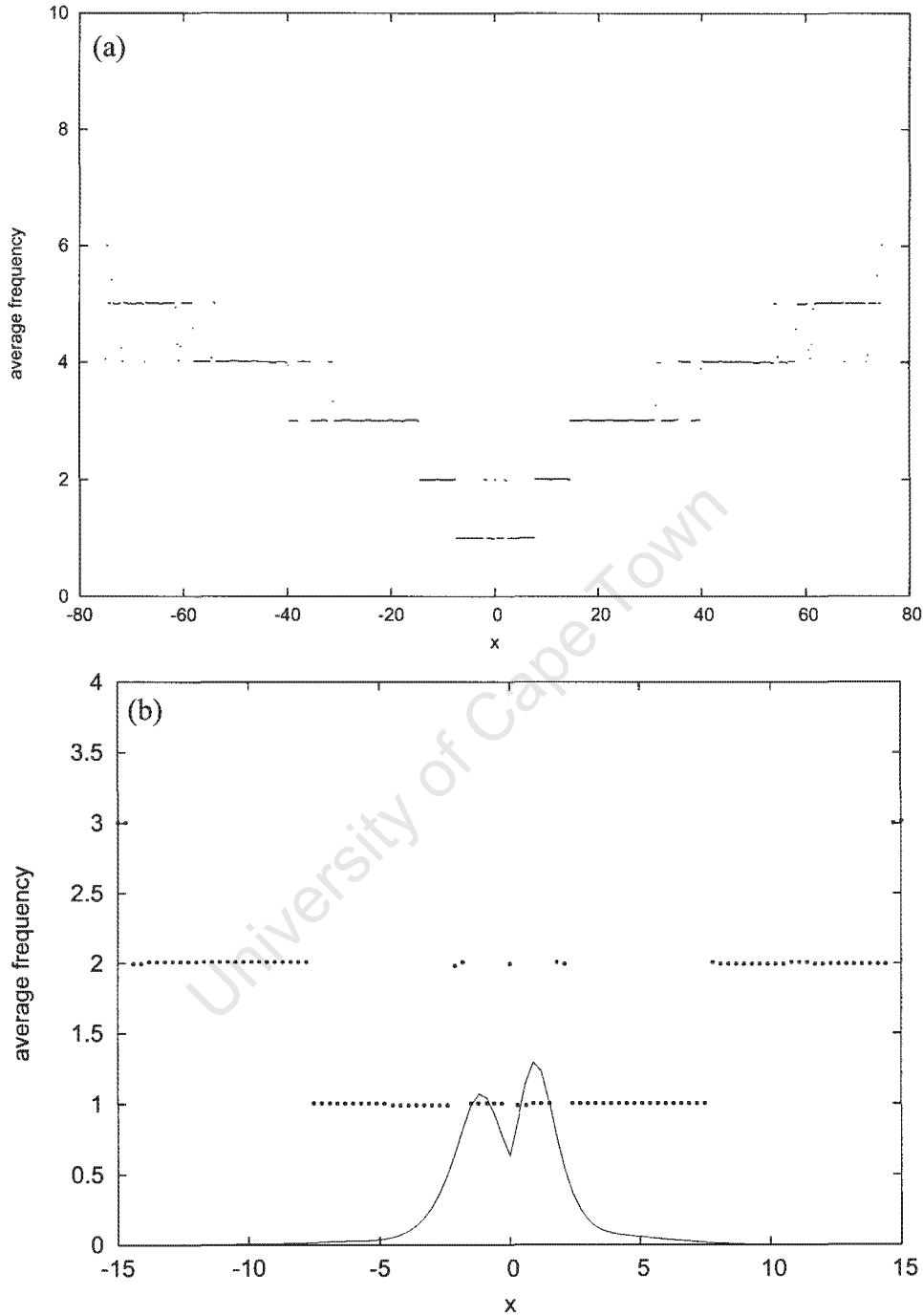

Figure 4.11: (a) Average frequency of oscillators in a chain exhibiting a double-humped soliton (Fig. 4.10). Here $q = -0.9$, $\gamma = 0.45$, $h = 0.6$ and $\Delta x = 0.3$. (b) The central portion of the chain with the soliton at $t = 1000$ superimposed.

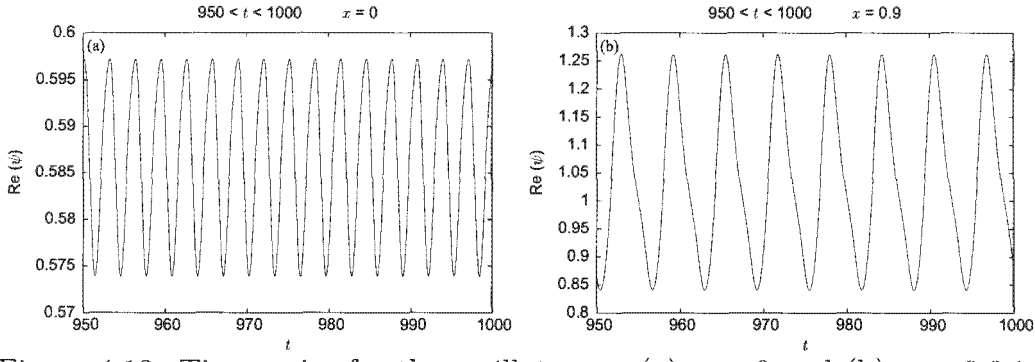

Figure 4.12: Time series for the oscillators at (a) $x = 0$ and (b) $x = 0.9$ in the array of the double-humped soliton (Fig. 4.10). Here $\gamma = 0.45$, $h = 0.6$, $q = -0.9$ and $\Delta x = 0.3$. Note that ψ_0 has double the frequency of adjacent oscillators.

of the soliton. Selected phase portraits are displayed in Fig. 4.13. The result that a second loop is about to emerge in the phase portrait in graph (f) is different to the result for the long impurity (Fig. 4.4) where only single loops in the phase portraits were observed.

4.4 Summary and Conclusions

All the results which were previously obtained for the continuous NLS equation with a δ-function impurity (using spectral techniques) have been replicated for the discrete equations. Thus the stability charts (Fig. 4.1) are still valid for small nonzero Δx. We have shown that this is the case for $\Delta x = 0.15$. In most cases, similar results were also observed for $\Delta x = 0.3$, but there were some differences.

The main features of the discrete system with an impurity are:

1. A long impurity may prevent an initial condition in the form of a soliton from degenerating into spatiotemporal chaos. A moderate strength impurity may allow an unstable soliton to oscillate with a fixed amplitude and frequency, while a stronger impurity can cause the soliton to become stationary.

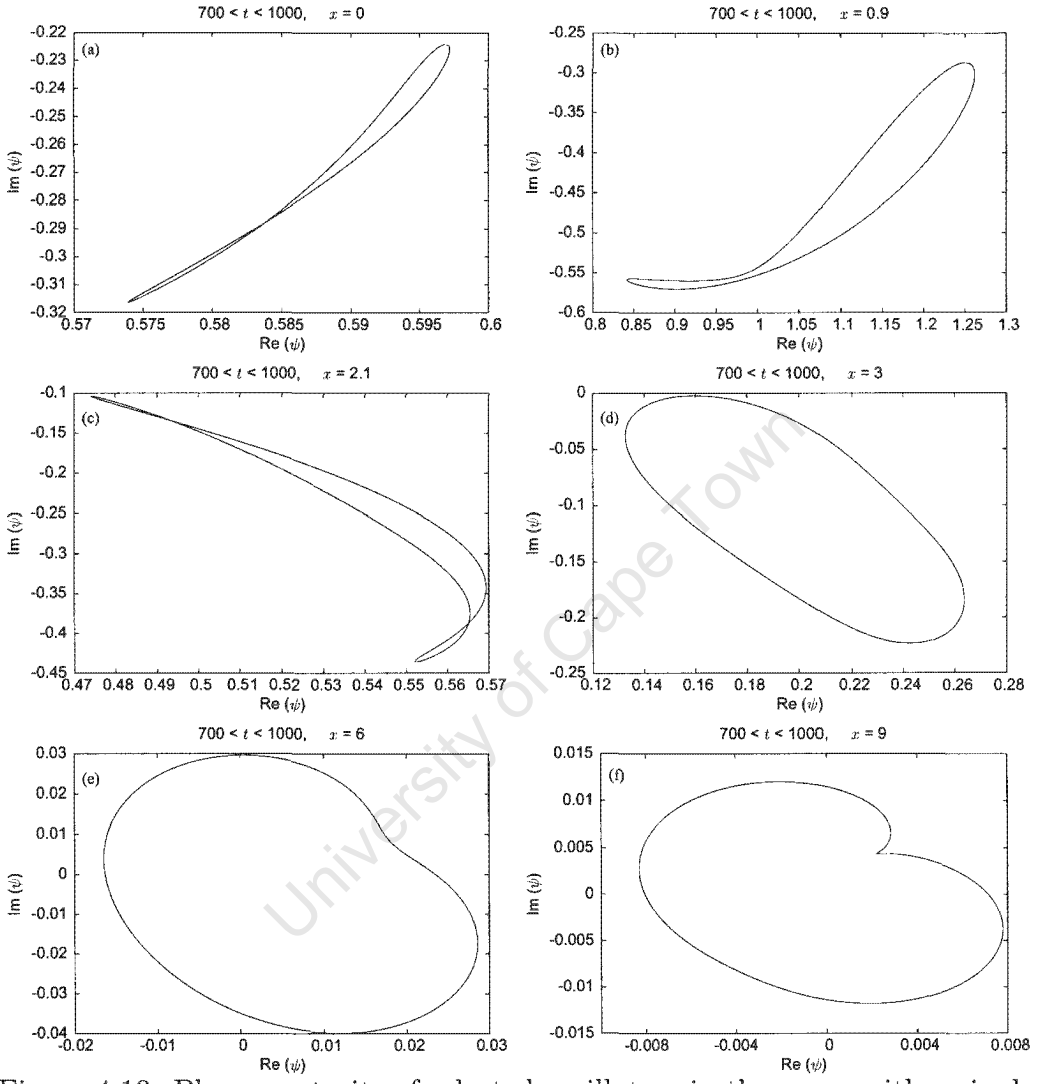

Figure 4.13: Phase portraits of selected oscillators in the array with a single short impurity at $x = 0$ for $\gamma = 0.45$, $h = 0.6$, $q = -0.9$ and $\Delta x = 0.3$. The cycle in graph (a) has double the frequency of that in graph (b), confirmed by the time series plots in Fig. 4.12. In graph (c) we clearly see that $\mathrm{Re}\,\psi$ has two maxima per cycle at $x = 2.1$. In graph (f) we see that a second loop in the phase portrait is about to emerge.

2. The stability of the stationary soliton is dependent on the discreteness. A soliton which is stable when Δx is small can lose its stability and begin to oscillate if Δx is increased.

3. We have observed that, when there is an impurity in the chain, the phase portraits for all the oscillators in the neighbourhood of a periodic soliton consist only of single loops. The impurity seems to reduce the amount of radiation produced, so that evidence of higher harmonics only appears much further from $x = 0$ than in the case of the homogeneous chain.

4. A soliton may form spontaneously at the site of a long impurity.

5. A long impurity may suppress a soliton if it is too strong.

6. Long impurities are attractive; short impurities are repulsive.

Having dealt with the dynamics of the chain of oscillators with a single impurity, we explore the effects of multiple impurities in various arrangements in the next chapter.

Chapter 5

Multiple impurities

In the previous chapter, we showed how a single impurity — either a longer or shorter pendulum in the chain — can affect the dynamics of our chain of oscillators. Now, we introduce disorder in the form of multiple impurities. That is, we investigate what happens when the lengths of *several* oscillators are changed. Our main objective is to explore under what conditions a set of impurities will suppress spatiotemporal chaos.

In Section 5.1, we present some examples showing the effects of different configurations of impurities and how they may stabilize the system. Scenarios we highlight include amplitude profiles which are static, oscillating regularly and chaotic. We also show that the dynamics has a sensitive dependence on the initial conditions. In Section 5.2, we progress to a systematic analysis of cases with equidistant long impurities of equal strengths. In Section 5.3, we present examples of possible behaviours when the distance between impurities is varied. In Section 5.4, we present the results of some simulations of arrays containing identical, equidistantly placed negative impurities. We summarize our results in Section 5.5.

5.1 A chain of oscillators with multiple impurities

We have shown how a single impurity can spontaneously nucleate a soliton in a chain of NLS oscillators (2.10),

$$i\frac{d\psi_n}{dT} + \kappa^2\left(\psi_{n+1} - 2\psi_n + \psi_{n-1}\right) - \psi_n + 2Q\delta_{n,0}\psi_n + 2\left|\psi_n\right|^2\psi_n = h\overline{\psi}_n - i\gamma\psi_n.$$

(The n-th oscillator is located at position x_n, and the separation between adjacent oscillators is Δx. The array of oscillators forms a ring, so that $\psi_{N+1} = \psi_1$ and $\psi_0 = \psi_N$. We remind that $\kappa = 1/\Delta x$ and $Q = q/\Delta x$. Here, q is the strength of the impurity, which corresponds to the length of the pendulum. The length of the chain is $L = 150$, so for a chain of 500 oscillators, $\Delta x = 0.3$.)

Now, we consider NLS chains containing *several* impurities. The impurities serve the purpose of disordering the chain. We explore how different configurations may suppress spatiotemporal chaos. We use initial conditions of the form

$$\text{Re}\,\psi_n = \text{Im}\,\psi_n = \alpha + \xi_n, \tag{5.1}$$

where α is a constant and each ξ_n is a uniformly distributed random number between 0 and 0.01.

In this section, we perform two simulations with different numbers of impurities. In the first simulation we have 7 impurities in the chain, while in the second simulation the chain contains 15 impurities. Our results demonstrate how the evolution of the chain depends on the number of impurities, the strength of the impurities and the value of α in the initial condition. Throughout this section, we use the parameter set ($\gamma = 0.33$, $h = 0.99$), which corresponds to the point marked with a black blob on the stability chart (Fig. 4.1).

A homogeneous chain with the small random initial condition (5.1) with $\alpha = 0$ evolves to $\psi \equiv 0$. We have shown how a single impurity can nucleate a pinned soliton from the same initial condition (Fig. 4.6). Now, we show that

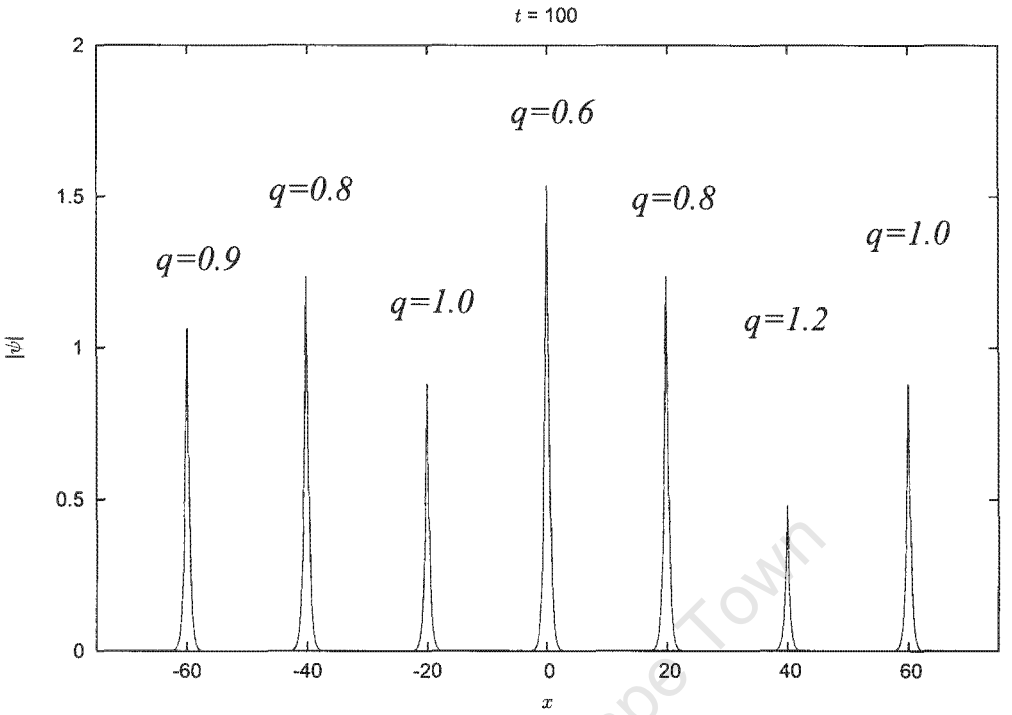

Figure 5.1: Starting from a small initial condition $\mathrm{Re}\,\psi_n = \mathrm{Im}\,\psi_n = \xi_n$, different impurity magnitudes give rise to 7 stationary solitons of different amplitudes. Here $\gamma = 0.33$, $h = 0.99$ and $\Delta x = 0.3$.

if more than one impurity is present in the chain, each is able to nucleate its own soliton. In Fig. 5.1, we see that seven solitons have formed, pinned on seven impurities of different strengths. The impurities are distributed evenly between $x = -60$ and $x = 60$, with an interval of 20 units. Solitons with smaller amplitudes form at sites of longer impurities, and solitons with larger amplitudes form at sites of shorter impurities. Here, all the emerging solitons are stationary.

For the parameters γ and h which we are using, initial conditions which have the form of equation (5.1) with $0 \leq \alpha < 0.07$ evolve to $\psi \equiv 0$ when the chain is homogeneous. By increasing α, we can induce spatiotemporal chaos in the homogeneous chain. For example, if we choose $\alpha = 0.1$, the 7 impurities used to generate Fig. 5.1 are insufficient to prevent evolution from degenerating into spatiotemporal chaos. However, chaos can be suppressed if

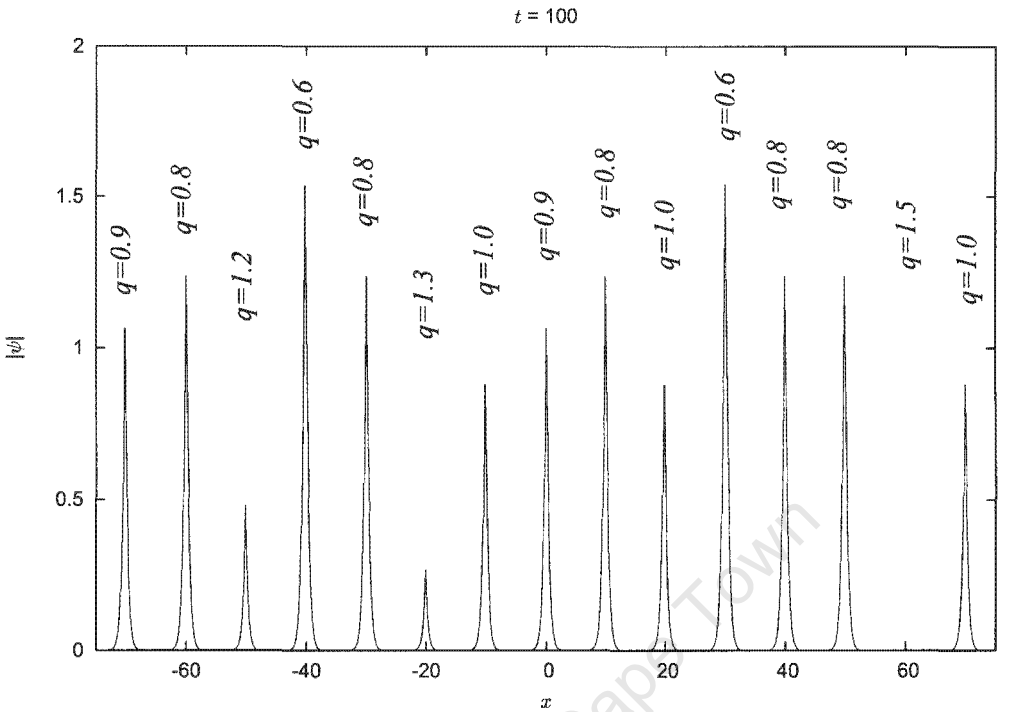

Figure 5.2: 15 impurities of various strengths stabilize the chain, even though a relatively large initial condition is used (Re ψ_n = Im $\psi_n = 0.1 + \xi_n$). Here $\gamma = 0.33$, $h = 0.99$ and $\Delta x = 0.3$.

we increase the number of impurities. We show an example of a configuration of 15 equidistant impurities which stabilizes the chain in Fig. 5.2. Here, the initial condition is (5.1) with $\alpha = 0.1$, and all formed solitons are stationary.

Note that the only differences between the two simulations (Fig. 5.1 and Fig. 5.2) are the initial conditions and the number of impurities present. When the 15 impurities we have chosen are included, a stationary soliton becomes pinned on each impurity, apart from at $x = 60$. We will now explain why the impurity at this point ($q = 1.5$) is too strong to nucleate a soliton.

In the case of a single impurity, solitons may be nucleated spontaneously if the driving strength h is greater than a critical value $\mathfrak{h}_{q,\gamma}$ where

$$\mathfrak{h}_{q,\gamma} = \sqrt{(1-q^2)^2 + \gamma^2}.$$

For fixed values of h and γ, this expression can be rearranged to give a critical

range of values $q_{\min} < q < q_{\max}$ for which solitons would be nucleated:

$$\sqrt{1-\sqrt{h^2-\gamma^2}} < q < \sqrt{1+\sqrt{h^2-\gamma^2}}. \tag{5.2}$$

For $h = 0.99$ and $\gamma = 0.33$, we have $0.258 < q < 1.390$. Consistent with this, note that in Fig. 5.2 a soliton is *not* nucleated by the impurity with $q = 1.5$ at $x = 60$. However, the presence of the impurity still helps to stabilize the chain. In fact, when the long impurity $q = 1.5$ was removed from its position at $x = 60$, spatiotemporally chaotic motion was observed in the neighbourhood of $x = 60$. These chaotic oscillations gradually spread in both directions along the array, to a maximum extent of about half its

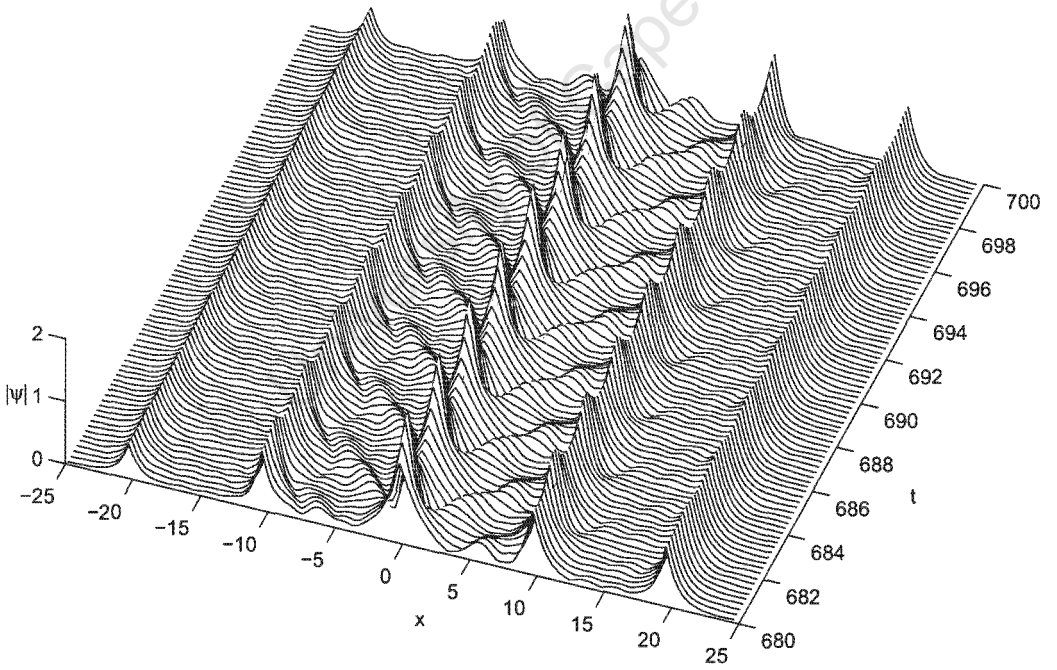

Figure 5.3: Long-term evolution of the central portion ($-25 < x < 25$) of an array with 15 impurities. The impurities are identical to those in Fig. 5.2, apart from at $x = 0$ where a rather weak impurity ($q = 0.3$) has been placed. Here $\gamma = 0.33$, $h = 0.99$ and $\Delta x = 0.3$. The initial condition is $\mathrm{Re}\,\psi_n = \mathrm{Im}\,\psi_n = 0.07 + \xi_n$

length. In the remainder of the array, the solitons retained their form, but small chaotic vibrations were present.

If an impurity is rather weak, it may nucleate an oscillatory soliton. We demonstrate this in Fig. 5.3 using a simulation with the same 15 impurities used in Fig. 5.2, apart from the impurity at the origin which is replaced by one of strength $q = 0.3$. The initial condition used is equation (5.1) with $\alpha = 0.07$. The soliton which forms at $x = 0$ oscillates periodically. Radiation from this soliton causes small periodic oscillations in the amplitudes of the other solitons pinned on impurities along the array. These oscillations become smaller further away from $x = 0$, as is shown in the phase portraits (Fig. 5.4). In this example, spatiotemporal chaos is totally absent from the system.

The shapes of the phase portraits for the oscillators at $x = 19.8$ and $x = 30$ show the presence of second harmonic radiation. This radiation is produced by the oscillating soliton at $x = 0$, and the waves travel along

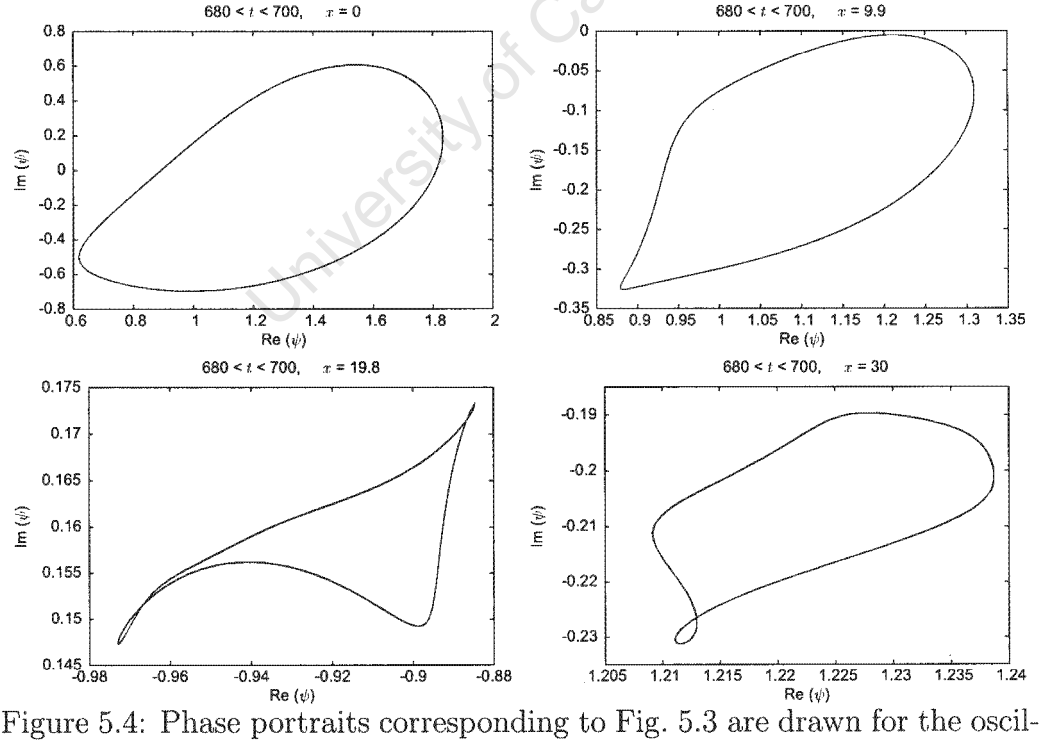

Figure 5.4: Phase portraits corresponding to Fig. 5.3 are drawn for the oscillators at $x = 0$, $x = 9.9$, $x = 19.8$ and $x = 30$, all points at which impurities exist and solitons have formed. Here $\gamma = 0.33$, $h = 0.99$ and $\Delta x = 0.3$.

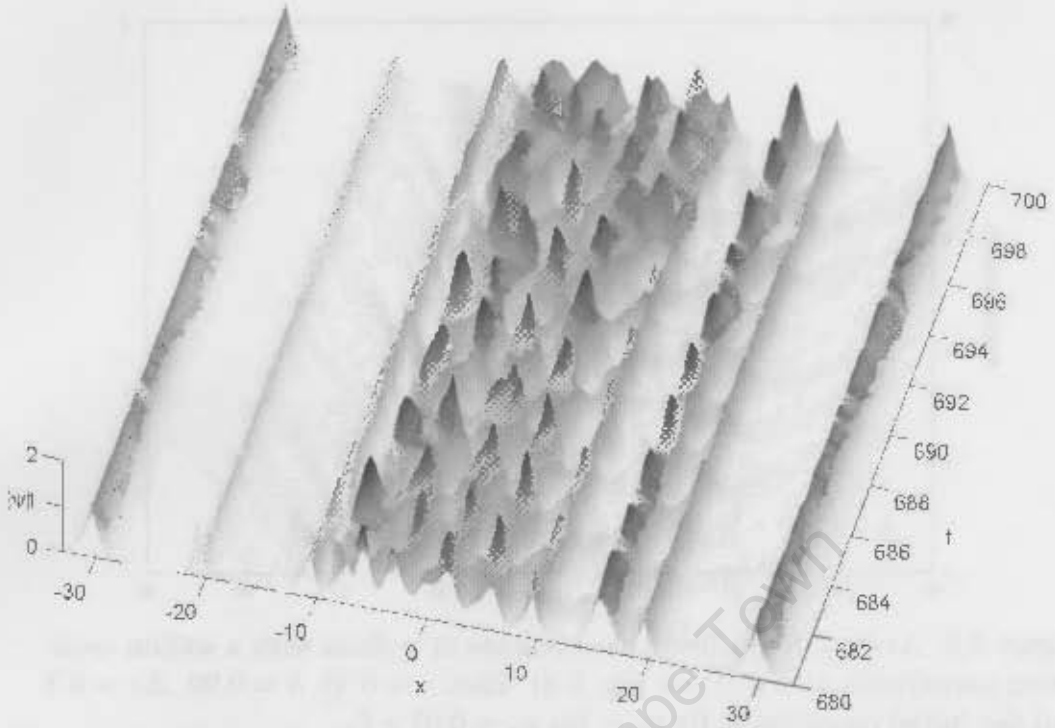

Figure 5.5: The configuration of impurities is identical to that in Fig. 5.3, but a larger initial condition has been used ($\mathrm{Re}\,\psi_n = \mathrm{Im}\,\psi_n = 0.1 + \xi_n$). Chaotic motion is evident in the region $-10 < x < 10$. Small chaotic waves radiate along the chain.

the whole chain. Note how the amplitude of the radiation decreases as the distance from the origin increases.

If the simulation is repeated with a larger initial condition, such as equation (5.1) with $\alpha = 0.1$, spatiotemporally chaotic motion is observed in the neighbourhood of $x = 0$ (Fig. 5.5). While many of the solitons which form along the array do not seem to be affected by the chaotic motion around the weak impurity, small chaotic waves propagate along the whole length of the chain. This is clearly illustrated by comparing the plots of the average frequencies (1.3) of each oscillator for the two scenarios in Fig. 5.6 and Fig. 5.7.

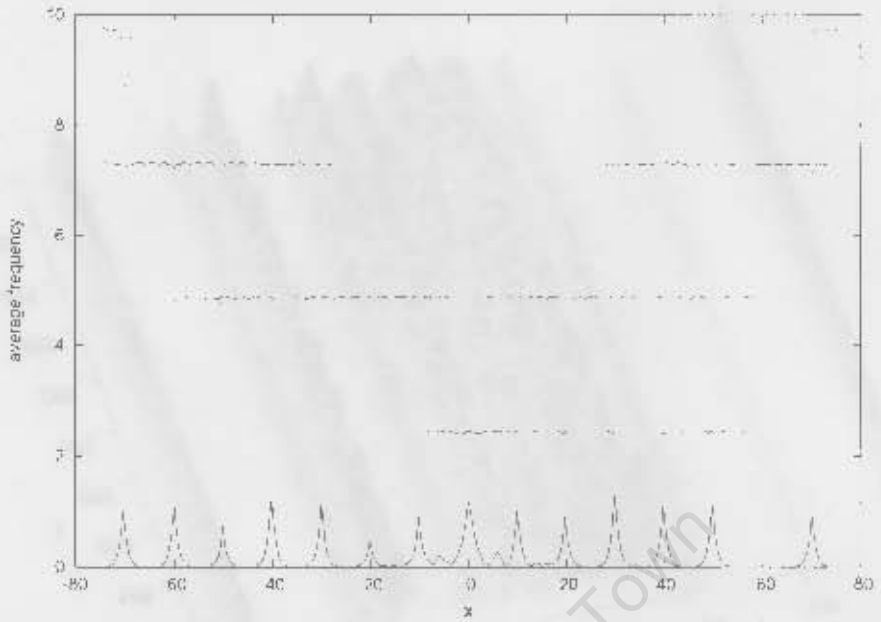

Figure 5.6: Average frequency measurements in a chain with a soliton oscillating periodically at $x = 0$ (see Fig. 5.3). Here $\gamma = 0.33$, $h = 0.99$, $\Delta x = 0.3$ and the initial condition is $\mathrm{Re}\,\psi_n = \mathrm{Im}\,\psi_n = 0.07 + \xi_n$.

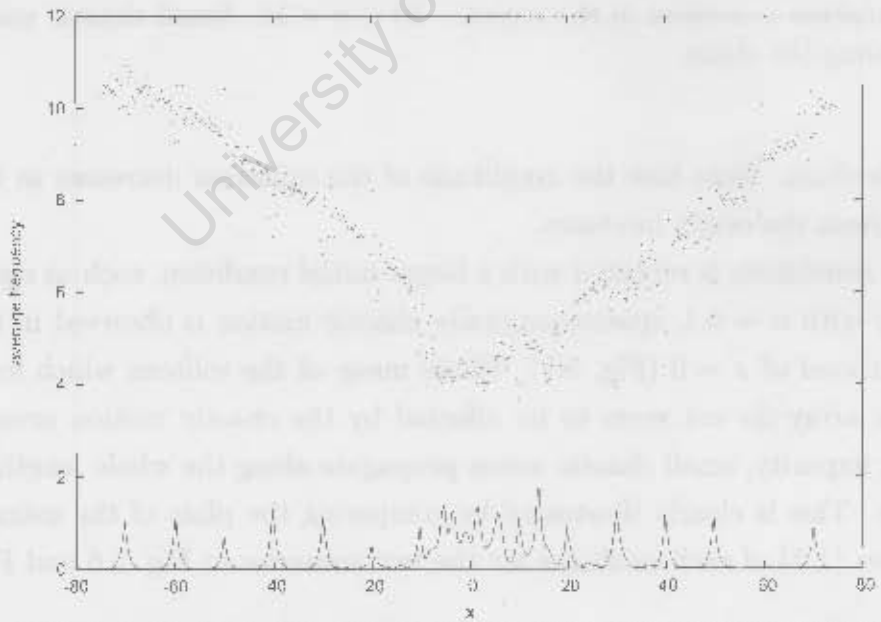

Figure 5.7: Average frequency measurements in a chain where spatiotemporal chaos is evident around $x = 0$ (see Fig. 5.5). Here $\gamma = 0.33$, $h = 0.99$, $\Delta x = 0.3$ and the initial condition is $\mathrm{Re}\,\psi_n = \mathrm{Im}\,\psi_n = 0.1 - \xi_n$.

5.2 Equidistant impurities of equal strength

In this section, we analyse the effects of impurities in the chain where all the impurities have equal strength and are placed equidistantly along the chain. (In the previous section, the impurities considered had different strengths and the spacing of the impurities around the ring was not uniform.) We have made a specific choice of system parameters ($\gamma = 0.3$, $h = 0.85$, $L = 150$, $\Delta x = 0.3$), and we use a common initial profile of

$$\mathrm{Re}\,\psi_n = \mathrm{Im}\,\psi_n = 0.2 + \xi_n, \qquad 0 < \xi_n < 0.01.$$

As described in the previous section, this initial condition evolves chaotically in the homogeneous system. The damping and driving parameters have been changed slightly here, but the evolution of the homogeneous chain is qualitatively the same.

For this choice of parameters and initial condition, up to 12 equidistant impurities have no stabilizing effect on the chain, and we observe spatiotemporal chaos (Fig. 5.8).

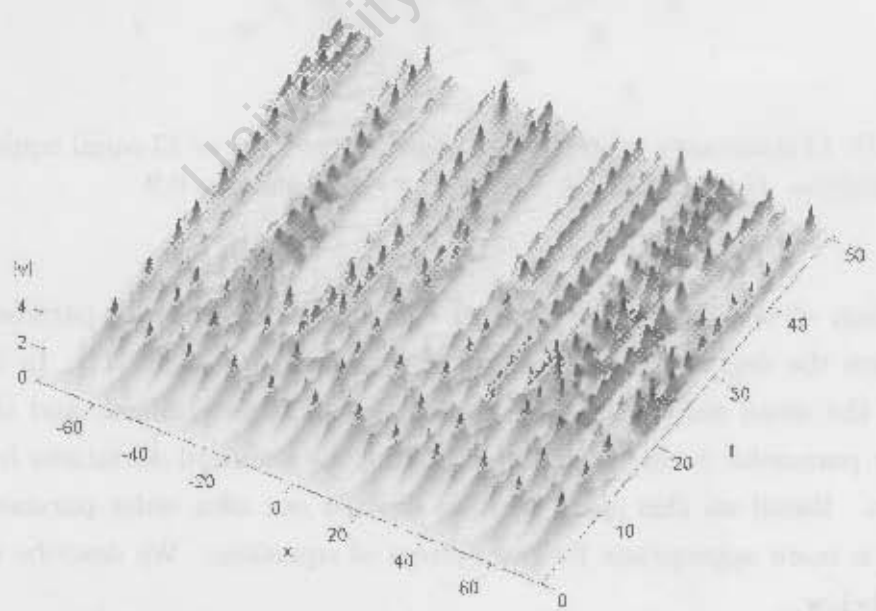

Figure 5.8: Spatiotemporal chaos in the system with 12 equal equidistant impurities. Here $\gamma = 0.3$, $h = 0.85$, $\Delta x = 0.3$ and $q = 0.9$.

This behaviour changes when a 13th impurity is added. Now, suddenly, each impurity cedes a soliton which is stable and stationary (Fig. 5.9). For this to occur, the impurity strength must be within a certain range, given approximately by inequality (5.2). This behaviour persists if more impurities are added.

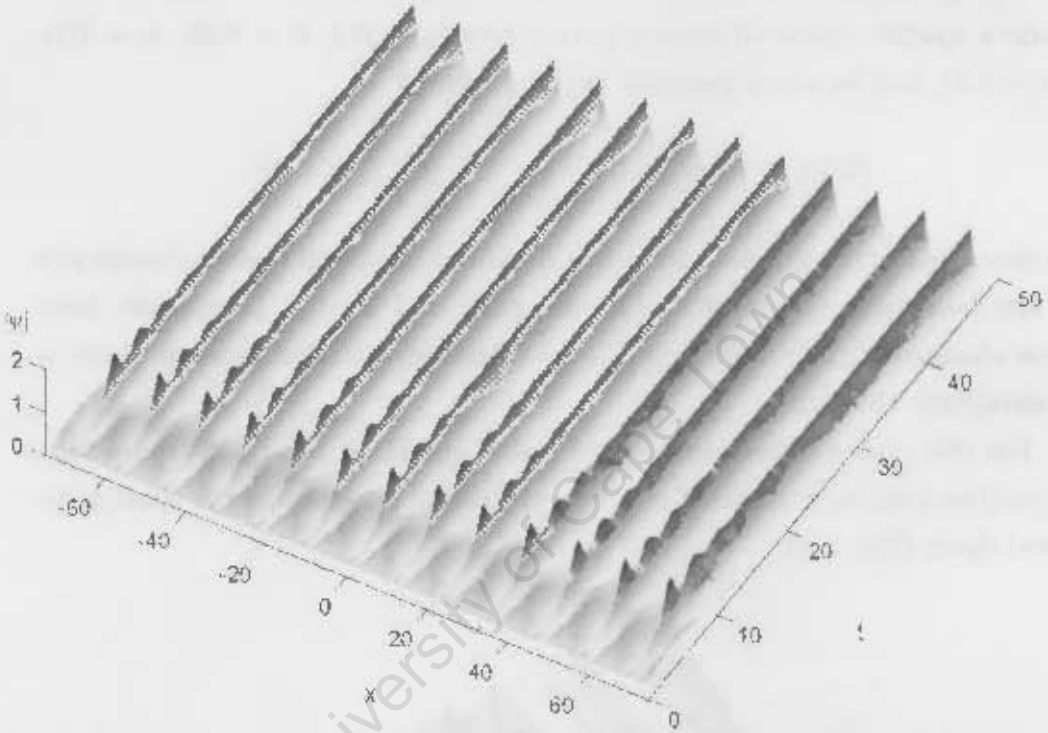

Figure 5.9: 13 stationary solitons are formed at the sites of 13 equal equidistant impurities. Here $\gamma = 0.3$, $h = 0.85$, $\Delta x = 0.3$ and $q = 0.9$.

Braiman *et al.* suggested a method for calculating an order parameter to measure the degree of synchronization present in a system [11]. In this method, the mean amplitude of all the oscillators is determined, and then the order parameter is calculated by averaging the standard deviations from the mean. Based on this idea, we have devised our own order parameter β which is more appropriate for our system of equations. We describe our method below.

Let N_I be the total number of impurities contained in the chain of oscillators. Our assumption is that if the impurities in the chain tame spatiotem-

poral chaos, pinned solitons will form at the sites of the impurities.

A stationary soliton which is pinned on an impurity of strength q has the form

$$\psi(x) = sA\,\mathrm{sech}(A|x| + \tilde{x})e^{-i\theta},$$

where

$$\cos 2\theta = \sqrt{1-\gamma^2/h^2}, \qquad A^2 = 1 + \sqrt{h^2-\gamma^2}, \qquad \tilde{x} = \mathrm{arctanh}(q/A)$$

and $s = +1$ or $s = -1$. In our simulations, we calculate the polarity s_k of the k-th soliton using

$$s_k(t) = \begin{cases} +1, & \text{if Re}\,\psi_n(t) > 0 \\ -1, & \text{if Re}\,\psi_n(t) < 0 \end{cases}$$

where n is the number of the oscillator at which the k-th impurity is located. Hence, for $1 \le k \le N_I$, after determining s_k, we subtract the pinned soliton of the corresponding polarity from $\psi_n(x)$, producing the real and imaginary parts of its perturbation:

$$\begin{aligned} X_k(t) &= \text{Re}\,\psi_n(t) - s_k A\,\mathrm{sech}(\tilde{x})\cos\theta \\ Y_k(t) &= \text{Im}\,\psi_n(t) + s_k A\,\mathrm{sech}(\tilde{x})\sin\theta. \end{aligned}$$

Next, we evaluate the frequency of the perturbation of the k-th soliton. If

$$X_k + iY_k = \rho_k(t)e^{i\varphi_k(t)},$$

then

$$\omega_k = \dot{\varphi}_k = \frac{d}{dt}\arctan\frac{Y_k}{X_k}.$$

We find the average frequency

$$\overline{\omega} = \frac{1}{N_I}\sum_{k=1}^{N_I}\omega_k$$

and then finally calculate the synchronization measure

$$\beta = \lim_{T\to\infty} \frac{1}{T} \int_{t_1}^{t_1+T} \frac{1}{|\overline{\omega}|} \sqrt{\sum_{k=1}^{N_I} (\omega_k - \overline{\omega})^2 dt}.$$

In order to eliminate the computational inaccuracies one obtains when dividing two very small numbers, we modified our algorithm so that the integrand would be set to zero at any time step at which $|\overline{\omega}| < 10^{-2}$.

This method is capable of identifying (by producing $\beta = 0$) not only oscillations which are in phase with one another, but also oscillations with a constant phase shift, even if the values of ρ_k are unequal and varying. Indeed, assume

$$\psi_n(t) = \rho_k(t) e^{i\varphi_0(t) + i\alpha_k} + sA\,\mathrm{sech}(\tilde{x}) e^{-i\theta},$$

where α_k are (constant) phase shifts. Then for all k we have $\omega_k = \dot{\varphi}_0$, whence $\overline{\omega} = \dot{\varphi}_0$ and so $\beta = 0$.

We have calculated β for different impurity strengths ($0.4 \leq q \leq 1.325$) and for different numbers of equidistant impurities ($10 \leq N_I \leq 36$). For each (q, N_I) pair, we have run a single simulation starting with identical initial conditions. The results of our calculations are summarized schematically in Fig. 5.10. The values of $\ln(1+\beta)$ are represented with a grey scale from 0 (black) to 4 (white). Darker shades indicate that a higher degree of synchronization occurs. The time at which averaging starts ($t_1 = 1000$) was chosen to be large enough to eliminate any transient effects from the results. The time period used for averaging was $T = 500$.

In Fig. 5.10, we see that spatiotemporal chaos always occurs when $N_I < 13$ and $q < 0.6$. Looking from left to right, an unexpected result is that the minimum value of q required to tame spatiotemporal chaos suddenly increases to $q = 0.8$ when $N_I = 22$. This minimum value then decreases steadily between $N_I = 24$ ($q = 0.85$) and $N_I = 34$ ($q = 0.65$), before another sharp increase at $N_I = 35$ to $q = 0.9$. These results indicate a more complicated relationship between N_I and q than what was anticipated.

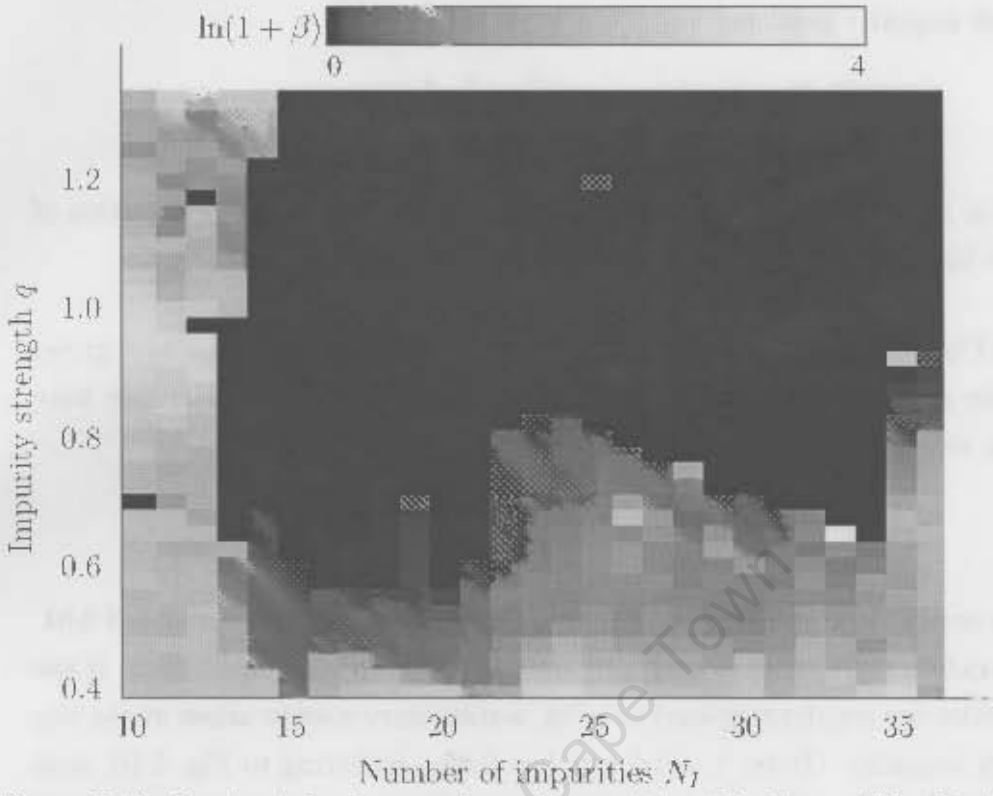

Figure 5.10: Horizontal axis: number of impurities $(10, 11, \ldots, 36)$. Vertical axis: impurity strength $(0.1 < q < 1.325$ at intervals of 0.025). Darker shades indicate better synchronization, that is, β is closer to zero. Here $\gamma = 0.3$, $h = 0.85$ and $\Delta x = 0.3$.

5.3 Disordered impurity positions

In this section, we explore possible outcomes of placing impurities of equal amplitude along the array at not quite regular intervals. Suppose we wish to include N_I impurities, and there are a total of N oscillators in the chain numbered from 1 to N, where N is even. An *even* distribution of impurities results by introducing the k-th impurity at the oscillator numbered

$$\frac{N}{2} + 1 - \left[(k-1)\frac{N}{N_I}\right] \mod N,$$

where $k = 1, \ldots, N_I$. (Square brackets denote rounding to integers.) In order to introduce disorder in the impurity positions, we add a random variable r_{ik}

to each impurity position:

$$\frac{N}{2} + 1 + \left[(k-1)\frac{N}{N_I}\right] + \left[\eta_k\right] \mod N.$$

Each η_k is normally distributed with a mean of 0 and standard deviation of σ. We increase the level of disorder by increasing σ.

In Fig. 5.11, we show an example of how the evolution changes as σ grows and the gaps between the impurities become more irregular. Here we have chosen to use $N_I = 14$ impurities. The initial condition used is

$$\text{Re}\,\psi_n = \text{Im}\,\psi_n = 0.2 + \xi_n,$$

where each ξ_n is a uniformly distributed random number between 0 and 0.01. The random number generator uses the same seed in each simulation. If the impurities are regularly spaced ($\sigma = 0$), a stationary soliton arises at the site of each impurity. (Here, $\gamma = 0.3$ and $h = 0.85$.) Referring to Fig. 5.10, note that at the point $(N_I = 14, q = 0.9)$ we have $\beta = 0$.

For small variations in the sizes of the gaps between impurities (small σ), we see no change from the case with even spacing. Thus, for $\sigma = 2$, 14 stationary solitons form at the sites of the impurities as before (Fig. 5.11a). We can see in the figure that the gaps between the lines are not all equal, but there are no oscillations.

When we increase the standard deviation to $\sigma = 3$, free-standing oscillating solitons appear in the larger gaps between impurities near $x = 39$ and $x = 61$ (Fig. 5.11b). Measuring the average frequency using equation (1.3) shows us that the oscillations are periodic, and radiation with higher harmonics travels along the length of the array (Fig. 5.12a). When $\sigma = 4$, another oscillating soliton appears near $x = -28$ in a gap between two impurities. The oscillations are still periodic (Fig. 5.12b). When we set $\sigma = 5$, a fourth oscillating soliton appears near $x = -50$. In this case, however, the oscillations in the whole array are chaotic (Fig. 5.12c).

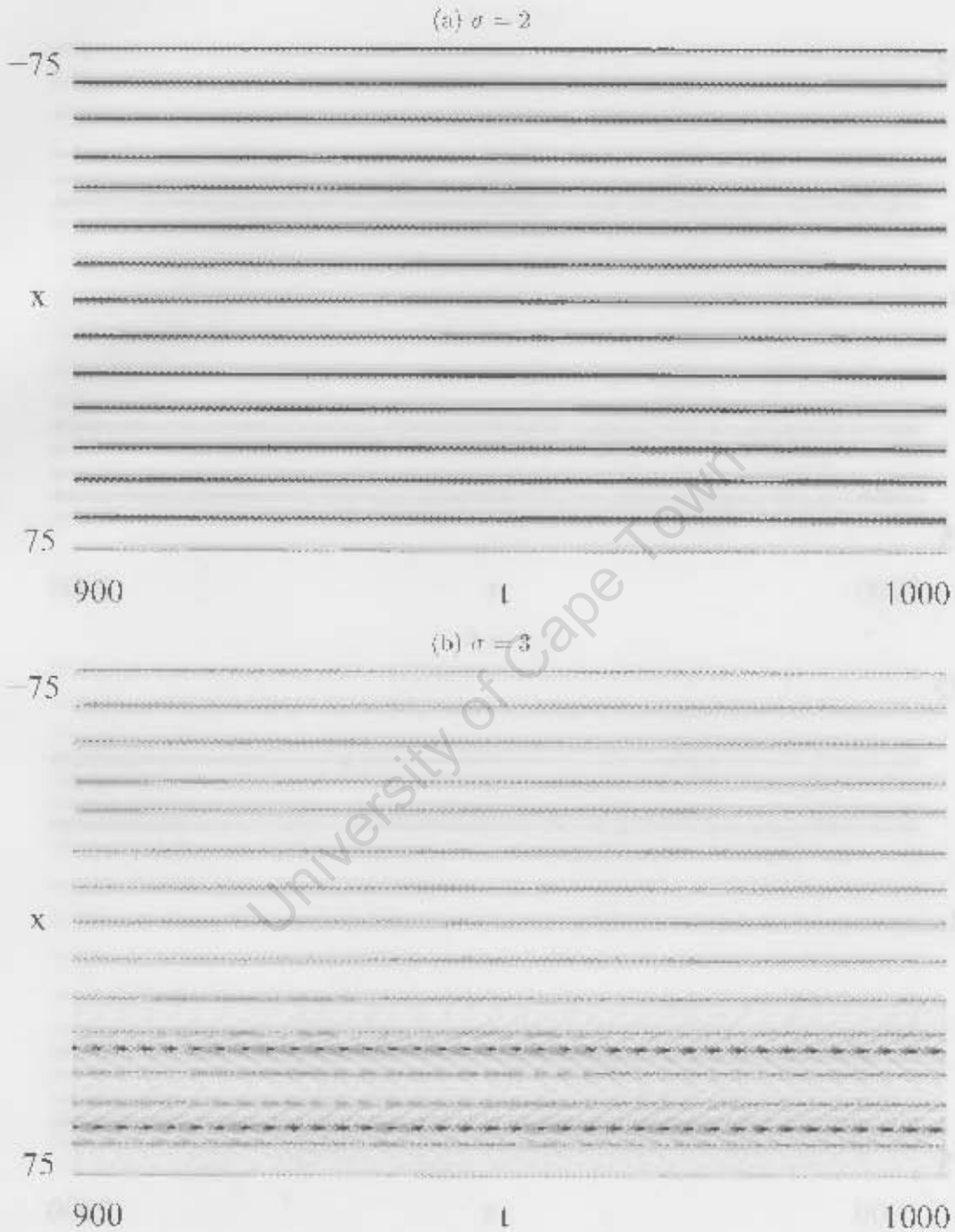

Figure 5.11: An array with 14 impurities, positioned with some randomness σ. Here $\gamma = 0.3$, $b = 0.85$, $q = 0.9$ and $\Delta x = 0.3$.

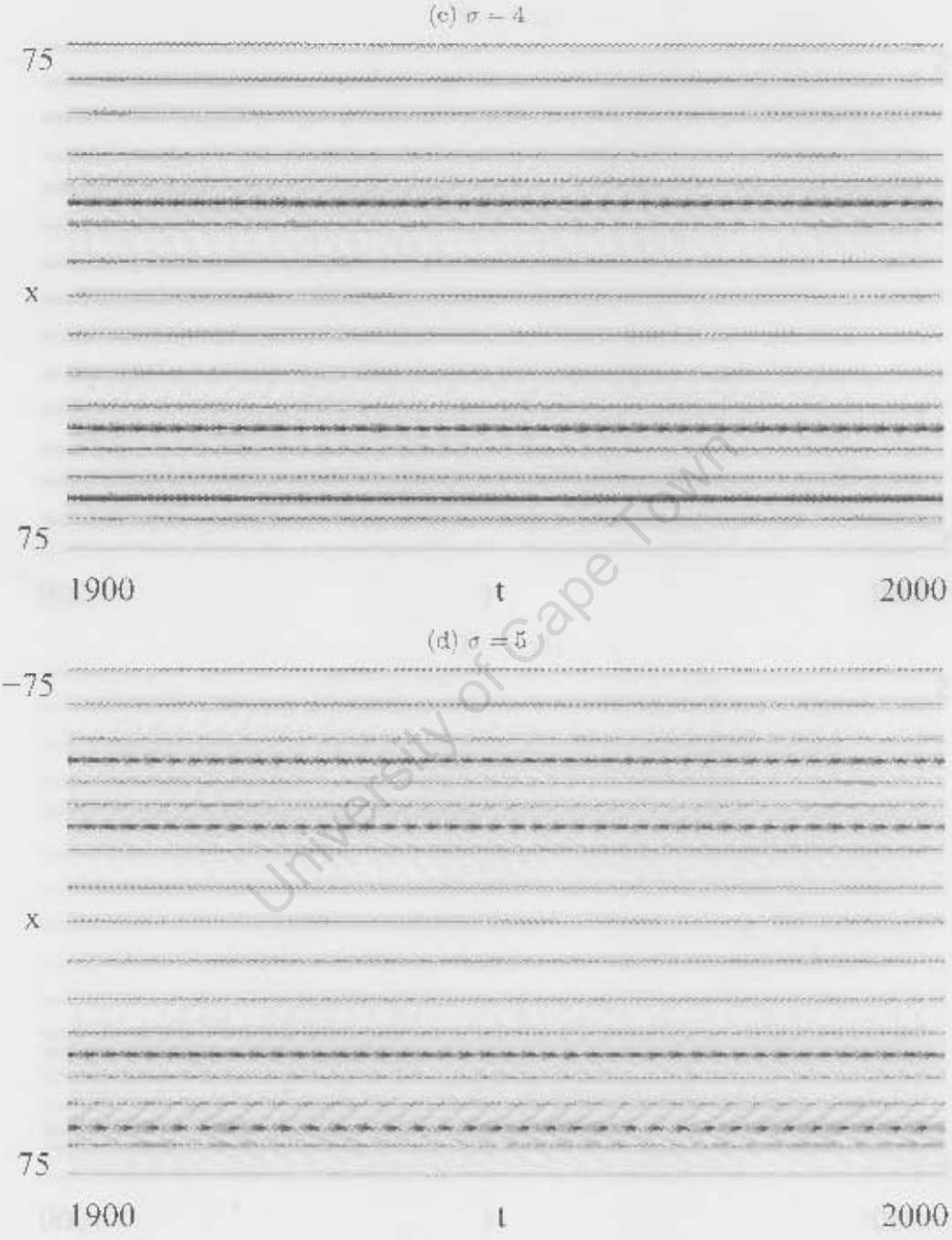

Figure 5.11: An array with 14 impurities, positioned with some randomness σ. Here $\gamma = 0.3$, $h = 0.85$, $q = 0.9$ and $\Delta x = 0.3$.

(a) $\sigma = 3$, $500 < t < 1000$

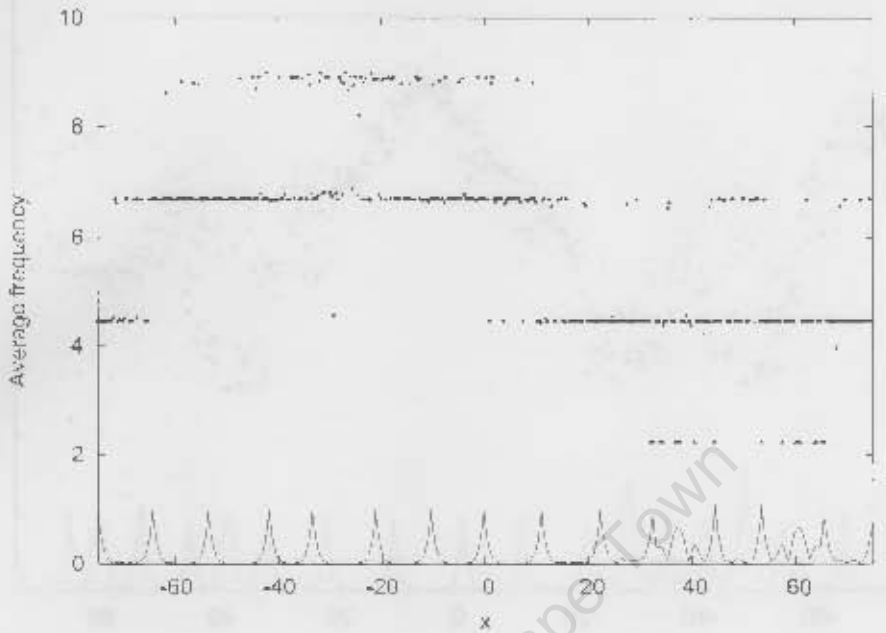

(b) $\sigma = 4$, $1000 < t < 2000$

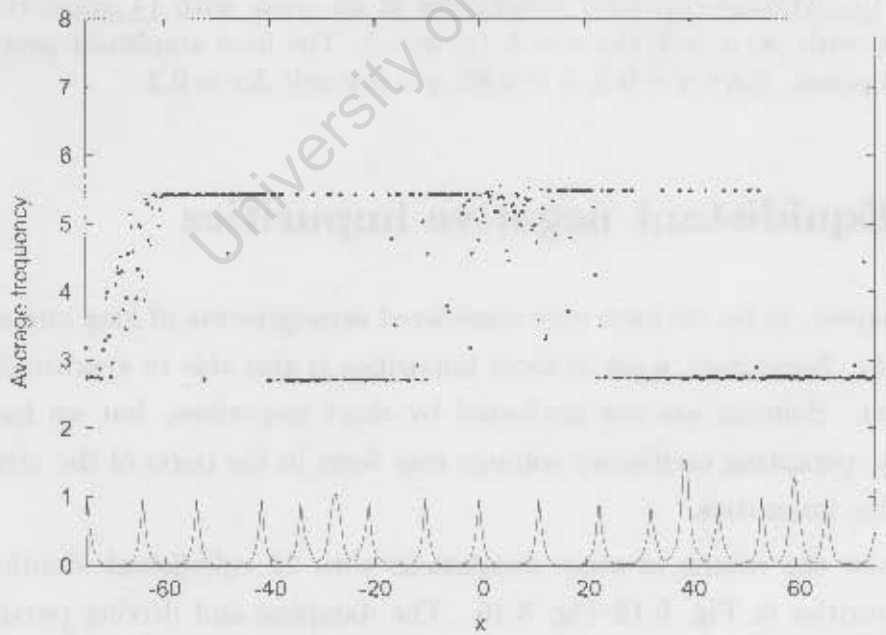

Figure 5.12

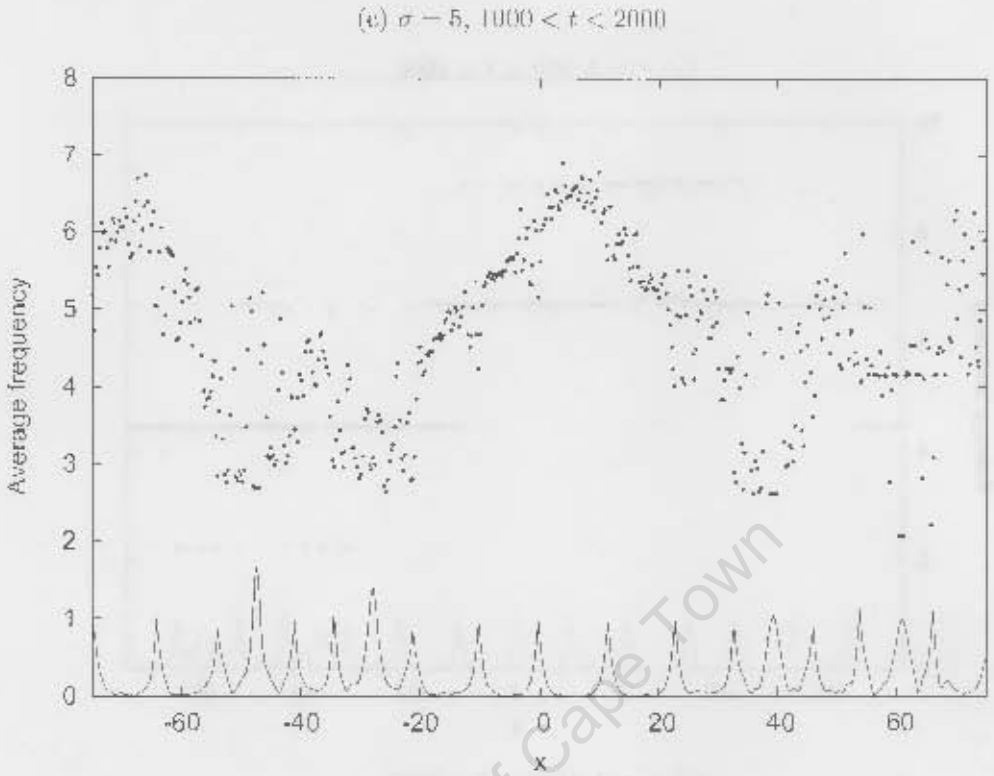

Figure 5.12: Average oscillator frequencies in an array with 14 impurities, positioned with (a) $\sigma = 3$; (b) $\sigma = 4$; (c) $\sigma = 5$. The final amplitude profile is superimposed. Here $\gamma = 0.3$, $h = 0.85$, $q = 0.9$ and $\Delta x = 0.3$.

5.4 Equidistant negative impurities

In this chapter, so far we have only considered arrangements of long impurities ($q > 0$). Sometimes, a set of short impurities is also able to synchronize the system. Solitons are not nucleated by short impurities, but we have found that persistent oscillatory solitons may form in the parts of the array between the impurities.

We show the results of some simulations with 21 equidistant identical short impurities in Fig. 5.13 Fig. 5.16. The damping and driving parameters used are $\gamma = 0.3$ and $h = 0.85$. (With these parameters, an initial condition in the form of a soliton degenerates into spatiotemporal chaos in the homogeneous chain.) The initial condition used in each simulation is

$\mathrm{Re}\,\psi_n = \mathrm{Im}\,\psi_n = 0.2 + \xi_n$, where each ξ_n is a uniformly distributed random number between 0 and 0.01. It was necessary to wait a long time for all transients to settle. In each figure, we plot the real part of $\psi(x,t)$, using a grey scale ranging from $\min\{\mathrm{Re}\,\psi\}$ (white) to $\max\{\mathrm{Re}\,\psi\}$ (black).

For $q = -0.2$, we observe spatiotemporal chaos (Fig. 5.13). As in the case of the spatiotemporally chaotic regime of the homogeneous array which was analysed in Chapter 3, we see that short-lived solitons are created and annihilated continuously.

The result is very different for $q = -0.4$. Now, the chaotic oscillations previously observed disappear, and only two periodic solitons remain (Fig. 5.14). These solitons are both positioned in a region of the chain between two adjacent impurities. They oscillate with a frequency of $\omega \approx 2.7$. We see from Fig. 5.14b that the solitons radiate at the frequency 2ω.

For stronger impurities, such as $q = -0.6$, we see more periodic solitons appearing. Solitons with both positive and negative polarity are formed here. Their frequency of oscillation is $\omega \approx 2.8$ (Fig. 5.15). As before, the solitons radiate at the frequency 2ω.

In Fig. 5.16, where $q = -0.8$, we see some interesting oscillatory solutions. The pair of solitons between $x = -40$ and $x = -20$ oscillate in phase, while the pair between $x = 40$ and $x = 60$ oscillate out of phase. At $x = -8$, we observe a double-humped soliton.

In an array with 21 stronger impurities ($q = -1.4$), a single stationary soliton was observed. When the value of q is decreased further, or when more impurities are introduced into the array, all amplitudes decay to zero.

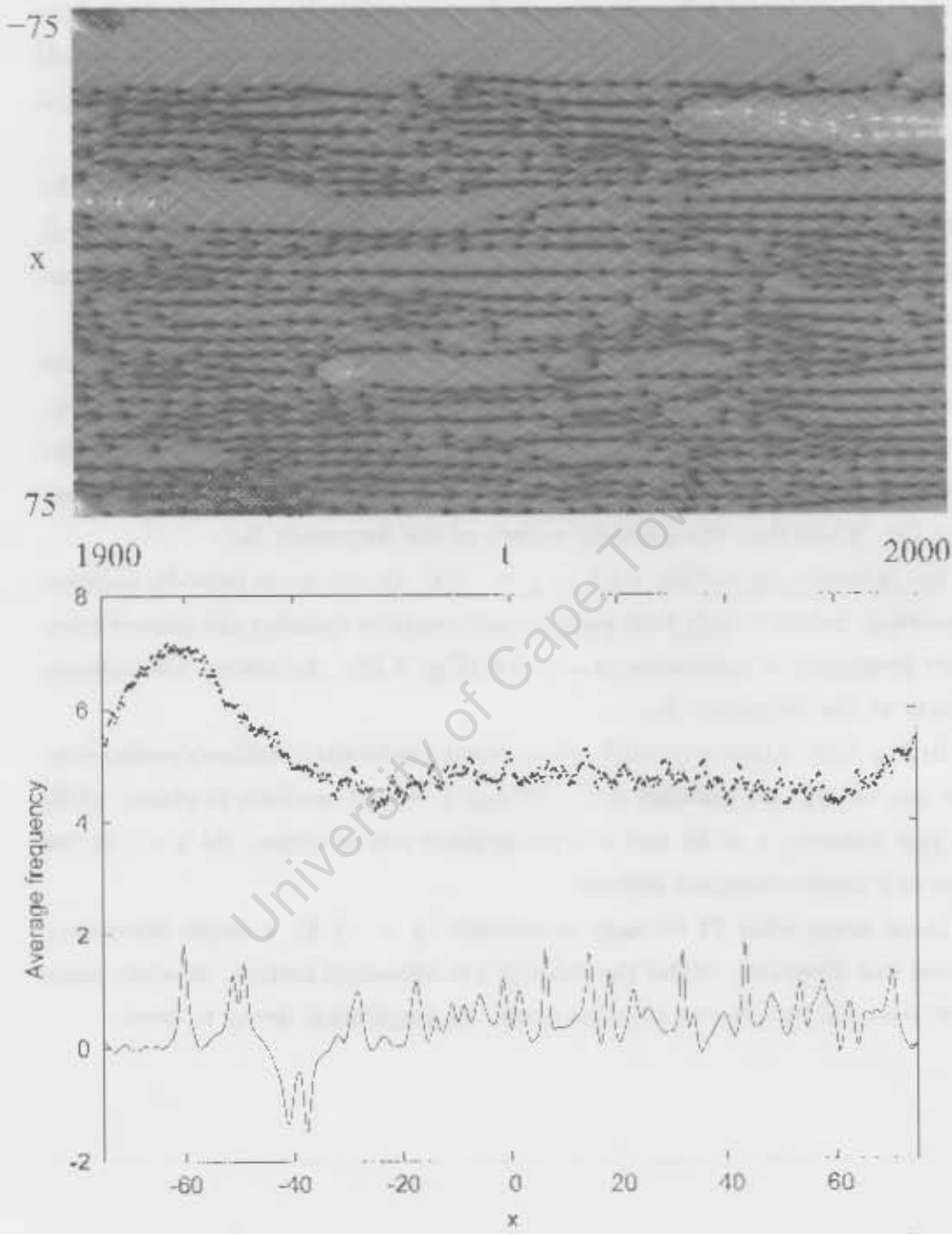

Figure 5.13: (a) Re $\psi(x,t)$ for 21 negative impurities with $q = -0.2$. Spatiotemporal chaos persists. (b) The average frequency is calculated for $1000 < t < 2000$, and a snapshot of Re ψ at $t = 2000$ is displayed. Here $\gamma = 0.3$, $h = 0.85$ and $\Delta x = 0.3$.

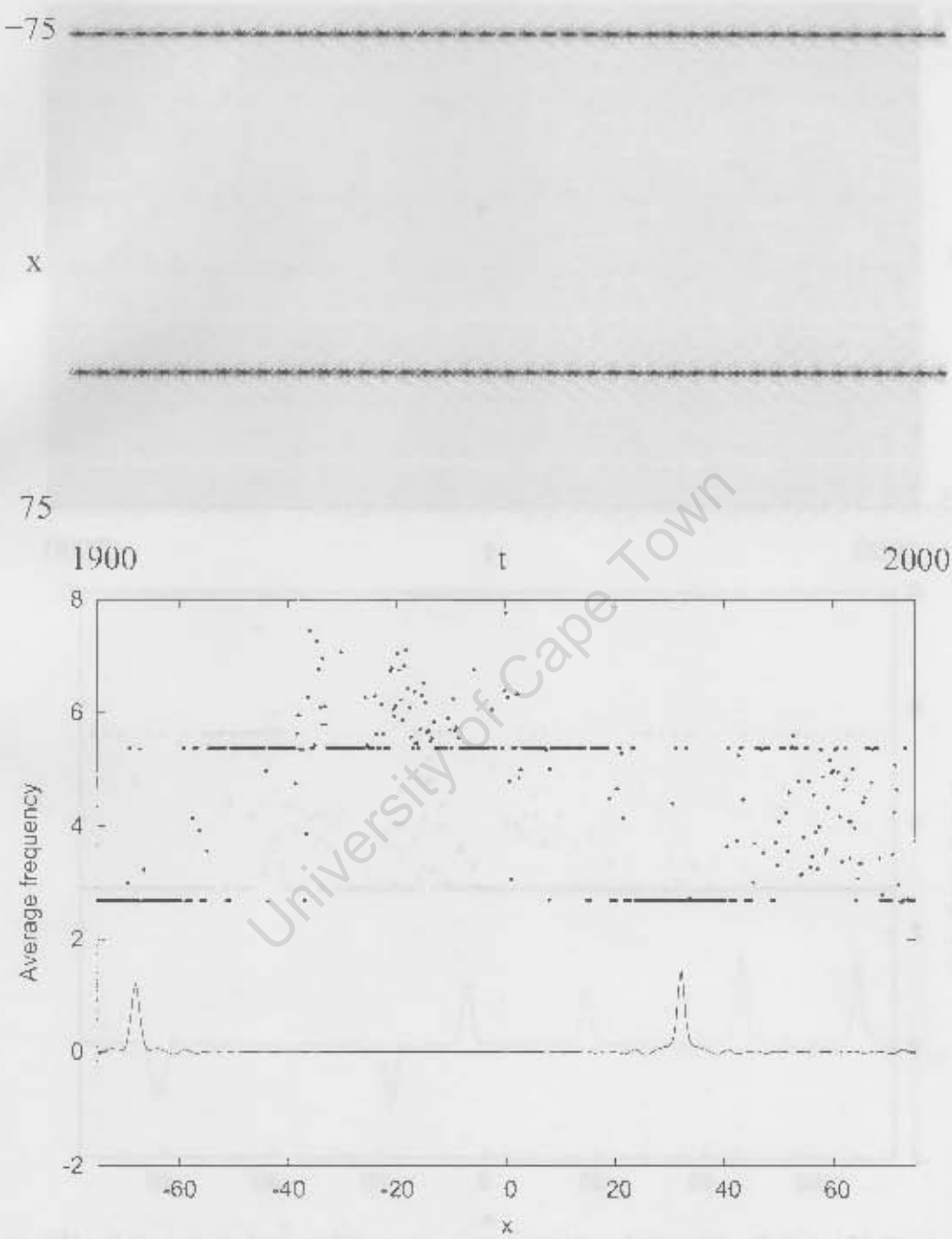

Figure 5.14: (a) Re $\psi(x,t)$ for 21 negative impurities with $q = -0.4$. Chaos is suppressed and two periodic solitons emerge. (b) The average frequency is calculated for $1500 < t < 2000$, and a snapshot of Re ψ at $t = 2000$ is displayed. Here $\gamma = 0.3$, $h = 0.85$ and $\Delta x = 0.3$.

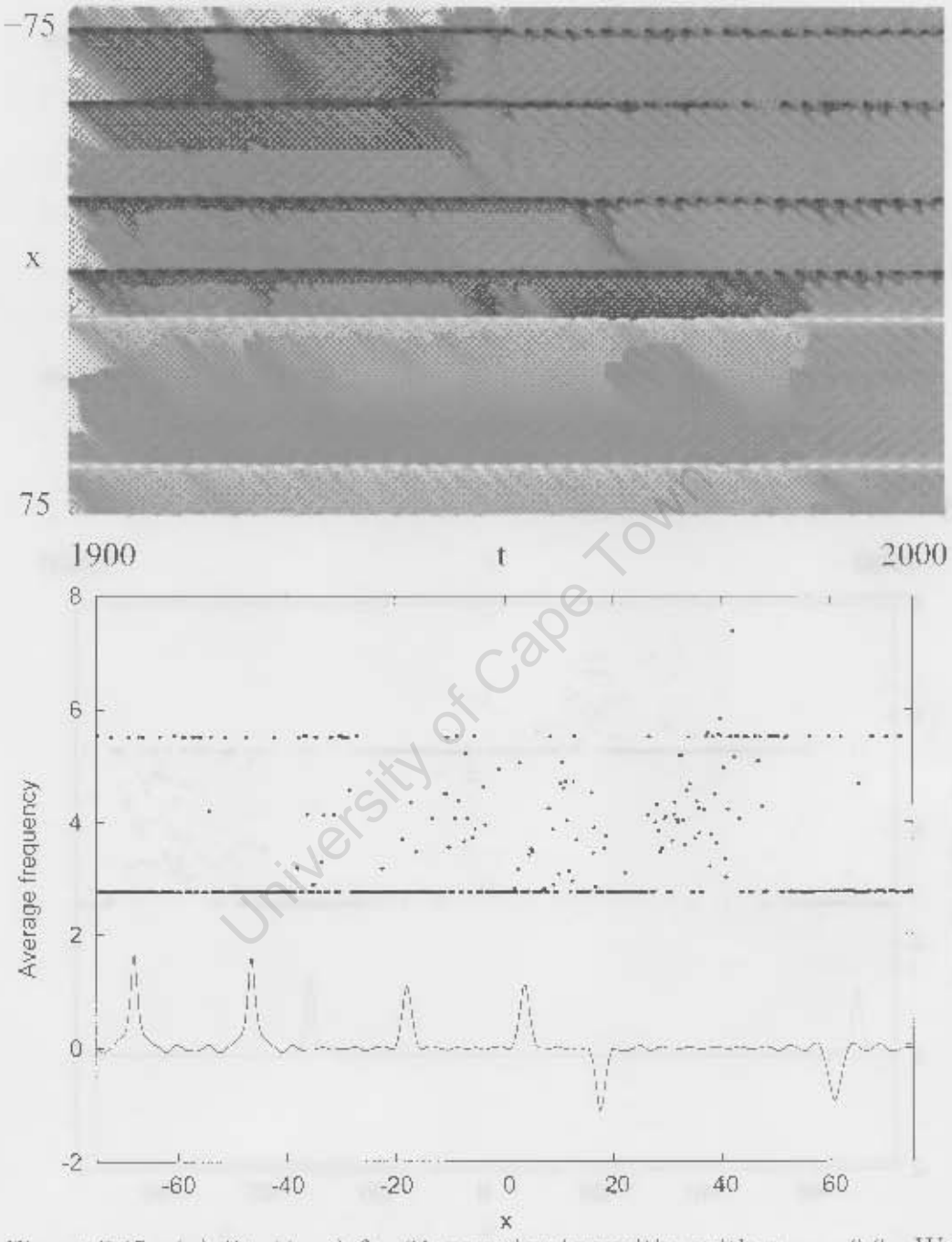

Figure 5.15: (a) Re $\psi(x,t)$ for 21 negative impurities with $q = -0.6$. We observe six periodic solitons. (b) The average frequency is calculated for $1500 < t < 2000$, and a snapshot of Re ψ at $t = 2000$ is displayed. Here $\gamma = 0.3$, $h = 0.85$ and $\Delta x = 0.3$.

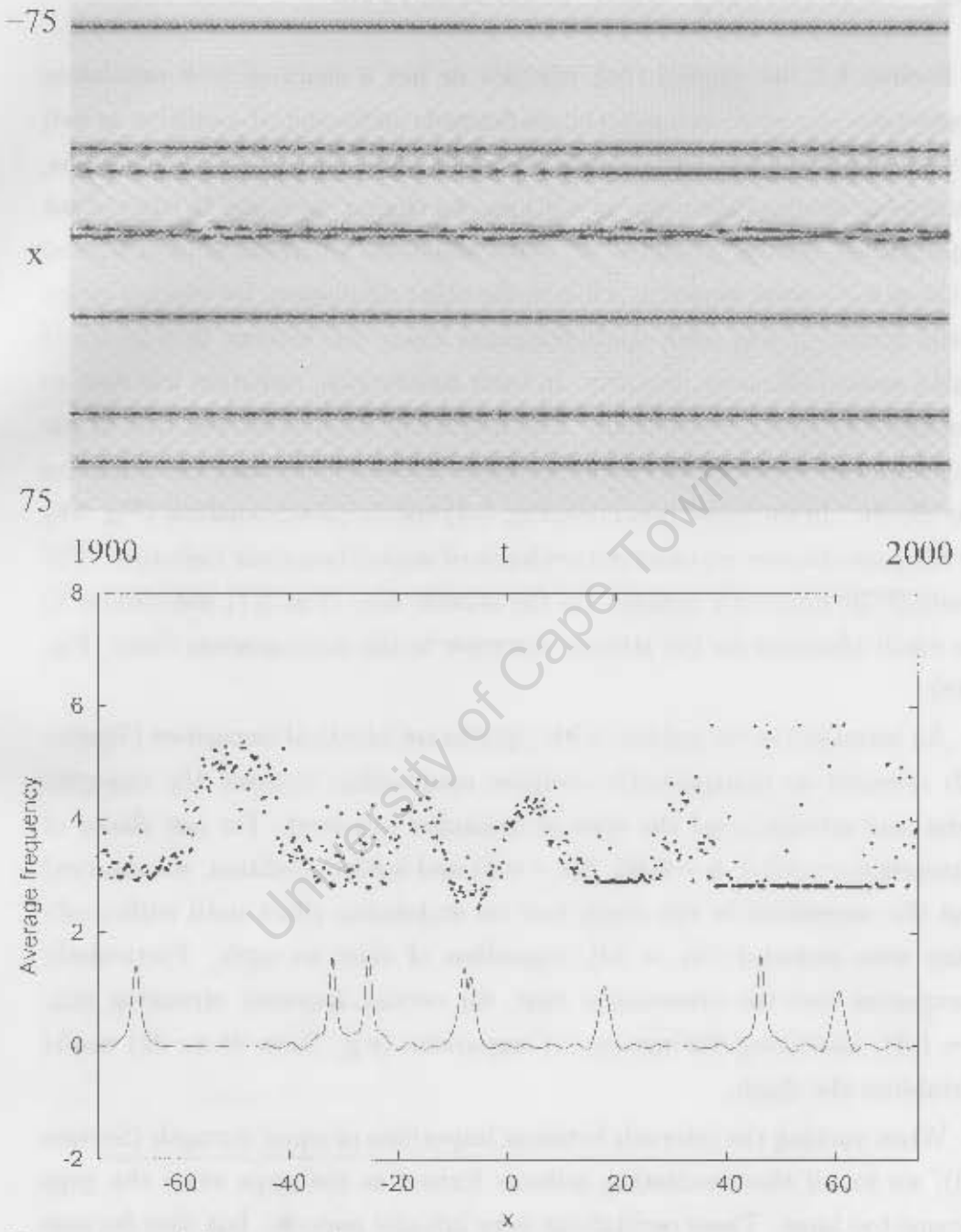

Figure 5.16: (a) Re $\psi(x,t)$ for 21 negative impurities with q -0.8. We observe seven oscillating solitons, including a double-humped soliton. (b) The average frequency is calculated for $1000 < t < 2000$, and a snapshot of Re ψ at $t = 2000$ is displayed. Here γ - 0.3, h 0.85 and $\Delta x = 0.3$.

5.5 Summary and Conclusions

In Section 5.1, we showed that whether or not a chain of NLS oscillators degenerates into spatiotemporal chaos depends on the initial condition as well as the number and strength of long impurities. We compared two simulations, identical apart from the initial condition, of a chain containing 15 equidistant impurities of various strengths. In one simulation, a periodic soliton formed at the site of a weak impurity, while in the other simulation, for which a larger initial condition was used, spatiotemporal chaos was evident in a localized region around the same impurity. In both simulations, radiation was seen to propagate along the whole chain. The frequency analysis showed that in the first case, the radiation was periodic, while in the second case, the radiation was chaotic. In the phase portraits (Fig. 5.4) and frequency analysis (Fig. 5.6) for the periodic case we observed evidence of second harmonic radiation. The result of the frequency analysis for the chaotic case (Fig. 5.7) was similar to the result obtained for the strange attractor in the homogeneous chain (Fig. 3.18).

An investigation of systems with equidistant identical impurities (Section 5.2) revealed an unexpectedly complex relationship between the impurity count and strength and the type of dynamics observed. For our choice of parameters ($\gamma = 0.3$, $h = 0.85$, $\Delta x = 0.3$) and initial condition, we observed that the impurities in the chain had no stabilizing effect until sufficiently many were included ($N_I = 13$), regardless of their strength. Particularly unexpected was the observation that, for certain impurity strengths (e.g. $q = 0.8$), increasing the number of impurities (e.g. from 21 to 22) would destabilize the chain.

When varying the intervals between impurities of equal strength (Section 5.3), we found that oscillating solitons formed in the gaps when the gaps became too large. These oscillations were initially periodic, but they became chaotic in cases which had more large gaps between impurities, and hence more solitons.

We also conducted some simulations with arrays containing equidistant negative impurities of equal strength (Section 5.4). We found that the

negative impurities were also capable of preventing spatiotemporal chaos in certain cases. With 21 short impurities, we observed chaotic motion for $q = -0.2$, but this was replaced by isolated oscillatory solitons for $-1.4 \leq q \leq -0.4$. The solitons appeared in the regions of the chain between the impurities. Occasionally, double-humped solitons were also observed.

Through our observations, we have made the following conclusions regarding the ability of a set of impurities to stabilize an array of oscillators (that is to prevent spatiotemporal chaos from emerging):

1. The impurities should be of sufficient strength. The strength required depends on the number of impurities and amplitude of the initial condition. In our simulations, impurities of strength $q \geq 0.6$ were used.

2. If the gaps between adjacent impurities are too large, free-standing oscillatory solitons tend to form in the gaps. Again, this depends on the initial condition. For example, when the initial condition used was $\mathrm{Re}\ \psi_n = \mathrm{Im}\ \psi_n = 0.2 + \xi_n$, the intervals between the x coordinates of the impurities needed to be less than 12 in order to prevent these oscillatory solitons from forming. The distance is independent of the impurity strengths.

3. We reiterate that the system studied is highly dependent on initial conditions. Generally, when the amplitude of the initial condition is larger, more impurities are required to stabilize the chain.

Chapter 6

Conclusion

In this thesis, we have simulated a chain of nonlinear Schrödinger oscillators numerically. We have studied the effects of various choices of parameters (damping γ, driving strength h and oscillator spacing Δx) on the dynamics. For larger driving strengths, the chain is prone to spatiotemporally chaotic evolution. Our main tasks were:

1. to study the advent of spatiotemporal chaos and to try to identify the fundamental structures which this chaos consists of, and

2. to explore how various configurations of impurities (number, strength and position) are able to synchronize the oscillators, suppressing spatiotemporal chaos.

We demonstrated through our simulations of a homogeneous chain that the discrete array of NLS oscillators exhibits similar behaviour to the continuous NLS equation. This includes the period-doubling transition from a periodic to a chaotic soliton solution (the strange attractor) as well as the degeneration of the soliton into spatiotemporal chaos for large driving strengths. Frequency analysis highlighted the fact that the spatiotemporally chaotic evolution is qualitatively different from the evolution of the strange attractor, where the chaos is spatially localized.

Our analysis of spatiotemporal chaos in the homogeneous chain revealed some new and interesting results. We identified many short-lived unstable

solitons distributed throughout the chain. All solitons had similar periods. We measured the average frequency of maxima of the oscillations at all sites along the chain. We found that this measurement converged to the same value along the whole chain. This value was approximately double the frequency of the oscillating solitons. Adjacent solitons tended to oscillate with a constant phase shift. We surmise that the mechanism for the synchronization of the frequencies of the solitons is coupling due to radiation produced by the solitons. This conclusion is supported by our measurement of the radiation speed which was remarkably close to the theoretical group velocity for linear waves with our measured average frequency.

Our next task was to explore how spatiotemporal chaos could be suppressed as a result of introducing intermittent disorder into our chain. In our work, we disordered the homogeneous chain by swapping one or more oscillators for longer or shorter ones. Since we only alter a few of the oscillators, the disorder we employ is rather weak.

When simulating a chain containing a single impurity, we replicated results previously obtained for the continuous NLS equation with a δ-function impurity. We showed how an impurity can prevent the periodic oscillations of a soliton from degenerating into spatiotemporal chaos, thus synchronizing the chain. We also demonstrated that a stationary soliton can form spontaneously at the site of a long impurity.

Lastly, we studied the effects of including multiple impurities in the chain. We showed that spatiotemporal chaos could often be suppressed if sufficiently many impurities were present. We showed that the number of impurities required depended on the initial condition, with larger initial conditions being more likely to produce chaos. We showed that spatiotemporally chaotic evolution could sometimes be contained in a small region of the chain, though radiation caused small chaotic vibrations throughout the array.

For a specific initial condition and fixed driving and damping, we systematically studied arrays with equal equidistant positive impurities. We varied the number of impurities as well as their strength. We found that for our chosen initial condition, we required at least 13 impurities for the oscillators to synchronize, regardless of their strength.

When we disordered the positions of evenly spaced impurities, we noticed that the chain lost its stability when the distances between the impurities were too large. It appears that if the gaps between the impurities are small enough, the dominant structures of the spatiotemporally chaotic regime (unstable solitons) cannot fit in, and they are therefore suppressed.

Negative impurities were also found to stabilize the chain in certain cases. These impurities do not nucleate solitons, but they can split the chain with periodic free-standing solitons forming between the impurities.

In summary, our results indicate that unstable solitons are the dominant structures which make up the spatiotemporally chaotic evolution of the chain. The oscillators in the chain can be synchronized if weak disorder is introduced in the form of impurities placed intermittently along the chain. This synchronization, which amounts to the suppression of spatiotemporal chaos, occurs if sufficiently many strong impurities are inserted into the chain.

When we disordered the positions of evenly spaced impurities, we noticed that the chain lost its stability when the distances between the impurities were too large. It appears that if the gaps between the impurities are small enough, the dominant structures of the spatiotemporally chaotic regime (unstable solitons) cannot fit in, and they are therefore suppressed.

Negative impurities were also found to stabilize the chain in certain cases. These impurities do not nucleate solitons, but they can split the chain with periodic free-standing solitons forming between the impurities.

In summary, our results indicate that unstable solitons are the dominant structures which make up the spatiotemporally chaotic evolution of the chain. The oscillators in the chain can be synchronized if weak disorder is introduced in the form of impurities placed intermittently along the chain. This synchronization, which amounts to the suppression of spatiotemporal chaos, occurs if sufficiently many strong impurities are inserted into the chain.

Bibliography

[1] N. V. Alexeeva, I. V. Barashenkov, and D. E. Pelinovsky, *Dynamics of the parametrically driven NLS solitons beyond the onset of the oscillatory instability*, Nonlinearity, **12** (1999), 103.

[2] N. V. Alexeeva, I. V. Barashenkov, and G. P. Tsironis, *Impurity-induced stabilization of solitons in arrays of parametrically driven nonlinear oscillators*, Physical Review Letters, **84** (2000), 3053.

[3] N. V. Alexeeva, I. V. Barashenkov, and G. P. Tsironis, *Taming spatiotemporal chaos by impurities in the parametrically driven damped nonlinear Schrödinger equation*, Journal of Nonlinear Mathematical Physics, **8** (2001), Supplement, 5.

[4] S. Ancoli-Israel, J. L. Martin, D. F. Kripke, M. Marler, and M. R. Klauber, *Effect of light treatment on sleep and circadian rhythms in demented nursing home patients*, Journal of the American Geriatrics Society, **50** (2002), 282.

[5] I. V. Barashenkov, unpublished.

[6] I. V. Barashenkov, M. M. Bogdan, and V. I. Korobov, *Stability diagram of the phase-locked solitons in the parametrically driven, damped nonlinear Schrödinger equation*, Europhysics Letters, **15** (1991), no. 2, 113.

[7] I. V. Barashenkov and E. V. Zemlyanaya, *Stable complexes of parametrically driven, damped nonlinear Schrödinger solitons*, Physical Review Letters, **83** (1999), 2568.

[8] I. V. Barashenkov, E. V. Zemlyanaya, and M. Bär, *Traveling solitons in the parametrically driven nonlinear Schrödinger equation*, Physical Review E, **64** (2001), 016603.

[9] J. Benford, H. Sze, W. Woo, R. R. Smith, and B. Harteneck, *Phase locking of relativistic magnetrons*, Physical Review Letters, **62** (1989), 969.

[10] M. Bondila, I. V. Barashenkov, and M. M. Bogdan, *Topography of attractors of the parametrically driven nonlinear Schrödinger equation*, Physica D, **87** (1995), 314.

[11] Y. Braiman, W. L. Ditto, K. Wiesenfeld, and M. L. Spano, *Disorder-enhanced synchronization*, Physics Letters A, **206** (1995), 54.

[12] Y. Braiman, J. F. Lindner, and W. L. Ditto, *Taming spatiotemporal chaos with disorder*, Nature, **378** (1995), 465.

[13] O. M. Braun and Y. S. Kivshar, *Nonlinear dynamics of the Frenkel-Kontorova model*, Physics Reports, **306** (1998), 1.

[14] J. Buck and E. Buck, *Mechanism of rhythmic synchronous flashing of fireflies*, Science, **159** (1968), 1319.

[15] W. Chen, B. Hu, and H. Zhang, *Interactions between impurities and nonlinear waves in a driven nonlinear pendulum chain*, Physical Review B, **65** (2002), 134302.

[16] G. B. Ermentrout and N. Kopell, *Frequency plateaus in a chain of weakly coupled oscillators, I*, SIAM Journal on Mathematical Analysis, **15** (1984), 215.

[17] A. Gavrielides, T. Kottos, V. Kovanis, and G. P. Tsironis, *Spatiotemporal organization of coupled nonlinear pendula through impurities*, Physical Review E, **58** (1998), 5529.

[18] P. Hadley, M. R. Beasley, and K. Wiesenfeld, *Phase locking of Josephson-junction series arrays*, Physical Review B, **38** (1988), 8712.

[19] M. V. Ivanchenko, G. V. Osipov, V. D. Shalfeev, and J. Kurths, *Phase synchronization in ensembles of bursting oscillators*, Physical Review Letters, **93** (2004), 134101.

[20] M. V. Ivanchenko, G. V. Osipov, V. D. Shalfeev, and J. Kurths, *Phase synchronization of chaotic intermittent oscillations*, Physical Review Letters, **92** (2004), 134101.

[21] I. Z. Kiss and J. L. Hudson, *Phase synchronization and suppression of chaos through intermittency in forcing of an electrochemical oscillator*, Physical Review E, **64** (2001), 046215.

[22] J. F. Lindner, B. S. Prusha, and K. E. Clay, *Optimal disorders for taming spatiotemporal chaos*, Physics Letters A, **231** (1997), 164.

[23] P. C. Matthews and S. H. Strogatz, *Phase diagram for the collective behavior of limit-cycle oscillators*, Physical Review Letters, **65** (1990), 1701.

[24] M. K. McClintock, *Menstrual synchrony and suppression*, Nature, **229** (1971), 244.

[25] G. V. Osipov and J. Kurths, *Regular and chaotic phase synchronization of coupled circle maps*, Physical Review E, **65** (2001), 016216.

[26] G. V. Osipov, A. S. Pikovsky, and J. Kurths, *Phase synchronization of chaotic rotators*, Physical Review Letters, **88** (2002), 054102.

[27] G. V. Osipov, A. S. Pikovsky, M. G. Rosenblum, and J. Kurths, *Phase synchronization effects in a lattice of nonidentical rössler oscillators*, Physical Review E, **55** (1997), 2353.

[28] G. V. Osipov and M. M. Sushchik, *The effect of natural frequency distribution on clustersynchronization in oscillator arrays*, IEEE Transactions on Circuits and Systems I: Fundamental Theory and Applications, **44** (1997), 1006.

[29] G. V. Osipov and M. M. Sushchik, *Synchronized clusters and multistability in arrays of oscillators with different natural frequencies*, Physical Review E, **58** (1998), 7198.

[30] V. Petrov, Q. Ouyang, and H. L. Swinney, *Resonant pattern formation in a chemical system*, Nature, **388** (1997), 655.

[31] A. Pikovsky, M. Rosenblum, and J. Kurths, *Synchronization*, no. 12 in Cambridge Nonlinear Science Series, Cambridge University Press, 2001.

[32] W. H. Press, S. A. Teukolsky, W. T. Vetterling, and B. P. Flannery, *Numerical Recipes in C*, Cambridge University Press, 1992, second ed.

[33] F. Qi, Z. Hou, and H. Xin, *Ordering chaos by random shortcuts*, Physical Review Letters, **91** (2003), 064102.

[34] R. Richter and I. V. Barashenkov, *Two-dimensional solitons on the surface of magnetic fluids*, Physical Review Letters, **94** (2005), 184503.

[35] M. G. Rosenblum and A. S. Pikovsky, *Controlling synchronization in an ensemble of globally coupled oscillators*, Physics Review Letters, **92** (2004), 114102.

[36] R. Roy and J. K. Scott Thornburg, *Experimental synchronization of chaotic lasers*, Physical Review Letters, **72** (1994), 2009.

[37] L. Rubchinsky and M. Sushchik, *Anomalous relationship between spatial and temporal patterns of dynamical behavior*, International Journal of Bifurcation and Chaos, **9** (1999), 2329.

[38] L. Rubchinsky and M. Sushchik, *Disorder can eliminate oscillator death*, Physical Review E, **62** (2000), 6440.

[39] N. F. Rulkova and M. M. Sushchik, *Experimental observation of synchronized chaos with frequency ratio 1 : 2*, Physics Letters A, **214** (1996), 145.

[40] V. S. Shchesnovich and I. V. Barashenkov, *Soliton-radiation coupling in the parametrically driven, damped nonlinear Schrödinger equation*, Physica D, **164** (2002), 83.

[41] W. L. Shew, H. A. Coy, and J. F. Lindner, *Taming chaos with disorder in a pendulum array*, American Journal of Physics, **67** (1999), 703.

[42] S. H. Strogatz, *Ordering chaos with disorder*, Nature, **378** (1995), 444.

[43] C. M. Ticos, E. Rosa, W. B. Pardo, J. A. Walkenstein, and M. Monti, *Experimental real-time phase synchronization of a paced chaotic plasma discharge*, Physical Review Letters, **85** (2000), 2929.

[44] T. J. Walker, *Acoustic synchrony: Two mechanisms in the snowy tree cricket*, Science, **166** (1969), 891.

[45] K. Wiesenfeld, P. Colet, and S. Strogatz, *Synchronization transitions in a disordered Josephson series array*, Physical Review Letters, **76** (1996), 404.